DEPARTMENT OF PHYSICS
UNIVERSITY OF JYVÄSKYLÄ
RESEARCH REPORT No. 13/2014

Spectroscopic studies of ^{173}Pt and ^{175}Pt

by

Pauli Peura

Academic Dissertation
for the Degree of
Doctor of Philosophy

To be presented, by permission of the
Faculty of Mathematics and Natural Sciences
of the University of Jyväskylä,
for public examination in Auditorium FYS1 of the
University of Jyväskylä on December 19th, 2014
at 12 o'clock noon.

JYVÄSKYLÄN YLIOPISTO

Jyväskylä, Finland
December 2014

Preface

The work presented here was carried out during the years 2007–2014 at the Department of Physics of the University of Jyväskylä.

I would like to express my gratitude to my supervisor Dr. Catherine Scholey for the guidance given to me during my studies. The interest she has constantly shown towards my work has been a great source of motivation. I would also like to express my gratitude to Prof. Rauno Julin for all the advice and encouragement during all the years. The advice given to me by Dr. Sakari Juutinen have been of great help. I express my special thanks to Prof. Matti Leino for all the help and support provided. I acknowledge the discussions together with Dr. David Joss, Dr. Juha Uusitalo and Dr. Jan Sarén which have given me insight into many different aspects of my work.

I thank all the past and present members of the RITU-Gamma group I have had a chance to work with. The time I have spent working at the detector hospital was spent mostly with Dr. Markus Nyman, Dr. Panu Ruotsalainen and Dr. Steffen Ketelhut, which made the work most pleasant. The friendly staff of the Department of Physics is thanked here for all the support provided. Dr. Timo Koponen deserves a big thank you for the guidance provided during many of the courses I took throughout my MSc studies.

Finally, I want to thank my family for all their support. For all the great joy and wisdom brought into my life I want to thank Ulrika.

Financial support from the University of Jyväskylä, The Finnish Cultural Foundation, The Finnish Academy of Science and Letters: Vilho, Yrjö ja Kalle Väisälä Foundation and Ellen and Artturi Nyyssönen Foundation is gratefully acknowledged.

Jyväskylä, December, 2014
Pauli Peura

Abstract

Peura, Pauli
Spectroscopic studies of ^{173}Pt and ^{175}Pt
Jyväskylä: University of Jyväskylä, 2014, 104 p.
Department of Physics Research Report No. 13/2014
ISSN: 0075-465X; 13/2014
ISBN: 978-951-39-5922-7 (paper version)
ISBN: 978-951-39-5923-4 (electronic version)
Diss.

Neutron-deficient ^{173}Pt and ^{175}Pt were studied using heavy-ion fusion-evaporation reactions. The JUROGAM Ge array and the GREAT spectrometer, in conjunction with the RITU gas-filled separator, were used for prompt–γ-ray and decay spectroscopy, respectively. The prompt γ rays of ^{173,175}Pt were selected using the recoil-gating and recoil-decay tagging techniques. For both nuclei, the known positive-parity bands were extended, and negative-parity bands were observed. An $i_{13/2}$ quasineutron alignment was observed for the positive and negative-parity bands of ^{173}Pt and ^{175}Pt, based on a cranked shell-model analysis. Observed low-frequency alignment irregularities of ^{175}Pt suggest a change of deformation within the rotational structure. Based on unhindered α decays of ^{173}Pt and ^{175}Pt, and the observation of subsequent $M1$ transitions in ^{169}Os and ^{171}Os, respectively, the ground-states of ^{173,175}Pt were assigned to have $I^\pi = (7/2^-)$. An isomeric state with a half-life of 9.0(5) μs was observed in ^{173}Pt. This isomeric state was assigned to have $I^\pi = (13/2^+)$, based on the observation of coincident $M2$ and $M1$ transitions following the decay of the isomeric state.

Keywords: nuclear spectroscopy, gamma-ray spectroscopy, alpha decay, recoil-decay tagging, neutron-deficient nuclei, cranked shell model

Author's address Pauli Peura
Department of Physics
University of Jyväskylä
Finland

Supervisor Dr. Catherine Scholey
Department of Physics
University of Jyväskylä
Finland

Reviewers Dr. Edward Paul
University of Liverpool
UK

Dr. Gregory Lane
Australian National University
Canberra, Australia

Opponent Prof. Philip Walker
University of Surrey
UK

Contents

Chapter 1

Introduction

The atomic nucleus can be characterised in numerous ways. For example the number of protons Z in the nucleus is used to label different atomic elements together with their given names. The element platinum refers to an atom with 78 protons in each nucleus. The isotopes of a given element can be identified by the number of neutrons N or by the mass number $A = Z + N$. To date, 39 Pt isotopes have been identified, ranging from the very-neutron deficient ^{166}Pt to the neutron rich ^{205}Pt.

Protons are known to have positive electric charge whereas neutrons are electrically neutral. Due to the fact that complex nuclei exist, there must be a strong force binding the protons and neutrons (nucleons) together to form a nucleus. This force has to be strong enough to overcome the Coulomb repulsion between the positively charged protons. Unlike the Coulomb force, the strong force has a short range. This becomes evident for the heaviest nuclei, which fission spontaneously, as the Coulomb repulsion overcomes the short-range binding force.

The experimental work presented in this thesis is centred around two isotopes of platinum, with mass numbers 173 ($N = 95$) and 175 ($N = 97$). The short half-lives of these radioactive isotopes call for the use of experimental facilities, to first create the nuclei, before they can be investigated experimentally. The closest stable isotope of platinum has mass number 190, thus these neutron-deficient isotopes are 17 (^{173}Pt) and 15 (^{175}Pt) neutrons away from ^{190}Pt. One of the motivations for this work is to continue the systematic study of the excited states in this region of nuclei, near the $Z = 82$ shell closure. In recent years, it has become possible to perform target-position γ-ray and focal-plane decay spectroscopy in a single experiment, when a recoil

separator is utilized. The correlations, between the observed signals[a] from various detectors in the experimental setup, depend on the properties of the nuclei emitting them. Thus, it is possible to make observations of nuclear structure by measuring, for example, electromagnetic radiation from an $A = 173$ platinum nucleus. Complimentary information to the γ-ray spectroscopy results can be gained by performing α-decay spectroscopy.

The Pt isotopes investigated here are situated just below the proton-magic number 82 of the spherical shell model. In Pb ($Z = 82$) and Hg ($Z = 80$) isotopes coexisting structures having different deformations have been well established [Hey11, GR14a]. The occurrence of these different nuclear shapes at low excitation energy is attributed to the energetically favourable multi-particle multi-hole (*mp-mh*) excitations. In this process the pair excitation lifts nucleons across a closed shell [Hey11]. These closed shells are explained by the nuclear shell model. For Pt isotopes similar shape coexistence, due to intruder *mp-mh* excitations, is not as well established, as it is for Hg and Pb isotopes [GR11]. However, for ^{174,176}Pt isotopes, coexisting shapes have been proposed due to observed irregularities in aligned angular-momentum plots at low rotational frequencies (ω) [Dra86, Dra91, Ced90, Goo04b]. These observations are supported by total Routhian surface (TRS) calculations, which predict well-defined prolate deformations at high-ω values. At low ω, the minimum-deformation value is not as well defined in ^{174,176}Pt [Ced90, Goo04b]. A change in deformation was also suggested to occur in a positive-parity band of ^{175}Pt based on observed low-frequency irregularities and TRS calculations [Ced90]. However, shape coexistence has not been observed in ^{177}Pt [Dra90].

The study of odd-A nuclei is important in order to obtain information of the single-particle orbitals, which are occupied by the odd nucleon. For ^{171}Pt, ^{167}Os and ^{163}W [Sch10], as well as for ^{175}Hg [O'D09] and ^{177}Hg [Mel03], the observation of $I^\pi = {}^{13}/_{2}^{+}$ isomeric states have been reported. These relatively long-lived states are assumed to be based on the $i_{13/2}$ unique-parity single-particle orbitals. Transitions of $M2$ character originating from these $I^\pi = {}^{13}/_{2}^{+}$ states have been observed to feed $I^\pi = {}^{9}/_{2}^{-}$ states of an $h_{9/2}$ origin [Sch10, O'D09, Mel03]. Support for the I^π assignments of ground states and excited states can be obtained from the study of α-decay properties of nuclei [Ras59a, Ras59b, GR11, Hey11]. An unhindered α decay is likely to be observed between initial and final states of similar nuclear configurations in mother

[a] For example the amplitude ($\propto$ energy) and time of detection.

and daughter nuclei, respectively. Additionally, α-decay studies compliment the study of excited states produced in heavy ion-fusion evaporation reactions. The excitation energy of fusion-evaporation reaction products is released mainly via the yrast states. In α decay, non-yrast states at low excitation energy can be populated with high probability. A recent outstanding example of the power of α-decay spectroscopy is the observation of the α decay from ^{190}Po. In this work, α decays to three $I^{\pi} = 0^{+}$ states in ^{186}Pb were observed by A. Andreyev *et al.* [And00]. These 0^{+} states are assumed to have different deformations, which is supported by the measured reduced widths for the α-decay branches.

Not all the parameters of interest in platinum isotopes can be measured with a single experimental setup. Therefore, in this work three main goals were set:

- extend the knowledge of the excited states,
- search for isomeric states, and
- investigate the fine-structure α decay,

in ^{173,175}Pt. The results obtained are from two different experiments performed at the Accelerator Laboratory of the University of Jyväskylä (JYFL). The experimental setup consisted of the JUROGAM[b] array, the RITU separator and the GREAT spectrometer. The nuclei studied were produced in fusion-evaporation reactions induced by heavy-ion beams of stable isotopes. Results for excited states in ^{173}Pt and ^{175}Pt are presented together with results from α decay of these isotopes. The results are interpreted using the cranked-shell model formalism and comparing the excited states of ^{173}Pt and ^{175}Pt to $N = 95$ and $N = 97$ Os, W and Hf isotones, respectively. An isomeric state with $I^{\pi} = (13/2^{+})$ was observed in ^{173}Pt, but not in ^{175}Pt. Additionally, α-decay fine structure was studied in ^{173}Pt and ^{175}Pt, revealing information on the excited states in ^{169}Os, ^{171}Os, respectively.

[b] The ^{175}Pt experiment used the JUROGAM I Ge array, whereas the JUROGAM II array was used in the ^{173}Pt experiment.

Chapter 2

Background

Atoms are known to consist of electrons surrounding a dense nucleus of protons and neutrons. The radii of atoms are of the order of 10^{-10} m whereas the radius of a nucleus is of the order of $R \approx 1.2 \times A^{1/3}$ fm $\approx 10^{-14}$ m [Gre55, p.7,38], [Eva72, p.30], for the nuclei studied in the present work. In atoms, electrons can be thought of as moving inside a central potential almost without interaction with each other. Placing electrons or nucleons into a confining potential, allows only a discrete set of energy states for the particles, which is explained by the quantum mechanical model of the system (see e.g. [Kra88, p.25]). However, within the nucleus the definition of a central potential is not as obvious as for atoms. The masses of the protons and neutrons are roughly the same[a] and their radii are comparable to the radius of the nucleus. Additionally, nuclei are bound together by a strong force with a short range. From this point-of-view the nucleons hardly seem like independent particles revolving around a common centre. Hence shell structure was originally not expected to occur in nuclei. However, there exists substantial experimental data that points towards certain numbers of Z and N, corresponding to nuclei that are observed to be especially stable. Based on these magic numbers, the picture of a shell structure appears.

2.1 Nuclear shell structure

One example of the aforementioned enhanced stability of magic nuclei, are the two-nucleon separation energies as a function of Z or N. The nucleon numbers where extra

[a]The mass of an electron is $\approx$ 511 keV/c^2, whereas the proton and neutron masses are $m_p \approx$ 938.3 MeV/c^2 and $m_p \approx$ 939.6 MeV/c^2, respectively [Moh12].

stability is seen are 2, 8, 20, 28, 50, 82. These are called the magic numbers. For neutrons $N = 126$ is also a magic number. Examples of the evidence for these magic numbers are given for instance in Refs. [May49, Kra65]. These shell structures can be explained assuming the nucleons move independently in a spherically symmetric central potential. In this potential, the allowed energy levels can be characterised by the orbital angular-momentum quantum number l of a nucleon. The notation used for the different l values is $s, p, d, f, g, h, i, \ldots$ for $l = 0, 1, 2, 3, 4, 5, 6, \ldots$, respectively. Due to the spherical symmetry of the potential, the $2l+1$ different angular orientations of $\bar{l}$, the magnetic substates m_l, have the same energy. Thus, the different l orbitals are said to be degenerate. The ordering and spacing of the orbitals depends on the shape of the confining potential. However, the magic numbers could only be reproduced by assuming a strong spin-orbit coupling between the spin s[b] and l of a particle [May49, Hax49]. Fermions – protons, neutrons and electrons – have s = 1/2, with possible projections $m_s = \pm 1/2$. When the spin of nucleons is taken into account, the resulting j orbitals are $(2j + 1)$ degenerate and $\bar{j} = \bar{l} + \bar{s}$ is called the total angular momentum. This is the independent-particle model (IPM) or shell model. Assuming that the strong force favours pairs of identical particles, which couple to zero total angular momentum, the IPM explains the experimental result $I^{\pi}_{\mathrm{gs}} = 0^+$ for even-Z, even-N nuclei [May50]. An even number of identical nucleons of the same j orbital coupling to zero angular momentum is called pairing. For odd-A nuclei the IPM, together with pairing, predicts that the I^{π} of a nucleus is determined by the last unpaired nucleon. This assumption is in good agreement with the experimental results for I^{π} for nuclei near the magic numbers [May50]. The independence of the single-particle motion in a nucleus is seen as a result of the Pauli exclusion principle, which prohibits two like fermions occupying the same quantum state [Bla60, pp.39-43]. On the left-hand side of Figure 2.1 the ordering of some of the spherical shell model single-particle orbitals for neutrons is shown. The spin-orbit coupling causes these l orbitals to be split, and the magic numbers 82 and 126 appear as large energy gaps, created by the splitting of the orbitals.

[b] The intrinsic angular momentum s of a particle is called spin. The word spin is often used for the total angular momentum I of a state, in addition to the intrinsic angular momentum.

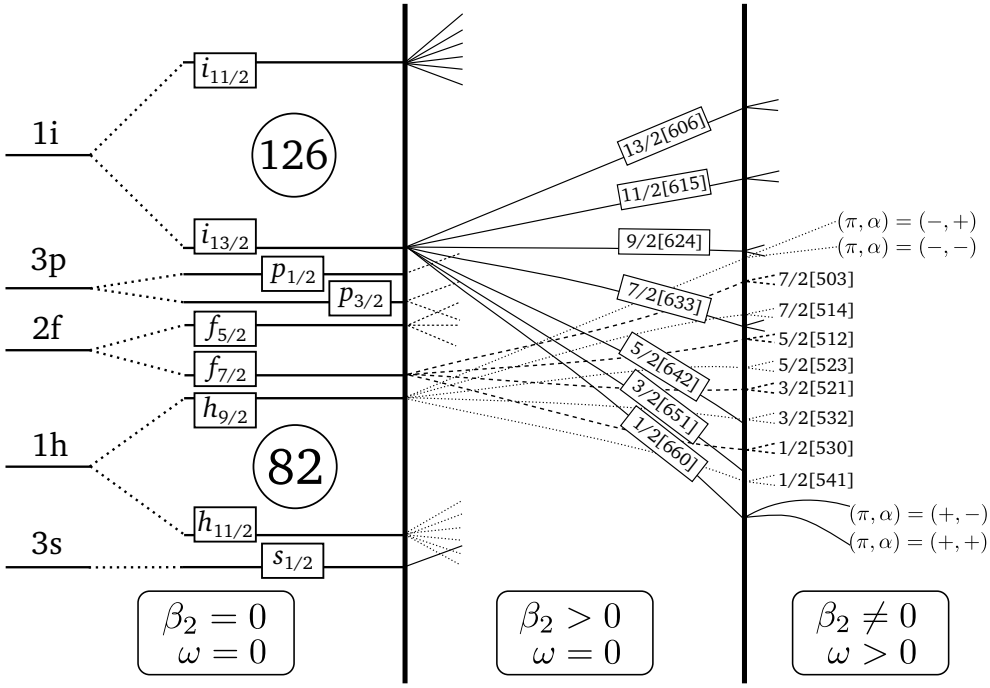

FIGURE 2.1: A schematic drawing of the evolution of the excitation energy of the neutron single-particle orbitals based on References [Kra88, Nil95]. On the left, the spherical shell model l-orbitals are split into two by the spin-orbit interaction. The l quantum numbers are labelled by letters $s, p, d, \ldots$ corresponding to $l = 0, 1, 2, \ldots$. In the middle the deformation (β_2) is increasing while moving from left to right. The $2j + 1$ degeneracy of the spherical potential is broken in the deformed potential (Nilsson model, Section 2.3) and the resulting orbitals are only 2-fold degenerate ($m_s = \pm 1/2$). On the right-hand side of the Figure, the deformation is fixed to a non-zero value while at the same time the angular velocity ω increases when moving to the right. The energy of the single-particle orbitals can be described in this case by the Cranking model (Section 2.4). Even the 2-fold degeneracy of the Nilsson model orbitals is broken by the rotation of the system. Only parity (π) and signature (α) can be used to uniquely define the resulting orbitals. Some of the Nilsson model orbitals are not drawn fully to maintain clarity of the Figure.

2.2 Unique-parity states

In the IPM the spin-orbit coupling divides the degenerate l orbitals in two. The split orbitals are labelled by the total angular momentum quantum number j. The splitting favours the high-j orbitals, while at the same time the low-j orbitals gain excitation energy. At certain particle numbers, this splitting can push an orbital originating from an odd-l (even-l) state among orbitals having only even-l (odd-l) values. As the

parity[c] of a given orbital is given by $(-1)^l$ (see e.g. [Eva72, p.174–175]), these intruding orbitals have unique parity compared with the nearby orbitals. These states are also called intruder states within the shell-model picture. In Figure 2.1 the splitting of the $1i$ orbital pushes the $i_{13/2}$ orbital down in energy making it an intruder state. A transition between states of different parity, and possibly with a large difference in angular momentum, is likely to be hindered. The large hindrance causes the half-life of the initial state to be longer, compared with a transition where a smaller change in angular momentum occurs. The $i_{13/2}$ orbital is chosen as an example, as the region where ^{173,175}Pt are located is known to be influenced by the presence of this unique-parity orbital [Sch10, O'D09, Mel03].

2.3 Rotational spectra and deformation

Nuclear deformation was introduced to explain the observed large quadrupole moments of, for example, ^{175,176}Lu [Tow49, Rai50], which were unexplained by the spherical shell model. If a nucleus is deformed it can rotate collectively. Alternatively, the collective motion may consist of vibrations about an equilibrium shape. A description of bound energy states of individual nucleons in a deformed nucleus was written, for the first time, by Nilsson [Nil55, Mot55]. The deformations considered in the Nilsson model are axially symmetric prolate and oblate shapes[d]. Small deformations can be described by the quadrupole-deformation parameter β_2 [Boh52, Nil69], describing prolate and oblate shapes when positive and negative, respectively. A prolate deformation corresponding to $\beta_2 \approx {}^{\Delta R}/_{R} = 0.2$ is shown in Figure 2.2. The difference between the two axis of an ellipsoid ΔR is taken to be $\Delta R = a - b$, where a and b are defined as in Figure 2.2. Furthermore, the average radius R is defined as $R \approx \frac{1}{3}(a + 2b)$ [Boh73, p.47].

The deformed shape of the potential breaks the $2j+1$ degeneracy of the spherical shell model leaving only the degeneracy due to the spin s of the nucleons. Furthermore, the energy states are labelled by the quantum numbers $\Omega^\pi\,[Nn_z\Lambda]$. In the notation Ω and Λ are the projections of the nucleon's total and orbital angular momenta, respectively, to the symmetry axis as shown in Figure 2.3. N is the total number of oscillator quanta and n_z is the number of nodes in the oscillations perpendicular to the symmetry

[c] Parity π is a reflection symmetry quantum number of the system. A system can possess positive $\pi = +$ or negative $\pi = -$ parity.

[d] A sphere stretched from opposite ends like a cigar and a compressed sphere similar to a pancake describe prolate and oblate shapes, respectively.

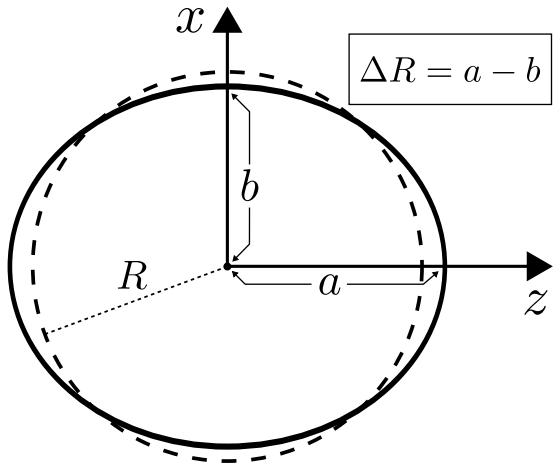

FIGURE 2.2: An ellipsoid (solid line) corresponding to a prolate deformation of $\beta_2 \approx {}^{\Delta R}/_{R} = 0.2$. The ellipsoid is compared with a circle (dashed line) of radius R having the same area as the ellipsoid. The deviation from the spherical symmetry ΔR is defined as $a - b$. The length of the ellipsoid is $2a$ along the z axis and $2b$ is the length along the x axis [Boh73, p.47].

axis [Mot59]. The total length of individual j projections on the nuclear symmetry axis (Ω_i), for a multi-particle state, is denoted as $K = \sum_i \Omega_i$. The splitting of the spherical shell model orbitals in the deformed potential is shown in the middle of Figure 2.1, where β_2 is increasing while moving to the right.

If the intrinsic motion of the individual nucleons can be separated from the collective motion of all the nucleons, the total angular momentum I consists of the angular momentum R of the rotating core and the angular momentum J of the independent nucleons. Then a fixed axially symmetric deformation of an even-even nucleus allows collective rotation perpendicular to the nuclear symmetry axis. The energy of the rotation for an even-even nucleus is then given as

$$E_{\text{rot}} = \frac{\hbar^2}{2\mathcal{J}} I(I+1), \quad I = 0, 2, 4, \ldots \tag{2.1}$$

where $\mathcal{J}$ is the moment of inertia of the nucleus and $K = 0$ [Boh53b, Boh53c, Boh53a]. The energy of the single-particle state determines the absolute position of the band head of the collective rotational structure. Experimentally Equation (2.1) is seen as a regular pattern of peaks in the measured radiation energy spectrum, where $\Delta E_{\text{rot}} = E_{\text{rot}}(I) - E_{\text{rot}}(I-2)$.

When rotational states in a deformed odd-A nucleus are considered, there are

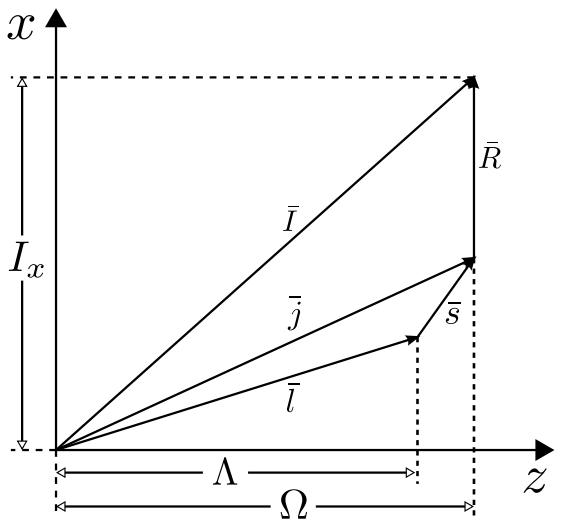

FIGURE 2.3: In the Nilsson model the projection of the orbital angular momentum $\bar{l}$ to the nuclear symmetry axis z is Λ. The projection of the particle's total angular momentum $\bar{j}$ to the symmetry axis is denoted by Ω. The total angular momentum $\bar{I}$ of the system is composed of $\bar{j}$ and the rotation of the core $\bar{R}$. The projection of $\bar{I}$ to the axis of rotation x is I_x.

different possibilities for the coupling between the rotating core and the odd nucleon. If the nucleus has a large deformation, the nucleon motion can be strongly coupled to the deformed core. In this strong-coupling model the projection of the nucleon's angular momentum to the symmetry axis (Ω) is a good quantum number [Boh51]. Equation (2.1) for the odd-A case in the strong-coupling limit is written as

$$E_{\text{rot}} = \frac{\hbar^2}{2\mathcal{J}}\left[I(I+1) - K(K+1)\right], \quad K \neq \frac{1}{2}, \quad I = 0, 1, 2, \ldots, \tag{2.2}$$

by taking into account the K value of the odd nucleon [Boh53a]. For $K = \frac{1}{2}$, the Coriolis force has a large effect on the rotational energy, which can be described by

$$E_{\text{rot}} = \frac{\hbar^2}{2\mathcal{J}}\left[I(I+1) + a\,(-1)^{I+\frac{1}{2}}\left(I+\frac{1}{2}\right)\delta_{K,\frac{1}{2}}\right], \quad K = \frac{1}{2}, \quad I = 0, 1, 2, \ldots, \tag{2.3}$$

where a is the decoupling parameter [Boh73, pp.31-34].

As the rotation of the core increases the influence of the Coriolis force becomes more significant. At high enough angular momentum it is to be expected that the coupling of the nucleon motion to the core rotation will overcome the tendency of the nucleons to align themselves along the axis of nuclear deformation. This rotation

coupling essentially decouples the motion of the nucleon from the core deformation, aligning the nucleon angular momentum along the rotational axis. Thus, the rotational spectrum in the decoupled limit should resemble the spectrum of the neighbouring even-A nucleus [Ste72, Ste75]. This decoupling can arise even in the low-I region when the Fermi surface[e] is near the low-Ω states of a given j orbital. Especially favourable candidates are orbitals originating from the spherical shell model intruder states, as the Coriolis energy can be estimated as

$$E_{\mathrm{Cor}}^{\max} \approx \frac{\hbar^2}{2\mathcal{J}}\ 2Ij, \tag{2.4}$$

where I is the total angular momentum of the system and j is the angular momentum of the nucleon [Ste75]. For example, the $i_{13/2}$ state has different parity and the highest j value compared to other states within the major shell that is located between magic numbers 50 and 82.

The deformed shell model has been successful in explaining the observed spins and parities in the regions where Z and N are in between magic numbers. If the deformation of the odd-A nucleus under study is known, the Nilsson model gives a prediction for the I^{π} of the ground state by the placement of the last nucleon onto an available single-particle orbital. On the other hand, the model of collective rotation explains the occurrence of rotational spectra whenever nuclei are deformed. Different coupling models can be used to gain information on nuclear deformation and single-particle orbitals involved.

In addition to the axially symmetric deformations, axially-asymmetric (triaxial) nuclear shapes are also possible. The magnitude of the axial asymmetry can be described by the γ-deformation parameter (see e.g. [Nil95, p.126]). When β_2 and γ parameters are used together for the description of a triaxial shape, β_2 can be taken to be a positive number. Then $\gamma = 0°$ and $\gamma = -60°$ describe prolate and oblate axially symmetric shapes, respectively, for collective rotations. Values of γ that are in between $0°$ and $-60°$, describe triaxial deformations [Nil95, p.126].

[e]The Fermi surface defines a boundary of occupied and unoccupied energy states of the system.

2.4 Cranking model

Equations (2.1) and (2.2) are good first approximations for deformed nuclei. However, when plotting the moment of inertia $\mathcal{J}$ against ω^2, a backbending of the moment-of-inertia curve was observed for certain nuclei [Joh71]. These pronounced effects in the moment of inertia have been attributed either to the breaking of a nucleon pair or a crossing of two rotational structures with different moments of inertia [Ste75].

A cranking-model description of the moment of inertia assumes an external rotation of the intrinsic coordinate system of the nucleons [Ing54]. The total Hamiltonian of a nucleus then has an additional term $-\hbar\omega I_x$, where ω is the fixed angular velocity of the deformed potential about the x axis[f] and I_x is the component of the total angular momentum operator along the x axis [Ing54, Ben79b]. Including also the pairing interaction, a good description of the experimentally observed moments of inertia can be obtained from the cranking model. The pairing interaction between nucleons was described by Belyaev using the independent quasi-particle formalism [Bel59], which has also been used in the cranked shell model of Bengtsson and Frauendorf [Ben79a, Ben79b, Ben86a]. The rotation of the deformed nuclear potential breaks the two-fold degeneracy of the orbitals and thus only parity π and signature[g] α are used for labelling the resulting states [Ben79b]. For nuclei with an odd particle number, α is either $+\frac{1}{2}$ or $-\frac{1}{2}$. The favoured signature of a j orbital is given by $\alpha_f = j$ mod 2. The right side of Figure 2.1 shows the breaking of the 2-fold degeneracy of the deformed nuclear potential as $\omega \neq 0$.

The idea of the Bengtsson and Frauendorf model is to take the measured transition energies $E(I)$ and transform them into the rotating system $E'(\omega)$. In addition, energy $e'(\omega)$ is defined as the energy with respect to a reference configuration $E'_r(\omega)$

$$e'(\omega) = E'(\omega) - E'_r(\omega). \tag{2.5}$$

The experimental rotational frequency is defined as

$$\omega(I) = \frac{E(I+1) - E(I-1)}{I_x(I+1) - I_x(I-1)}, \tag{2.6}$$

[f] The x axis is the axis of the rotation of the system, the symmetry axis of the system being the z axis.

[g] Signature α is a quantum number describing the rotation of the system about the x axis [Ben79b].

where I is the so called intermediate angular momentum between two excited states and I_x is the projection of I to the x-axis [Ben79b]. The projection I_x is given as

$$I_x = \sqrt{(I + 1/2)^2 - K^2}, \tag{2.7}$$

by the Pythagorean theorem and the energy in the rotating system, the Routhian, is [Ben79b]

$$E^{'}(I) = \frac{1}{2}\left[E(I+1) + E(I-1)\right] - \omega(I)I_x(I). \tag{2.8}$$

The experimental $E^{'}(I)$ values define a discrete set of points which are plotted with respect to the experimental rotational frequencies $\omega(I)$. Furthermore it is now possible to define aligned angular momentum $i(\omega)$

$$i(\omega) = I_x(\omega) - I_{xr}(\omega), \tag{2.9}$$

where I_{xr} is the angular momentum of the reference configuration [Ben79b]. According to this definition, changes in the rotational structure will be highlighted clearly whenever the I_{xr} configuration is different from the configuration crossing the reference configuration at given angular momentum.

The reference configuration describing the rotating core, can be taken to be for example the ground-state band of the neighbouring even-even nucleus. Due to the crossing of the reference band by the higher-lying band, the angular momentum I_x of the reference configuration is extrapolated using the Harris parametrization of the angular momentum [Har65]

$$I_{xr} = \omega\left(\mathcal{J}_0 + \mathcal{J}_1\omega^2\right). \tag{2.10}$$

Extrapolation of the reference energy is defined as [Ben79b]

$$E_r^{'} = -\frac{1}{2}\omega^2\mathcal{J}_0 - \frac{1}{4}\omega^4\mathcal{J}_1 + \frac{1}{8}\frac{\hbar^2}{\mathcal{J}_0}. \tag{2.11}$$

2.5 Nuclear decay

The decay of a nuclear state can be described by the radioactive-decay law, where the decay constant λ is defined by the rate of decay

$$\lambda = -\frac{1}{N}\frac{dN}{dt}, \tag{2.12}$$

where N is the number of nuclei in the decaying sample (see e.g. [Eva72, p.470–473]). By integration of Equation (2.12) the decay of the radioactive sample can be described as

$$N = N_0 e^{-\lambda t}, \tag{2.13}$$

where N_0 is the number of decaying nuclei at $t = 0$. Furthermore, the time when half of the nuclei in a given sample have decayed, is called the half-life

$$t_{\frac{1}{2}} = \frac{\ln 2}{\lambda}, \tag{2.14}$$

for the nuclei in the sample. If energetically possible, the nuclear decay is very likely to proceed via particle emission. Only if particle emission is hindered, for example due to a repulsive barrier, or when there is not enough energy available, is electromagnetic (EM) radiation able to compete with particle emission. The probability of the transition depends on the energy available for the decay, the conservation of angular momentum, parity and charge [Eva72, Bla60]. When the half-life of a state is long compared with the half-lives of other excited states in a nucleus, it is called an isomeric state.

2.6 Electromagnetic transitions and internal conversion

Electromagnetic radiation can be classified by angular momentum, carried by the emitted photons (l_γ) and the z-component of the angular momentum (m_γ). For photons l_γ is always greater than zero. The type of radiation can be either electric or magnetic for each value of l_γ, and the parity of the radiation with l_γ is obtained by [Bla60]

$$\begin{aligned} \text{electric:} \quad & \pi_\gamma = (-1)^{l_\gamma}, \\ \text{magnetic:} \quad & \pi_\gamma = -(-1)^{l_\gamma}. \end{aligned} \tag{2.15}$$

Conservation of the total angular momentum in a transition between states I_i^π and I_f^π restricts l_γ to values

$$|I_i - I_f| \leq l_\gamma \leq I_i + I_f. \tag{2.16}$$

Often $l_\gamma = |I_i - I_f|$, due to the fact that the γ-ray emission probability is proportional to $(R/\lambda\!\!\!^{-})^{2l_\gamma}$ [Eva72, Bla60]. Considering a γ-ray energy of 1 MeV $\left(\lambda\!\!\!^{-} \approx 10^{-12}\text{ m}\right)$ and $R \approx 10^{-14}$ m, it becomes apparent that the probability of EM radiation decreases rapidly as l_γ increases. If there is a change in parity between the initial and final

states, l_γ is odd (even) for electric (magnetic) transitions, as parity is conserved in the process. When the parity is unchanged, l_γ is even (odd) for electric (magnetic) transitions. For the same multipole order, a magnetic transition compared with an electric transition is slower by a factor $\frac{v}{c}$ [Bla60, p.623], where v is the velocity of the nucleons. Thus, only if the electric transition for a given l_γ is forbidden by parity conservation, is a magnetic transition of the same multipole order expected to compete with an electric transition. Transitions from a state based on a high-j unique-parity orbital are often hindered, as they not only include a change in parity, but also may involve a large change in angular momenta between the initial and final states.

Useful estimates for the transition probabilities T of the EM transitions can be obtained assuming that the emitted radiation to is due to a transition of a single proton in the nucleus [Wei51]. These Weisskopf estimates can be used to normalize the experimental transition probabilities ($T^{\text{exp}} = \ln 2 \;/\; t_{\frac{1}{2}}^{\text{exp}}$), to give a reduced transition probability

$$B(\sigma l) = T^{\text{exp}}/T^{\text{W}}, \tag{2.17}$$

where σ distinguishes between electric (E) and magnetic (M) transitions, and T^{W} is the Weisskopf estimate for the transition probability. These estimates are to be taken as order of magnitude estimates for the transition rates [Wei51]. If $B(\sigma l) \gg 1$ the transition cannot be solely due to a single proton, hence a collective behaviour can be assumed.

Alternatively to photon emission the excitation energy can also be transferred to a bound electron of the atom. The electron in this internal conversion process is then ejected from the atom with an energy

$$E_c = (E_i - E_f) - B = E_\gamma - B, \tag{2.18}$$

where B is the binding energy of the electron, and E_i and E_f are the excitation energies of the initial and final states, respectively. The total decay constant of Equation (2.12) is the sum of the partial decay constants: $\lambda = \lambda_\gamma + \lambda_c$. The ratio of these partial decay constants is the total conversion coefficient $\alpha = \lambda_c/\lambda_\gamma$. Furthermore, α is the sum of all partial conversion coefficients α_K,α_L,α_M... [Eva72]. The letters K, L, M,... correspond to the atomic electron orbitals, starting with the orbital having the lowest energy.

2.7 Alpha decay

In α decay an α particle (a ${}^4_2$He nucleus) is emitted from the mother nucleus $\left({}^A_Z X_N\right)$. The resulting daughter nucleus can be denoted as ${}^{A-4}_{Z-2}X'_{N-2}$. An α particle has zero intrinsic angular momentum and $\pi_\alpha = +$. The conservation of the total angular momentum demands that

$$|I_i - I_f| \leq l_\alpha \leq I_i + I_f, \tag{2.19}$$

where l_α is the angular momentum carried away by the α particle. Only even l_α are allowed when there is no change in parity between I_i^π and I_f^π. If $\pi_i \neq \pi_f$, only odd values of l_α are possible, due to parity conservation.

In addition to angular momentum and parity, the α particle has an electric charge, $q_\alpha = 2e$. Consequently an α particle experiences a Coulomb potential barrier due to the electric charge $q = (Z-2)e$ of the daughter nucleus. According to classical physics an α particle, confined within a potential, would never be able to penetrate this potential barrier. The quantum-mechanical tunnelling through the Coulomb potential was originally considered by Gamow [Gam28] and separately by Gurney and Condon [Gur28].

The decay constant λ in α decay can be defined as

$$\lambda = fP, \tag{2.20}$$

where f is the collision rate of the α particle with the barrier [Per57]. P denotes the barrier-penetration factor, which can be evaluated as

$$P \approx \exp\left[-2\int_{R_i}^{R_o} \frac{\sqrt{2M}}{\hbar}\sqrt{V(r) + \frac{Z_1 Z_2 e^2}{r} + \frac{\hbar^2}{2mr^2}l_\alpha(l_\alpha+1) - E}\; dr\right], \tag{2.21}$$

where M is the reduced mass[h]. Proton numbers of the α particle and the daughter nucleus are Z_1 and Z_2, respectively. The energy E of an α particle in Equation 2.21 takes into account the decrease of the observed α-particle energy due to electron screening. The nuclear potential $V(r)$ and the Coulomb and centrifugal terms form the total potential experienced by the α particle. The integral is evaluated numerically within the classical inner and outer turning radii R_i and R_o of the α particle, respectively [Ras59a]. The energy E available for the α particle inside the nucleus depends on the difference of the masses of the initial and final systems. This energy difference is also called the

[h]The reduced mass is $m_\alpha m_{X'} / \left(m_\alpha + m_{X'}\right)$.

Q value of the decay, defined as

$$Q = (m_X - m_{X'} - m_\alpha)c^2, \tag{2.22}$$

where m_X, $m_{X'}$ and m_α are the atomic masses of mother and daughter nuclei and the α particle, respectively.

To compare different measured decay rates, λ, it is usual to define the reduced width, δ^2, by [Per57]

$$\delta^2 \approx hf = \frac{h\lambda}{P}, \tag{2.23}$$

where the rates are scaled by the barrier-penetration factor P. Decay rates in α decay can be compared using the reduced hindrance factors F. The reference value for the decay rate is taken to be the ground-state to ground-state α decay of an even-even nucleus [Ras59a, Ras59b]. For an even-even nucleus F can be defined as [Ras59a]

$$F = \frac{\delta^2_{\text{gs}}}{\delta^2}, \tag{2.24}$$

where δ^2_{gs} is the reduced width of the ground-state to ground-state α decay. For an odd-A nucleus an average value of nearest even-even isotopes is used as a reference. The hindrance factor can then be described as [Ras59b]

$$F = \frac{\delta^2_1 + \delta^2_2}{2\delta^2_{\text{odd}}}, \tag{2.25}$$

where δ^2_1 and δ^2_2 are the reduced widths of the $(A-1)$ and $(A+1)$ isotopes, respectively. Reduced hindrance-factor values less than 4 (favoured decay) are usually taken to represent α decays between initial and final states of similar configurations. Values larger than four are associated with unfavoured α decays.

2.8 Systematics of platinum isotopes

An appreciable amount of research has been carried out on the excited states of neutron-deficient platinum isotopes. In the odd-A Pt isotopes between $A = 187 - 194$, the observed decoupled bands can be explained by assuming an oblate deformation. For oblate deformation, the Fermi surface for these nuclei is close to the low-Ω Nilsson orbitals of $\nu i_{13/2}$ origin [Pii75]. For even-A $^{182-186}$Pt isotopes, a prolate ground-state

deformation was suggested [Bur67, Bes76]. The perturbed low-I structures of ^{176,178}Pt were assumed to be due to shape-coexistence [Dra86, Ben86b, Ben87, Ced90]. Most recently, the results reported for the very-neutron deficient Pt isotopes of $A = 167-172$ reveal a change towards a vibrational character of the low-lying excited states [Ced98, Jos05, GH09].

Comparing the excited states of the odd and even-mass Pt isotopes provides an insight in to the coupling of the odd neutron to the even-A Pt core. The systematics of yrast states of $A = 168 - 194$ Pt isotopes is shown in Figure 2.4. Around the neutron mid shell ($N = 104$) the addition an odd neutron has an effect on the excitation energy, when compared with the even-A isotopes. This is a consequence of the deformation of Pt nuclei around $N = 104$, thus making it possible for the odd neutron to be strongly coupled to the deformed core. However, the odd-even staggering of the excitation energy presented in Figure 2.4, can also be attributed to a difference in deformation between the odd-A and even-A nuclei. When moving away from the neutron mid shell, the odd neutron is seen to become decoupled from the deformed core. This is seen in Figure 2.4 as the odd-A Pt isotopes' excitation energies become similar to the excitation energies observed in the even-A Pt isotopes (moving to the left from $N = 97$ and to the right from $N = 109$).

A more direct observation of the ground-state properties of nuclei is provided by laser spectroscopy. Results for the $^{183-198}$Pt [Hil92] and $^{178-183}$Pt isotopes [Le Blanc99] agree with the assumptions made about the ground-state deformations based on γ-ray spectroscopy. The results from laser spectroscopy highlight the general trend of increasing prolate deformation below $A = 188$. Information on the deformation of low-lying configurations can also be obtained through lifetime measurements. The $B(E2)$ values reported for the low-lying states in even-A $^{176,180-186}$Pt isotopes are all significantly larger than the corresponding single-particle estimates [Dra86, Gar86, Wil06, Wal12, Gla12]. These values signify the collective character of the observed rotational structures. For these nuclei, the $B\left(E2, 4^+ \rightarrow 2^+\right)$ values were observed to increase significantly, compared with the $B\left(E2, 2^+ \rightarrow 0^+\right)$ values. This increase was interpreted as a sign of configuration mixing due to coexisting deformed configurations. For ^{175}Pt, the $B\left(E2, {}^{17}/_{2}^{+} \rightarrow {}^{13}/_{2}^{+}\right)$ and $B\left(E2, {}^{21}/_{2}^{+} \rightarrow {}^{17}/_{2}^{+}\right)$ values of 88.5(5) W.u. and 290(5) W.u., respectively, were reported [Wat11]. A change in the deformation in ^{175}Pt was assumed to take place in the rotational band that is based on the $i_{13/2}$ configuration by Watkins [Wat11].

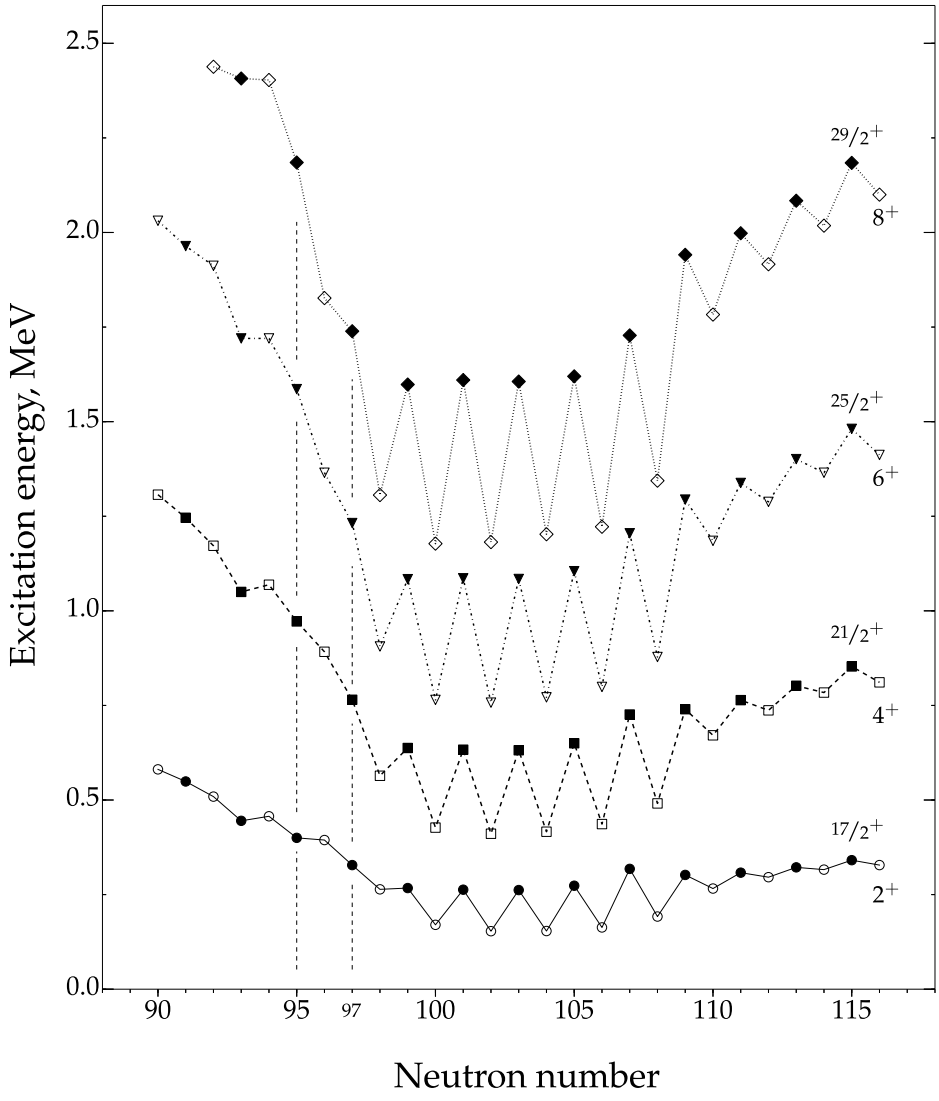

FIGURE 2.4: Systematics of yrast states in $A = 168 - 194$ Pt isotopes as a function of the neutron number N. The even-A isotopes (open symbols) are plotted with respect to the 0^+ ground state. Positive-signature states of odd-A isotopes (filled symbols) are plotted taking the $^{13}/_2{}^+$ state as a reference. Vertical dashed lines highlight $N = 95, 97$ of ^{173,175}Pt, respectively. Around the neutron mid shell ($N = 104$) the excitation energies of these yrast states have a pronounced staggering between the odd-A and even-A nuclei. When moving away from the neutron mid shell, the motion of the odd neutron is seen to become weakly coupled to the core deformation. This is seen from the similarity of the excitation energy between even and odd-A Pt isotopes at $N \leq 97$ and $N \geq 109$. Data are taken from [Pii75, Jan88, Bes76, Nyb90, Bur67, De Voigt90, Bag09, Dra86, Dra90, Dra91, Ced98, Jos05, GH09].

Chapter 3

Experimental techniques

3.1 Production of ^{173,175}Pt nuclei

All experiments of the present work were performed at the Accelerator Laboratory of the Department of Physics, University of Jyväskylä (JYFL). Both ^{173}Pt and ^{175}Pt nuclei were produced in fusion-evaporation reactions induced by heavy-ion beams. Here, the fusion of two stable nuclei was accomplished by producing an ion beam from a chosen isotope. The ion beams were provided by an electron-cyclotron resonance (ECR) type ion source. This ion beam was then accelerated, using the K130 cyclotron, to an energy required for a fusion-evaporation reaction to occur. After the cyclotron, the ions were guided into the RITU cave, where the beam impinged on a thin target. Table 3.1 lists the reactions, beam energies, target thicknesses and beam intensities used in the experiments. In addition, the estimated cross section (σ) for each reaction is given in Table 3.1.

The kinetic energy needed for the fusion of a beam particle with a target nucleus to be possible is determined by the repulsive Coulomb force between the two nuclei. Additionally, the reaction Q value effects the excitation energy of the fused system. For the reactions used in the present work, the Q values are negative. In the fusion process the nuclei are assumed to form a semi-stable compound nucleus with no memory of its past state [Boh36]. The compound nucleus is in a highly excited state and it decays mainly via particle emission within $\left(10^{-19} - 10^{-16}\right)$ s [Frö96]. After particle emission the excitation energy of the system is released by the emission of statistical γ rays – mainly of dipole character. Finally, the excitation energy of the residual nucleus reaches

TABLE 3.1: The isotopes of the target and beam materials used in the experiments are listed together with the particle-evaporation channels leading to ^{173,175}Pt. The beam energy E_b^{lab}, target thickness d, average beam intensity I_b^{avg}, beam on target time and the estimated cross section (σ) for the corresponding reaction channels are also provided. All the Mo targets used were self supporting and their isotopic enrichment was more than 97 %. The targets were combined together with a (40–50)-μg/cm^2 carbon reset foil, which was placed downstream from the target.

Reaction	E_b^{lab}, MeV	d, mg/cm^2	I_b^{avg}, particle-nA (pnA)	Beam time, h	σ, 10^{-27} cm^2 (mbarn)
$^{92}\mathrm{Mo}(^{86}\mathrm{Sr}, 2pn)^{175}\mathrm{Pt}$	403	0.60	8	168	4
$^{92}\mathrm{Mo}(^{84}\mathrm{Sr}, 2pn)^{173}\mathrm{Pt}$	392	0.60	6	140	0.3
	400	0.60	6	145	0.3
$^{92}\mathrm{Mo}(^{84}\mathrm{Kr}, 3n)^{173}\mathrm{Pt}$	362	0.55	4	36	0.5

the yrast line, from where it decays towards the ground state. Typically half-lives of the states in the yrast cascade are in the picosecond range [Ste72]. An important aspect of heavy-ion induced fusion reactions is the possibility to transfer a large amount of angular momentum, $\bar{l} = \bar{r} \times \bar{p}$, to the compound system. The emitted particles and statistical γ rays carry mainly excitation energy away from the compound system, hence the yrast levels can be populated in this way at high angular momentum [Ste72].

3.2 The JUROGAM I and II Ge-detector arrays

The residual nuclei following the reactions given in Table 3.1 still have high velocities $\left(\frac{v}{c} \approx 4\ \%\right)$ after penetrating the remaining part of the thin target material. However, due to the short half-lives of the excited states, the γ rays are typically emitted within a 1 mm distance from the point of the fusion reaction. For this reason, information about the excited states can be gained by observing γ rays emitted by the reaction products at the target position. The residual nucleus formed in the fusion-evaporation reaction is called hereafter a recoil.

The measured γ-ray energies need to be corrected for the Doppler shift. The Doppler-shifted γ-ray energy $E_\gamma^{'}$ is

$$E_\gamma^{'} = E_\gamma \left(1 + \frac{v}{c}\cos\theta\right), \tag{3.1}$$

where E_γ is the unshifted energy, v is the velocity of the recoils and the angle of emission θ is measured with respect to the beam direction. The angle θ is rather well defined for the γ rays emitted by the recoils, since for the reactions used, the recoil distribution is forward focused.

Good energy resolution is generally required to separate the observed γ-ray energies. Also, as many of the emitted photons as possible should be absorbed by the detector material, for high detection efficiency. The interaction of the electromagnetic radiation with matter is a statistical process, showing an exponential decay of the original intensity when passing through matter [Eva72]. The main interaction processes with matter, considering the X-ray and γ-ray energies of this work, are the photoelectric effect, Compton scattering and pair production. In pair production a high energy[a] photon is absorbed and an electron-positron pair is created. Also in the photoelectric effect the total photon energy in absorbed, now by an atomic electron. This electron is then ejected from the atom. In the Compton-scattering process, the photon scatters from a nearly free atomic electron. The outcome of the scattering is a photon of lower energy and a scattered electron.

Currently the best compromise in detection efficiency and energy resolution, for the detection of γ rays, is achieved by the use of high-purity germanium (HPGe) detectors. Although the proton number of Ge is low ($Z = 32$), making the photoelectric absorption probability small, the excellent energy resolution compensates for this shortcoming. In the JUROGAM I array 43 GASP [Ros93] and EUROGAM Phase 1 [Bea92] type HPGe detectors were placed into 6 rings around the target position. Additionally the Ge detectors were surrounded by anti-Compton bismuth germanate (BGO) shields. Vetoing events that are simultaneous in the Ge and scintillator detectors improves the peak-to-background ratio of the measured γ-ray energy spectra.

Before the ^{173}Pt experiment, the JUROGAM I array was replaced by the JUROGAM II array consisting of 15 GASP and Phase 1 type Ge detectors together with 24 clover-type [Duc99] Ge detectors. The detectors in JUROGAM II form 4 rings surrounding the target position. Each of the clover detectors houses four separate Ge crystals. Signals from each crystal can be added-back to reconstruct the scattered events between the crystals of a single detector. With the add-back method high photon-detection efficiencies can be achieved [Duc99]. Unfortunately ring 1 of JUROGAM II,

[a] $E_\gamma \geq 2m_e c^2 = 1.022$ MeV

which holds 5 Ge detectors at an angle $\theta = 157.6^o$, was not in place in the ^{173}Pt experiment. Additionally, one clover detector was not used in the ^{173}Pt experiment because of inferior energy resolution.

The Ge detectors were energy and efficiency calibrated using ^{133}Ba and ^{152}Eu radiation sources [Fir96]. The absolute γ-ray detection efficiencies, $\epsilon_{\rm abs}$, extracted for the 1.33-MeV γ-ray energy using a ^{60}Co radiation source, were 4.2 % and 3.9 %, for JUROGAM I and II, respectively.

Angular distributions of the EM radiation can be measured after the heavy-ion fusion reactions due to the well-defined beam direction and the large angular momentum of the recoils [Dia66, New67]. From the angular distributions it is possible to determine the multipole order of EM radiation [Bla60, p.594]. The angular distributions were fitted as [New67]

$$W(\theta) = A_0 + A_2 P_2(\cos\theta) + A_4 P_4(\cos\theta), \tag{3.2}$$

where $P_2(\cos\theta) = \cos\theta$ and $P_4(\cos\theta) = \frac{1}{2}\left(\cos^2\theta - 1\right)$ are the Legendre polynomials [Boa83, p.487,766]. Stretched $\Delta I = 2$ transitions have positive values for A_2/A_0, whereas a negative value suggests a pure stretched $\Delta I = 1$ transition [Dia66]. For weaker prompt transitions at higher I, only the ratio of the anisotropy could be extracted from the data for ^{175}Pt, defined as

$$R_{\rm J1} = \frac{I_\gamma(157.60^\circ)}{I_\gamma(94.16^\circ) + I_\gamma(85.84^\circ)}, \tag{3.3}$$

where I_γ is the efficiency-corrected γ-ray intensity measured at a given angle. The notation $R_{\rm J1}$ refers to the JUROGAM I array.

Analysis of the extracted $\gamma\gamma$-matrix and $\gamma\gamma\gamma$-cube data was performed using the programs ESCL8R and LEVIT8R, respectively, from the Radware software package [Rad95a, Rad95b]. The time-coincidence condition was set to 100 ns between γ-ray events accepted into a matrix or cube.

3.3 The RITU separator

Both Ge-detector arrays were used in conjunction with the gas-filled recoil separator RITU [Lei95], which is located downstream from the target position. The RITU separator consists of a quadrupole, a dipole and two further quadrupole magnets. The first quadrupole focuses the recoils vertically for better acceptance of the recoils into the

dipole chamber [Lei95]. The magnetic field B of the dipole bends particles according to their average magnetic rigidity, which for a gas-filled separator is independent of the initial charge states and velocities of the particles [Lei95]. As the beam ions have a smaller magnetic rigidity compared with the recoils, separation of beam from the recoils is accomplished in the dipole field. During operation RITU was filled with helium gas at about 1 mbar pressure. Recoils colliding with the He atoms attain a well-defined average charge state, which leads to a smaller recoil image size at the focal plane of RITU. Thus, the recoil transmission of the separator is increased [Lei97].

3.4 The GREAT spectrometer

At the focal plane of RITU is the Gamma Recoil Electron Alpha Tagging (GREAT) spectrometer [Pag03]. As recoils leave RITU, they fly through an isobutane-filled multi-wire proportional counter (MWPC) where the energy-loss and time of the recoils are recorded. Downstream from the MWPC, recoils are implanted into a double-sided silicon strip detector (DSSD). There are two adjacent DSSDs consisting of 1 mm strips, each detector forming an active area of (60×40) mm^2 [Pag03]. Combined, the 60 vertical strips and the 40 horizontal strips in each detector define a total of 4800 pixels. The time and energy signals from the DSSD strips are recorded for the recoil-hit events. Possible subsequent radioactive decays (e.g. α and β decays) after a recoil implantation can also be detected by the DSSDs. The probability of the α particle escaping the DSSD is estimated in this work to be 50 %, based on the geometry of the implantation. The implantation depth of the recoils is $\sim (1-10)$ μm [Pag03], giving the α particle a high probability of escape into the upstream direction. The DSSDs used in the experiments were 300-μm thick.

Upstream from the DSSDs are 28 Si PIN-type detectors (PINs) for the detection of escaping α particles or conversion electrons. The 500-μm thick detectors form a box around the DSSDs as shown in Figure 3.1. Downstream behind the DSSDs is a double-sided planar-Ge detector for γ and X-ray detection. The planar-Ge detector is segmented with 24 vertical strips facing the DSSDs and 12 horizontal strips on the rear face of the detector. The segmentation makes it possible to perform $\gamma\gamma$-coincidence analysis using only the planar detector. Facing the DSSDs is a 500-μm thick beryllium window of the planar detector, allowing low-energy γ rays to pass through with minimum attenuation. Directly above the DSSDs, outside the vacuum

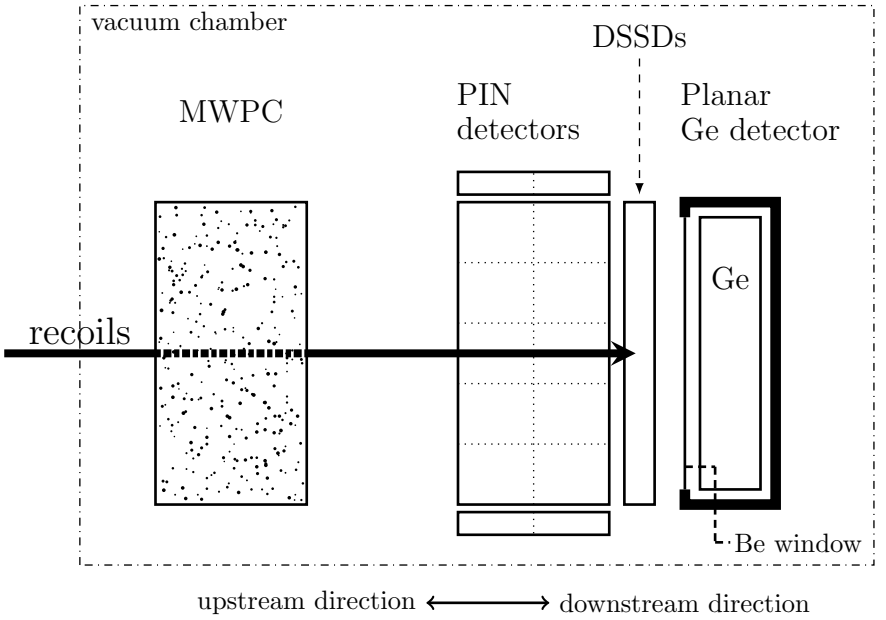

FIGURE 3.1: A schematic top-view diagram of recoils entering the GREAT spectrometer downstream from the RITU separator. The recoils leave energy in the MWPC after which they are implanted into the DSSD. Subsequent decays of the recoils are detected by the DSSD, PIN, planar and clover detectors, depending on the type of emitted radiation. The GREAT clover-Ge detector is located outside the vacuum chamber directly above the DSSDs. See Section 3.4 for a more detailed description.

chamber, is a segmented clover-Ge detector with a BGO-suppression shield, for high-energy γ-ray detection [Pag03]. Relative positions of the GREAT detectors are shown in Figure 3.1.

The calibration of the GREAT DSSD strips was first performed using ^{239}Pu, ^{241}Am and ^{244}Cm α-decay sources. Furthermore, the DSSD strips were calibrated off line using known α-particle energies emitted by the recoils produced in the reactions used. In the off-line calibration the α decay occurs within the active detector material and the recoil energy of the daughter nucleus is also accounted for. The planar and clover-Ge detectors were calibrated using the known γ-ray energies from ^{133}Ba and ^{152}Eu calibration sources [Fir96]. The calibration of the PIN diodes was performed by using conversion electrons from an open ^{133}Ba source [Fir96]. The efficiencies of the Ge detectors and the PIN diodes were based on the results of a Monte-Carlo simulation [And04], as the available point-like radiation source does not represent the distribution of the implanted recoils in the DSSD.

3.5 Data acquisition

Collecting and storing the data from all the channels for every registered event in the JUROGAM–GREAT setup is a major undertaking. The data acquisition (DAQ) system would commonly be setup with adjustable time-delay and time-coincidence condition units. In this way the well-defined flight time of the recoils through RITU into the DSSDs can be accounted for. Similarly, for the observation of decay events after the recoil implantation, coincidence-time units would be needed. A common trigger condition for all the DAQ channels introduces a collective dead time for all the data channels in the system. The total data readout (TDR) method, used in the present work, eliminates the need for a common dead-time condition by recording all data from all individual channels at an accuracy of 10 ns [Laz01]. This accuracy is achieved using a 100-MHz metronome. What remains are the dead times of the single channel analog-to-digital converters (ADC). The single-channel data were time ordered on line into a single data stream, first by collate units and finally by the merge PC. Before writing the data to storage, a software prefiltering was applied taking a 5-μs slice of the data from all channels preceding any focal-plane event.

For the JUROGAM array an upgrade of the signal-processing chain was carried out when the JUROGAM II array was built. The analogue signal-processing units for the energy and time signals were replaced by digital Lyrtech-ADC cards. Each Lyrtech unit has 16 input channels and the detector preamplifier signals are digitized by 100-MHz flash ADCs. The preamplifier signal shaping in the Lyrtech ADCs results in a trapezoidal signal for the amplitude measurement. The flat top of the trapezoidal-shaped signal is more tolerant, than a Gaussian shape, against the preamplifier signal rise-time fluctuations. These fluctuations arise due to the large Ge-crystal size [Rad72]. The signal-shaping times used in the Lyrtech ADCs reduce the single-detector dead time for JUROGAM II on average by 40 %, compared with the semi-Gaussian shaping used for JUROGAM I.

3.6 Recoil-decay tagging method

The coupled system of JUROGAM, RITU and GREAT allows the collection of prompt target-position events and delayed events[b] observed at the RITU focal plane. As all observed focal-plane events are stored together with selected prompt JUROGAM data, the data can be sorted later by demanding an observation of certain logical chains of events. In the recoil-decay tagging (RDT) method [Sch86, Sim86] a chain of prompt-recoil-α events is searched for from the data. The recoil at the focal plane is selected by its energy loss in the MWPC and the flight time between the MWPC and the DSSD pixel. An α-decay event is searched for in the same DSSD pixel after the recoil has been selected. The search-time for an α-decay event was set to be $3 \times t_{\frac{1}{2}}$, where $t_{\frac{1}{2}}$ is the half-life of the state in question. This search-time is defined separately for each different decay branch that is being searched for. With this condition the probability of not observing the α decay due to a finite search time is less than 13 %. In addition, there should not be a simultaneous MWPC event observed, if the recoil is observed to α decay inside the DSSD. If a correlated pair of recoil-hit and α-decay events is found, then the prompt γ rays, time correlated with the recoil-implantation events, can be selected from the data. Naturally the logic presented here can also be modified. For example, it is possible to correlate the recoils with γ rays originating from a decay of an isomeric state and detected by the planar-Ge or clover detector. If the condition of a correlated recoil-alpha event pair is removed, recoil-gated (RG) prompt γ rays can be selected by the recoil–prompt-γ time-coincidence condition. The recoil time-of-flight, from the target position to the focal plane of RITU, determines the delay between the prompt γ-ray events and the subsequent recoil-implantation event. For the ^{173}Pt and ^{175}Pt experiments time-of-flight values of $\approx$ 0.3 μs and 0.4 μs were measured, respectively. Sorting the data for the RG, RDT and decay spectroscopy methods was performed using the Grain software package [Rah08].

[b] A delayed event is a detected event delayed with respect to the formation of the recoil at the target position. The word *event* includes the observation of both the time and energy of a decay or implantation event.

3.7 Decay spectroscopy

In addition to the RDT method, decay spectroscopy was performed for the α decays of ^{173,175}Pt. The α-particle energies were determined for α decays in correlated recoil-alpha chains. The search-time for an α-decay event was set to $3 \times t_{\frac{1}{2}}$. If the α-particle energy was known, the time-differences between a recoil-implantation event and an α-decay event could be measured. Only those α-event candidates that passed the defined α-particle energy condition, were accepted for the time-difference measurement. The maximum allowed time between a recoil event and an α-decay event during the half-life measurement was 80 s. When waiting for a new event it is possible that a random event, resembling the recoil-implantation event or the decay-of-interest, is observed. These random coincidences can be seen in the time-difference plots as a second exponentially decaying component. The event rate in an experiment should be chosen in such a way that the probability of a random correlation is not too high (see also Section 4.1). The α-decay half-lives were extracted from two-component fits using the method proposed by Karl-Heinz Schmidt *et al.* [Sch84].

Fine-structure α decay[c] and the possible subsequent decay of an excited state were also investigated. In addition to the correlated recoil-α pair, a 150-ns time condition was demanded between the observed α decay and the detection of radiation in either the focal-plane Ge detectors or the PIN-diode detectors. This 150-ns time condition was applied in software during the off-line analysis.

[c]The term α-decay fine structure is often used to describe α decay from a single initial state to different final states of the daughter nucleus.

Chapter 4

Results

4.1 Event-rate considerations for RDT

In this section the average event rates for the reactions of Table 3.1 are considered. For this discussion an event is defined as any signal[a] spatially and temporally correlated in a certain pixel of the DSSDs. If the average event frequency in an RDT experiment is high, compared with λ of the nucleus of interest, the probability of correlating a recoil-implantation event with the subsequent correct α-decay event is low.

For the reactions employing ^{84}Sr and ^{84}Kr beams, for the production of ^{173}Pt, the average event rates (f_{avg}) per pixel were 0.3 Hz and 0.6 Hz, respectively. On the other hand, an average event rate defines an average time $T = f_{\text{avg}}^{-1}$ between two consecutive events in a DSSD pixel. The probability P of observing an α-decay event after the recoil-implantation within time T is

$$P = \left[1 - \exp\left(-\frac{\ln(2)}{t_{\frac{1}{2}}}\ T\right)\right] * 100\%. \tag{4.1}$$

As the half-life of ^{173}Pt is 382(2) ms [Bag08], estimates for the α-decay probabilities within time T can be determined. Probabilities 99.8 % and 95.1 % for the ^{84}Sr and ^{84}Kr beam parts of the experiment, respectively, are obtained. Only the Sr-beam reaction data were used for the isomeric-state and α-decay measurements. For the prompt γ-ray spectroscopy, data from both reactions were combined for the analysis to maximize the number of observed γ-ray events.

[a] For example a recoil-implantation event, an α-decay event or a β-decay event.

In the ^{175}Pt experiment the average event-rate per pixel was 0.5 Hz. This event rate was chosen for the production of ^{175}Hg ($t_{\frac{1}{2}} \approx 11$ ms) [O'D09]. Using the known ^{175}Pt half-life of 2.53(6) s [Bas04] a value of $P = 42$ % was obtained, which is not an optimal value for ^{175}Pt recoil-α correlations. However, the peripheral y strips of the DSSDs had noticeably lower event rates compared with the y strips in the middle of the DSSDs. These y strips were selected in software and used for the recoil-α correlations in the present work. This technique was first reported by Joss *et al.* for the study of ^{167,168}Os [Jos01]. The distribution of events as a function of the y-strip number is shown in Figure 4.1 together with the excluded region. The average event-rate per pixel, using only the outer y strips defined in Figure 4.1, was 0.13 Hz, yielding $P = 88$ %. The half-lives from the ^{175}Pt experiment data, reported in the present work, were obtained using only the peripheral y strips for recoil-α correlations. All y strips were used for the RG and RDT in-beam γ-ray spectroscopy with the JUROGAM I array.

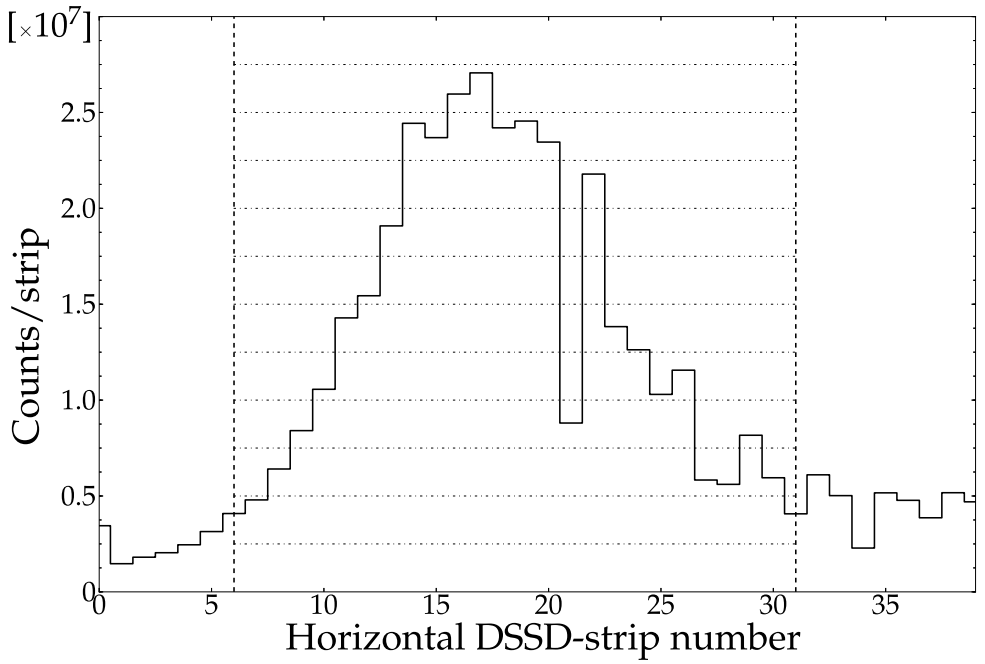

FIGURE 4.1: The histogram represents the distribution of events with respect to the horizontal y strips of the DSSDs from the ^{175}Pt experiment. The peripheral y strips outside the hashed-out area, that is marked by the horizontal dot-dash lines, were used for recoil-α correlations where indicated in the text. The figure is from [Peu14].

4.2 Previous experimental studies on ^{173,175}Pt

Alpha-particle energies of ^{173}Pt and ^{175}Pt α decays were reported, for the first time, by Siivola to be $E_\alpha = 6.19(2)$ MeV and 5.95(1) MeV, respectively [Sii66]. Siivola reported also a half-life of 2.1(2) s for the ^{175}Pt α decay. These E_α values were later confirmed by Gauvin *et al.* [Gau73], who also reported a value of $t_{\frac{1}{2}}\left(^{175}\mathrm{Pt}\right) = 2.52(8)$ s. For ^{175}Pt Hansen *et al.* reported the total ^{175}Pt α-branching ratio B_α to be 75(15) % [Han71]. The total α-branching ratios $B_\alpha = 84(6)$ % and $B_\alpha = 64.5(52)$ % were reported in 1979 by Hagberg *et al.* for ^{173}Pt and ^{175}Pt, respectively [Hag79]. All these B_α values were obtained from the ratio of the parent (Hg) and daughter (Pt) intensities in a singles α-particle-energy spectrum [Han71, Hag79].

The ^{173}Pt half-life was reported first by Della Negra *et al.* to be 325(20) ms [Della Negra81]. A year later Enge *et al.* reported the value $t_{\frac{1}{2}} = 360(20)$ ms for ^{173}Pt [Eng82]. The ^{173}Pt α-decay properties have more recently been reported by Page *et al.* [Pag96], Rowe *et al.* [Row02] and Goon [Goo04a]. Weighted averages of the reported values are: $t_{\frac{1}{2}} = 382(2)$ ms, $E_\alpha = 6211(6)$ keV and $B_\alpha = 86(4)$ % [Bag08]. Goon also reported fine-structure α decays with $E_\alpha = 6067$ keV, 6100 keV and 6133 keV[b]. The $E_\alpha = 6067$-keV and 6100-keV α-decay branches were presented to be in coincidence with subsequent $E_\gamma = 171.2$-keV and 136.2-keV transitions, respectively [Goo04a]. The observation of excited states in ^{173}Pt was reported for the first time by Joss *et al.* in an RDT study [Jos05, Jos06]. The observed yrast states were assigned to be based on an $I^\pi = (13/2^+)$ band head. The band structure feeding the band head was observed up to $I^\pi = (41/2^+)$ [Jos05, Jos06].

The observation of α-decay fine structure in ^{175}Pt was reported, for the first time, by Hagberg *et al.* [Hag79]. They reported the observation of α-particle energies of 5831(10) keV ($b_\alpha = 4.7(10)$ %), 5964(5) keV ($b_\alpha = 55(5)$ %) and 6038(10) keV ($b_\alpha = 4.8(8)$ %). The partial α-decay branching ratios b_α were given, normalized to the decay of the ^{175}Pt ground state[c]. The $E_\alpha = 5964$ keV α-decay branch was observed in coincidence with a γ-ray transition of $E_\gamma = 76.4(10)$ keV. Transitions with $E_\gamma = 134.4(10)$ keV and 211.8(10) keV were furthermore observed in coincidence with an α-decay branch of $E_\alpha = 5831$ keV. Reports on α-particle energies and branching ratios for ^{175}Pt were also published by Keller *et al.* [Kel86] and Page *et al.* [Pag96].

[b] $E_\alpha = 6133$ keV α-decay branch was reported as a tentative assignment [Goo04a].

[c] The percentages of individual α-decay branches from a state (b_α^i) sum up to the total α-decay branch ($B_\alpha = \sum_i b_\alpha^i$) of the state.

Excited states in ^{175}Pt were reported, for the first time, by Cederwall *et al.* [Ced90] in a $\gamma\gamma$-coincidence analysis combining a recoil separator and a Ge detector array. Band structures feeding an $I^{\pi} = (13/2^{+})$ band head were reported up to $I^{\pi} = (45/2^{+})$ by Cederwall *et al.*.

4.3 ^{173}Pt

4.3.1 Decay of an isomeric state

Due to the $i_{13/2}$ unique-parity orbital, isomeric states with $I^{\pi} = 13/2^{+}$ are known to exist in many even-Z odd-A nuclei close to ^{173}Pt. Scholey *et al.* reported the observation of an $I^{\pi} = (13/2^{+})$ isomeric state in ^{171}Pt, ^{167}Os and ^{163}W [Sch10]. Furthermore, in ^{175}Hg [O'D09] and in ^{177}Hg [Mel03] an isomeric state with $I^{\pi} = (13/2^{+})$ exists. All these reported isomeric states have half-lives in the microsecond range.

If a nucleus has an isomeric state, with a half-life comparable to or greater than the flight time through a separator, the decay of the isomeric state can be observed at the focal plane of the separator. The time-of-flight through the separator sets the lower limit on the observable half-life. This lower limit depends also on the intensity of the transitions depopulating the isomeric state. Observation of γ rays or conversion electrons originating from an approximately 1-μs isomeric state in ^{173}Pt was possible, as the flight time of the ^{173}Pt recoils was measured to be less than 0.5 μs.

A search for γ rays following the decay of an isomeric state within ^{173}Pt was conducted. In this case, the time window between a γ-ray event in the planar-Ge detector and a recoil-implantation event in a DSSD pixel ($\Delta t_{r,\gamma}$) was set to $(0-70)$ μs. In addition, the recoil-implantation event was demanded to be followed by an ^{173}Pt α-decay event of $E_{\alpha} = 6200$ keV within 1 s ($\Delta t_{r,\alpha}$) from the implantation of a recoil. Two γ rays, with energies of 103.5(2) keV and 145.0(2) keV, were observed to follow the recoil events with a half-life of $t_{\frac{1}{2}} = 9.0(5)$ μs, as shown in Figure 4.2. These γ rays were observed to be coincident within 100 ns in a $\gamma\gamma$ matrix[d] of the planar-Ge x-strip events. The time-difference ($\Delta t_{r,\gamma}$) data and the result of the single-exponential fit of Equation (2.13), are shown in the inset of Figure 4.2. The planar-Ge detector γ-ray events, for the inset of Figure 4.2, were accepted only if the 103.5-keV and 145.0-keV transitions were observed in coincidence in the planar-Ge detector x strips.

[d]Unless otherwise stated, when referring to the planar-Ge $\gamma\gamma$ coincidences, the 100-ns time-coincidence condition was always required.

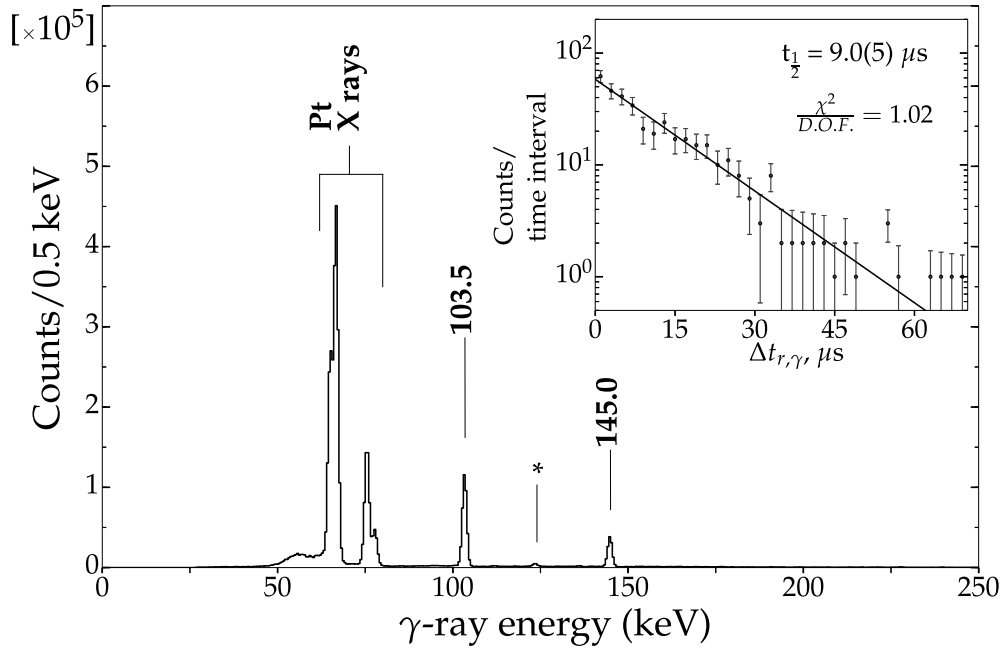

FIGURE 4.2: The ^{173}Pt γ rays emitted after recoil implantation and detected by the planar-Ge detector within 70 μs of a recoil event. The inset shows the time-difference $\Delta t_{r,\gamma}$ spectrum of the detected $\gamma\gamma$ events together with the result of the single-exponential fit to the data. The time-difference was defined between the time of the coincident 103.5-keV and 145.0-keV γ rays and the time of recoil-implantation event. The time-coincidence condition for the γ rays was 100 ns. A randomly correlated 123-keV γ ray from the ^{172}Os β^+-decay chain is marked with a star.

The K-conversion coefficient $\left(\alpha_K^{\text{exp}}\right)$ for both transitions following the decay of the 9.0-μs isomeric state was determined from

$$\alpha_K^{\text{exp}} = \frac{I_X\left(K_\alpha\right) + I_X\left(K_\beta\right)}{I_\gamma}, \tag{4.2}$$

where the intensities $I_X\left(K_\alpha\right)$, $I_X\left(K_\beta\right)$ and I_γ were corrected for the planar-Ge detector efficiency at the given energy. This ratio was obtained using the $\gamma\gamma$ matrix of γ-ray events detected in the x strips of the planar-Ge detector. When the energy condition in the $\gamma\gamma$ matrix was set on the 145.0-keV transition, $\alpha_K^{\text{exp}}\left(103.5\text{ keV}\right) = 4.6(4)$ was obtained. Similarly when the energy condition was set on the 103.5-keV transition a value of $\alpha_K^{\text{exp}}\left(145.0\text{ keV}\right) = 9.6(8)$ was obtained. These α_K^{exp} values are compared with the theoretical α_K values obtained from the BrIcc v2.3S conversion-coefficient

TABLE 4.1: The calculated [Kib08] α_K values for different electric and magnetic multipolarities for the 103.5-keV and 145.0-keV transitions in ^{173}Pt. These values are compared to the α_K^{exp} values obtained from the experiment. The last column gives the deduced assignment for the transition type.

		α_K^{calc}						deduced
E_γ (keV)	α_K^{exp}	$E1$	$M1$	$E2$	$M2$	$E3$	$M3$	σl
103.5	4.6(4)	0.301	4.97	0.684	34.4	1.14	98.8	$M1$
145.0	9.6(8)	0.129	1.90	0.368	10.5	0.930	35.7	$M2$

calculator [Kib08] in Table 4.1. Based on this comparison the 103.5-keV and the 145.0-keV transitions were assigned an $M1$ and an $M2$ character, respectively.

The single-particle estimates of transition probabilities T (see Section 2.6) for $M1$-type and $M2$-type γ-ray transitions are [Kra88, p.332]

$$\begin{aligned} T(M1) &= 5.6 \times 10^{13} \times E_\gamma^3 \, \frac{1}{s}, \\ T(M2) &= 3.5 \times 10^{7} \times A^{\frac{2}{3}} \times E_\gamma^5 \, \frac{1}{s}, \end{aligned} \tag{4.3}$$

where the transition energies E_γ are given in units of MeV and A is the mass number. Taking into account the corresponding total-conversion coefficients α [Kib08], estimates for the total half-lives are obtained as

$$\begin{aligned} t_{\frac{1}{2}}(M1; 103.5 \text{ keV}) &= \frac{\ln 2}{[T(M1) \times (1+\alpha)]} = \frac{\ln 2}{[T(M1) \times (1+6.04)]} \approx 1.6 \text{ ps}, \\ t_{\frac{1}{2}}(M2; 145.0 \text{ keV}) &= \frac{\ln 2}{[T(M2) \times (1+\alpha)]} = \frac{\ln 2}{[T(M2) \times (1+14.73)]} \approx 0.6 \ \mu\text{s}. \end{aligned} \tag{4.4}$$

It is unlikely that a 103.5-keV $M1$-type transition could be so strongly hindered compared with the Weisskopf estimate, that it would de-excite the $t_{\frac{1}{2}} = 9.0$-μs state. Therefore the 145.0-keV $M2$ transition is assigned to de-excite the isomeric state. Based on the α decay of ^{173}Pt (see Section 4.3.2), the ground state of ^{173}Pt is assigned to have $I^\pi = (7/2^-)$. As the isomeric state feeds the ground state via the coincident $M1$ and $M2$ transitions, the isomeric state is assigned to have $I^\pi = (13/2^+)$. Hence, in ^{173}Pt, a $(9/2^-)$ state is fed by the observed $M2$ transition, and the 103.5-keV transition is assigned to de-excite the $I^\pi = (9/2^-)$ state.

4.3.2 Alpha decay

Based on the known α-decay half-life of 382(2) ms of the ^{173}Pt ground state [Bag08], the time-coincidence condition between the recoil-implantation events and the α-decay events was set to $\Delta t_{r,\alpha} \leq 1.0$ s. The resulting total α-particle energy spectrum is shown in Figure 4.3(a), revealing many different α-decaying nuclei produced in the experiment. A good selectivity for the ^{173}Pt α-decay events was obtained by demanding the recoil events to be followed by the decay of the 9.0-μs isomeric state. Gamma rays originating from the decay of the isomeric state were observed by the planar-Ge detector within a 30-μs search time. Figure 4.3(b) displays the α-particle energies observed for these recoil-γ-α chains. A large reduction of the observed α-decaying nuclei is achieved. When γ rays subsequent to these α decays were searched for in the planar-Ge detector, the (E_α, E_γ)-matrix of Figure 4.3(c) was obtained. The α-γ time-coincidence condition was 150 ns for events shown in Figure 4.3(c). Three γ-ray energies at 35.0 keV, 135.7 keV and 170.8 keV are observed together with Os X rays. The 35.0-keV transition was

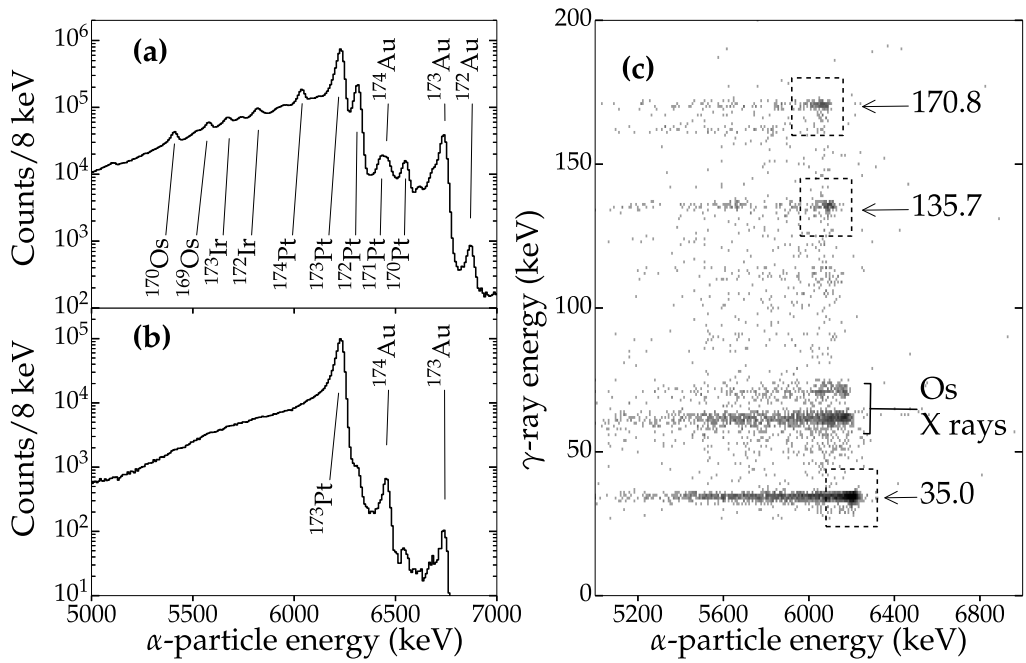

FIGURE 4.3: Total α-particle energy spectrum (a) obtained from the ^{92}Mo$(^{84}$Sr$, x)$ reaction with $\Delta t_{r,\alpha} \leq 1.0$ s. In (b) only recoil-implantation events, followed by the 103.5-keV or the 145.0-keV transition in the planar-Ge detector within $\Delta t_{r,\gamma} = 30$ μs, are accepted. Alpha-decay events of (b) are furthermore seen to be in coincidence with γ rays detected by the planar-Ge detector (c) within a 150-ns time condition.

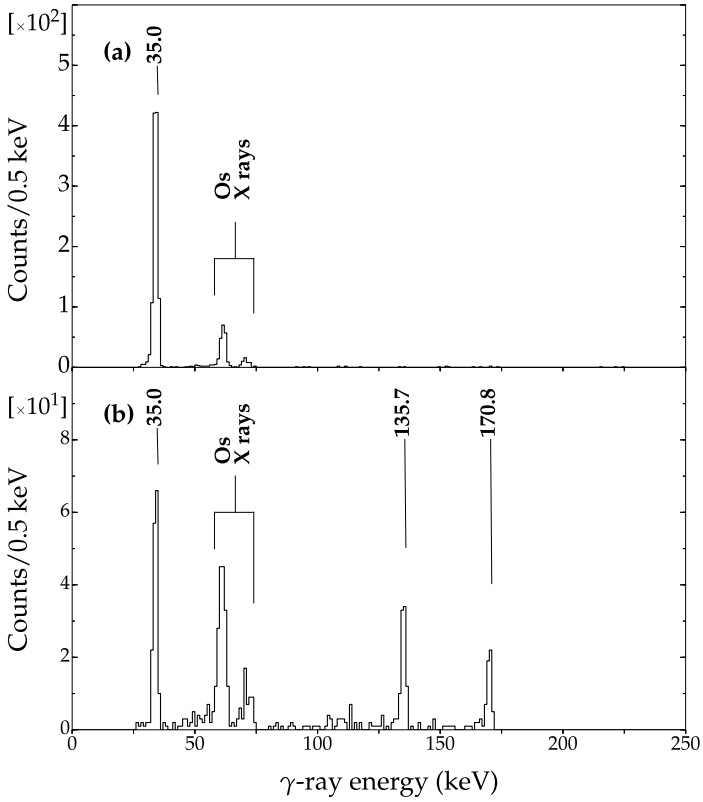

FIGURE 4.4: The Os γ rays and X rays observed with the planar-Ge detector following ^{173}Pt α-decay events. The α-particle energy conditions were set on the 6201 keV and 6063 keV peaks for Figures (a) and (b), respectively. A time condition of 150 ns was demanded between the DSSD α-decay events and the γ-ray events detected by the planar-Ge detector. The Os K-X rays in (a) are in coincidence with the E_α = 6201-keV transition due to summing of the internal-conversion electron energies of the 35.0-keV and 135.7-keV transitions to the α-particle energy (see Figure 4.3(c)).

seen in coincidence with the E_α = 6201(8)-keV α-decay branch (Figure 4.4(a)). All three γ-ray transitions are observed to be in coincidence with the E_α = 6063(8)-keV α-decay branch (Figure 4.4(b)).

A $\gamma\gamma$ matrix of the planar x-strip events, following the ^{173}Pt α decays, showed the 35.0(2)-keV and 135.7(2)-keV transitions to be in coincidence with each other. The sum of these energies (170.7(3) keV) is the same, within errors, as the energy of the 170.8(2)-keV transition. Hence, the two transitions were assumed to follow a decay path parallel to the 170.8-keV transition. An internal conversion coefficient of

$\alpha_K^{\mathrm{exp}}(135.7\ \mathrm{keV}) = 1.9(6)$ was obtained by setting the energy condition on the 35.0-keV transition in the $\gamma\gamma$ matrix. This value compares well with the calculated value $\alpha_K(M1) = 1.951$ [Kib08].

The decay energy of the 35.0-keV transition is well below the Os K-electron binding energy of 73.9 keV, which forbids the decay to proceed via internal K conversion. In addition, the Os L-X rays have energies of $\approx$ 10 keV, which was below the energy threshold of the planar-Ge detector. Thus, it was not possible to obtain an α_L^{exp} value for the 35.0-keV transition. However, α_{tot} values are 1.32 and 21.2 for 35.0-keV $E1$- and $M1$-type transitions, respectively [Kib08]. The α-particle energies observed in this experiment were always $\approx$ 20 keV above $E_\alpha = 6201$ keV, if the 35.0-keV γ ray was not in coincidence with the α-decay events. If the 35.0-keV transition would have a $\alpha_{\mathrm{tot}} \approx 1$, there should have been two α-particle energies detected for ^{173}Pt (Figure 4.3(b)). This is due to conversion-electron energy summing to the α-particle energy inside the DSSD [Kel86]. The summing of conversion electrons to the observed α-particle energies is seen in Figure 4.3(c). The 135.7-keV γ ray should be in coincidence with the same E_α as the 170.8-keV transition. Instead, the observed E_α is shifted up in energy as the conversion-electron energy, originating from the 35.0-keV state decay, sums up with E_α. Hence, the 35.0-keV transition was assumed to be of $M1$ type.

With the 135.7-keV transition assumed to have $M1$ character, an estimate for the $\alpha_K^{\mathrm{exp}}(170.8\ \mathrm{keV}) = 0.1(2)$ was obtained, based on the γ-ray energy spectrum shown in Figure 4.4(b). Taking into account the Os K-X rays emitted after the internal K conversion of the 135.7-keV transition, an estimate for the K-X ray intensity from the K conversion of the 170.8-keV transition was obtained. The BrIcc values in best agreement with this estimate are $\alpha_K(E1) = 0.081$ and $\alpha_K(E2) = 0.254$. An $E2$ character was assigned for the 170.8-keV transition as it does not require a change in parity between the initial and final states. This is supported also by the parallel $M1$ transitions.

The results of ^{173}Pt α-decay spectroscopy are presented in Table 4.2 and in Figure 4.5. The α-decay half-life was obtained from a two-component fit to the data plotted according to the K.-H. Schmidt method [Sch84]. Separate fits were carried out for each of the ^{173}Pt α-particle energy and ^{169}Os γ-ray combinations, resulting in the half-lives given in Table 4.2. The weighted average of these individual half-lives is 366(7) ms, in agreement with the previously reported values [Bag08]. The result of the

TABLE 4.2: Decay spectroscopy data from the ^{92}Mo$(^{84}$Sr$, 2pn)$ reaction. For the ^{173}Pt ground-state half-life the weighted-average value of the fitted half-lives is 366(7) ms. The half-lives were fitted to the recoil-α time-difference spectra where the α-decay event was demanded to be followed by a γ-ray event within 150 ns. The γ-ray energy conditions used are given in the table (see also Figure 4.5). The reduced widths δ^2 and the hindrance factors F were obtained using Equations (2.23) and (2.25), respectively. The $\delta^2_{\text{Ref}} = \frac{1}{2}\left(\delta^2_1 + \delta^2_2\right) = 108(10)$ keV was obtained from the δ^2 values for the nearest even-even neighbours ^{172,174}Pt.

Nucleus	E_α (keV)	$t_{\frac{1}{2}}$ (s)	b_α (%)	δ^2 (keV)	F	I^π_f	E_γ (keV)	α^{exp}_K
^{173}Pt	6063(8)	0.36(2)[a]	2.0(2)	10.1(9)	11(2)	$(9/2^-)$	170.8(2)	0.1(2)
^{173}Pt		0.36(2)[b]					135.7(2)	1.9(6)
^{173}Pt	6201(8)	0.368(7)[c]	81(8)	65(5)	1.7(2)	$(7/2^-)$	35.0(2)	

[a] E_γ = 170.8 keV in coincidence with E_α = 6063 keV required.
[b] E_γ = 135.7 keV in coincidence with E_α = 6063 keV required.
[c] E_γ = 35.0 keV in coincidence with E_α = 6201 keV required.

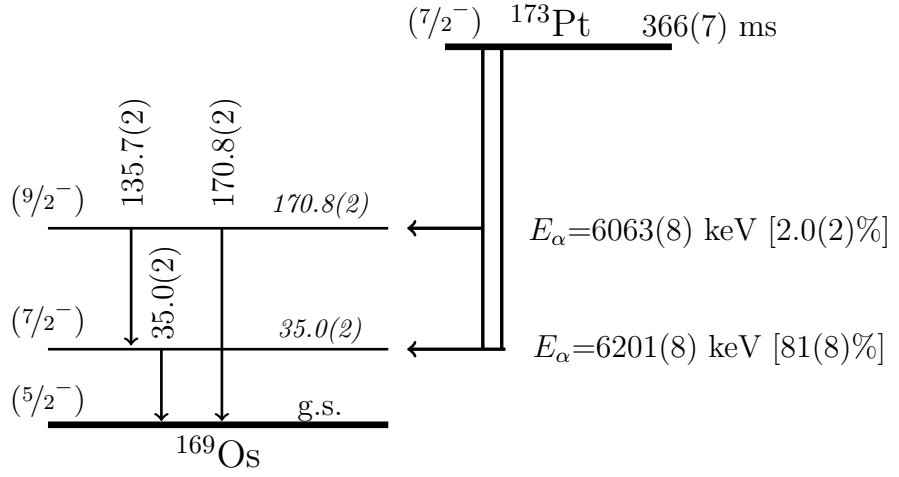

FIGURE 4.5: The ^{173}Pt α-particle energies are presented together with the transitions depopulating the excited states in ^{169}Os. The values in brackets following E_α indicate the α-decay branching ratios b_α. In this work the total α-decay branch B_α of the ^{173}Pt ground-state was measured to be 83(7) %. The total angular momenta and parities of the states are based on the systematics of the Os and Pt isotopes, α-decay hindrance factors and the deduced γ-ray transition types from the α^{exp}_K values.

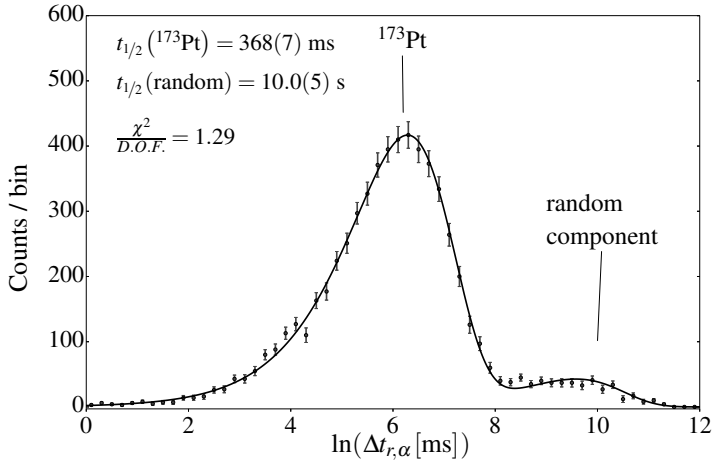

FIGURE 4.6: The plot of time-differences between the recoil-implantation event and the 6201-keV ^{173}Pt α-decay event. Additionally a 35.0-keV γ-ray event in the planar-Ge detector, within 150 ns after the α-decay event, was demanded. The time differences on the x axis are plotted taking the natural logarithm of the observed time difference $\Delta t_{r,\alpha}$ (in ms units) [Sch84]. The result of the two-component fit to the data is shown by the solid line.

fit to the time-difference data, where $E_\alpha = 6201$ keV and $E_\gamma = 35.0$ keV were required, is shown in Figure 4.6. The total α-decay branch of ^{173}Pt, $B_\alpha = 83(7)$ %, was obtained from the comparison of the intensities of the recoil-gated and α-tagged 103.5-keV and 145.0-keV transitions detected by the planar-Ge detector. This value is in agreement with the values reported earlier [Bag08]. The partial α-decay branching ratios from the present work are $b_\alpha(6063\ \mathrm{keV}) = 2.0(2)$ % and $b_\alpha(6201\ \mathrm{keV}) = 81(8)$ %. These b_α values are based on the total intensities of transitions in ^{169}Os that follow the ^{173}Pt $E_\alpha = 6063$ keV or 6201 keV α-decay events. A ground-state to ground-state α-decay branch was not observed for ^{173}Pt.

4.3.3 Prompt γ-ray spectroscopy

The level scheme for ^{173}Pt from this work is shown in Figure 4.7. Measured γ-ray energies and intensities together with the level energies are given in Table 4.3. Temporal correlations between the γ rays were established using an RDT-$\gamma\gamma$ matrix. The $\gamma\gamma$ matrix consisted of 4.9×10^6 events. Additionally, it was possible to confirm the coincidences, between the observed γ rays in bands 1 and 2, using an RDT-$\gamma\gamma\gamma$ cube

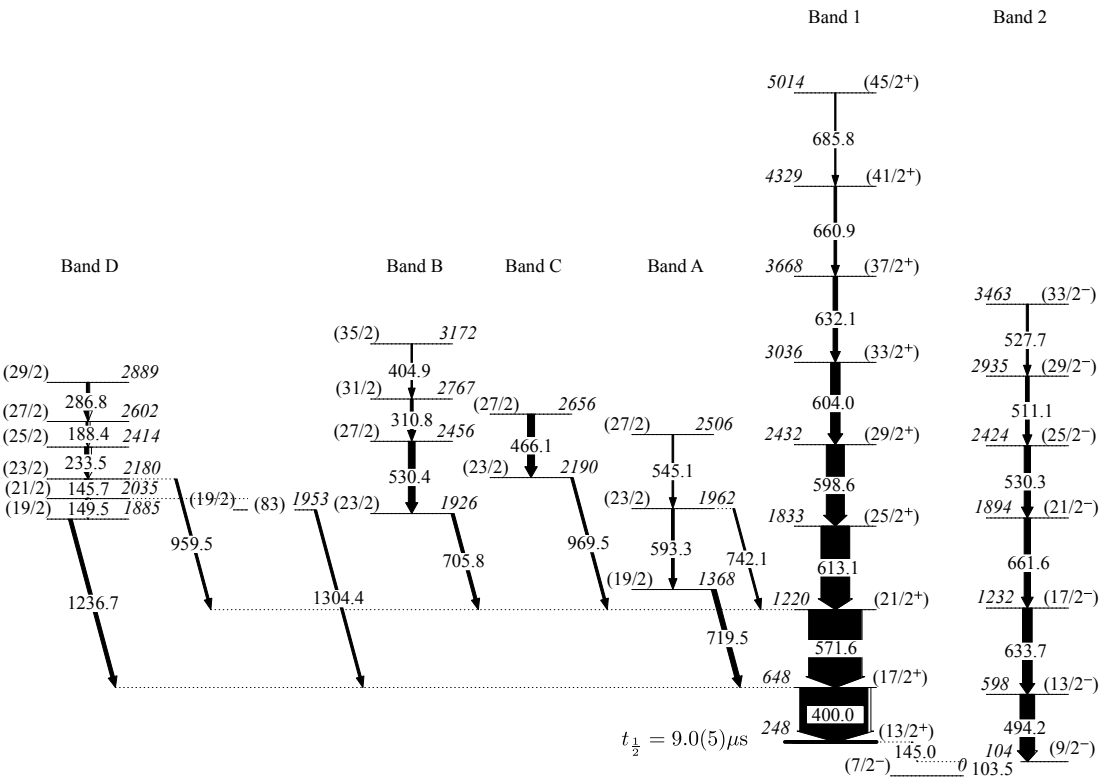

FIGURE 4.7: The proposed level scheme for ^{173}Pt. The width of the arrows shows the relative intensity of the transitions. The transition energies (normal font) and level energies (italics) are given in units of keV. The I^{π} assignments are based on the measured intensities, as well as α-decay and ground-state properties of ^{177}Hg, ^{173}Pt and ^{169}Os. For the states with only I values in brackets the transition-multipolarity estimate is based on systematics in this region of nuclei. The unobserved (83)-keV transition is drawn only to highlight the observed coincidence between the 1304.4-keV and 145.7-keV transitions.

with 5.9×10^6 events[e]. A 100-ns time-coincidence condition was demanded for the γ-ray events in the $\gamma\gamma$ matrix and the $\gamma\gamma\gamma$ cube.

With only three θ angles in JUROGAM II available in this experiment[f], it was not possible to measure angular distributions for the γ-ray transitions in ^{173}Pt. However, for ^{173}Pt, angular-distribution-intensity ratios R were given by Joss *et al.* also for some transitions which were not placed in the published level scheme [Jos06, Table III]. Based on the similar energies and intensities measured in the present work, and

[e]The RDT cube was created with the ^{173}Pt α-particle-energy condition including also escape-α events ($E_\alpha \approx 1-2$ MeV). Hence the $\gamma\gamma\gamma$ cube has more events than the $\gamma\gamma$ matrix.

[f]The JUROGAM II clovers form two rings, $\theta_{C1} = 104.5^\circ$ and $\theta_{C2} = 75.5^\circ$, which are symmetric about $\theta = 90^\circ$ after the add-back of the scattered events is performed.

TABLE 4.3: Gamma-ray transition energies, intensities and level energies for ^{173}Pt obtained in this work. Assignments for I^π are given based on angular-distribution measurements of Joss *et al.* [Jos06], for the marked transitions, and systematics in this region of nuclei. The transition intensities are normalized to the $(\frac{17}{2}^+) \rightarrow (\frac{13}{2}^+)$ 400.0-keV transition.

E_γ (keV)	E_{level} (keV)	I_γ	I_i^π	I_f^π
104.0(4)	104.0(4)	4.2(4)	$(9/2^-)$	$(7/2^-)$
145.7(4)	2180(1)	2.8(2)	(23/2)	(21/2)
149.5(4)	2034.8(9)	2.3(2)	(21/2)	(19/2)
188.4(4)	2602(2)	2.8(3)	(27/2)	(25/2)
233.5(4)	2414(2)	6.1(3)	(25/2)	(23/2)
286.8(4)	2889(2)	3.6(3)	(29/2)	(27/2)
310.8(4)	2767(1)	3.8(4)	(31/2)	(27/2)
400.0(4)[c]	648.5(5)	100(6)	$(17/2^+)$	$(13/2^+)$
404.9(5)	3172(2)	2.0(4)	(35/2)	(31/2)
455.3(4)		5(1)		
466.1(4)[a]	2656(1)	10(1)	(27/2)	(23/2)
494.2(4)[c]	598.2(6)	21(2)	$(13/2^-)$	$(9/2^-)$
503.2(4)		8(1)		
511.1(4)	2935(1)	5.3(4)	$(29/2^-)$	$(25/2^-)$
527.7(4)	3463(2)	3(1)	$(33/2^-)$	$(29/2^-)$
530.3(4)[bc]	2423.8(9)	9(1)	$(25/2^-)$	$(21/2^-)$
530.4(4)[c]	2456.3(9)	9.7(4)	(27/2)	(23/2)
545.1(5)	2506(2)	2.3(3)	(27/2)	(23/2)
571.6(4)[c]	1220.1(7)	77(5)	$(21/2^+)$	$(17/2^+)$
593.3(5)	1961.4(8)	3.9(6)	(23/2)	(19/2)
598.6(4)	2431.8(9)	26.1(9)	$(29/2^+)$	$(25/2^+)$
604.0(4)	3036(1)	13.7(7)	$(33/2^+)$	$(29/2^+)$
613.1(4)[c]	1833.1(8)	41.6(9)	$(25/2^+)$	$(21/2^+)$
632.1(4)[c]	3668(2)	6.6(3)	$(37/2^+)$	$(33/2^+)$
633.7(4)	1231.9(7)	14(1)	$(17/2^-)$	$(13/2^-)$
660.9(4)	4329(2)	3.8(4)	$(41/2^+)$	$(37/2^+)$
661.6(4)	1893.5(8)	9.2(4)	$(21/2^-)$	$(17/2^-)$
685.8(6)	5014(2)	1.8(3)	$(45/2^+)$	$(41/2^+)$
705.8(4)	1925.9(8)	4.5(5)	(23/2)	$(21/2^+)$
719.5(4)	1368.0(7)	7.0(6)	(19/2)	$(17/2^+)$
742.1(5)	1962.2(8)	2.7(5)	(23/2)	$(21/2^+)$
837.0(6)		4(1)		
853.9(5)		2.0(3)		
959.5(6)	2179.6(9)	3.5(7)	(23/2)	$(21/2^+)$
969.5(6)	2189.6(9)	3.7(6)	(23/2)	$(21/2^+)$
1037.6(4)		4.8(7)		
1236.7(6)	1885.2(8)	5.3(7)	(19/2)	$(17/2^+)$
1304.4(7)	1952.9(9)	3.6(6)	(19/2)	$(17/2^+)$

[a] Non-coincident doublets, only one of which is placed in the level scheme.
[b] Self-coincident doublet.
[c] Angular distribution measurement by Joss *et al.* [Jos06].

on the published R-ratio values of Joss *et al.*, these transitions in bands 1 and 2 were assigned to be of $E2$ character. For other transitions in bands 1 and 2 the transition-type assumption is based on the systematics in this region of nuclei. For all other transitions in Figure 4.7 either dipole or quadrupole character was assumed. The I^{π} assignments for the $(^{7}/_{2}^{-})$, $(^{9}/_{2}^{-})$ and $(^{13}/_{2}^{+})$ states are based on the observed α-decay and the 9.0-μs isomeric-state decay properties of ^{173}Pt.

The total γ-ray energy spectra of ^{173}Pt are shown in Figures 4.8(a) and 4.8(b). The energy spectrum of Figure 4.8(a) was obtained from an RDT analysis, where the recoil-implantation events were followed by ^{173}Pt α-decay events with $E_{\alpha} = 6201$ keV. In Figure 4.8(b) the recoils are tagged with the γ rays emitted after the decay of the $(^{13}/_{2}^{+})$ isomeric state. The 103.5-keV or 145.0-keV transitions emitted after the decay of the isomeric state were observed by the planar-Ge detector within 30 μs from the recoil events. The time-difference condition between the recoil and α-decay events was $0 \leq \Delta t_{r,\alpha} \leq 1.0$ s for both figures. The most notable difference between these figures is the reduction of the observed γ-ray transition intensity at certain γ-ray energies in Figure 4.8(b) compared with Figure 4.8(a). The positions of the γ-ray energies whose intensity has decreased the most are marked by arrows in Figure 4.8(b). These transitions belong to a negative-parity band, which feeds the ground state of ^{173}Pt. They are not observed in Figure 4.8(b), which indicates that the feeding from this negative-parity band to the positive-parity band is weak.

In Figure 4.9(a) γ rays from the $\gamma\gamma$ matrix in temporal coincidence with the 400.0-keV transition of band 1 are shown. When the γ-ray energy condition is placed on the 604.0-keV transition in band 1, coincidences with only the members of band 1 are seen in Figure 4.9(b). The results obtained in the present work agree with assignments of Joss *et al.* [Jos06] for the positive-parity band in ^{173}Pt. Joss *et al.* assigned the observed prompt band structure to a $I^{\pi} = (^{13}/_{2}^{+})$ band head. The results from the delayed γ-ray spectroscopy, in the present work confirm the previously made assignments. The positive parity band is extended up to $I^{\pi} = (^{45}/_{2}^{+})$ from $I^{\pi} = (^{41}/_{2}^{+})$.

In Figure 4.9(c) the γ-ray energies of the transitions in band 2 are shown in coincidence with the 494.2-keV transition. Observation of the 494.2-keV transition was already reported by Joss *et al.*. Also the 633.7-keV, 661.6-keV and 530.3-keV transitions were reported, as the transitions in the positive-parity band with similar energies were marked as doublets. However, these transitions were not placed in the

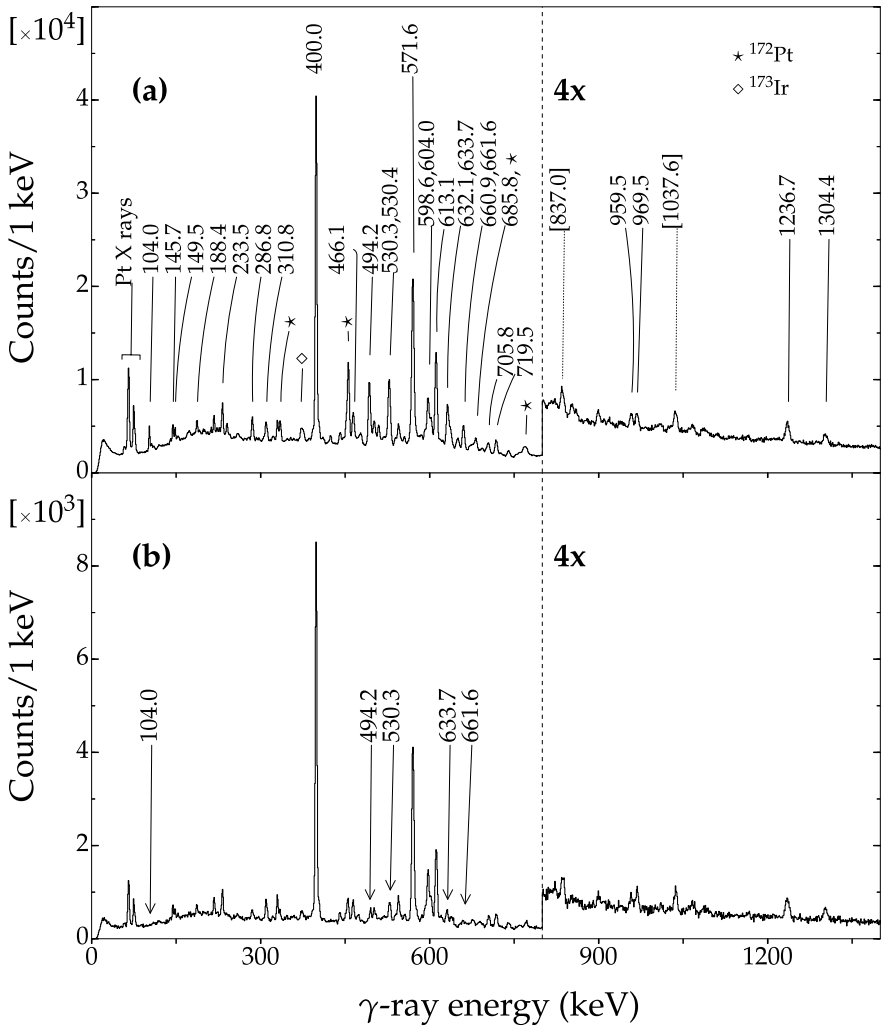

FIGURE 4.8: (a) Prompt γ rays in coincidence with recoil-implantation events tagged with the ^{173}Pt $E_\alpha = 6201$-keV α decays. In (b), the recoil events are accepted only if they are followed by a decay of the 9.0-μs ($^{13}/_{2}^{+}$) state. The decays from the isomeric state (103.5-keV or 145.0-keV transitions) were observed in the planar-Ge detector within 30 μs from the recoils. Transition energies written in square brackets in (a) are observed in coincidence with ^{173}Pt γ rays, but it was not possible to place them in the level scheme. The positions of transitions in band 2, which were not in coincidence with the decay of the isomeric state, are highlighted with arrows in (b). The time-coincidence condition between the recoil-implantation and α-decay events was set to $0 \leq \Delta t_{r,\alpha} \leq 1$ s, for (a) and (b).

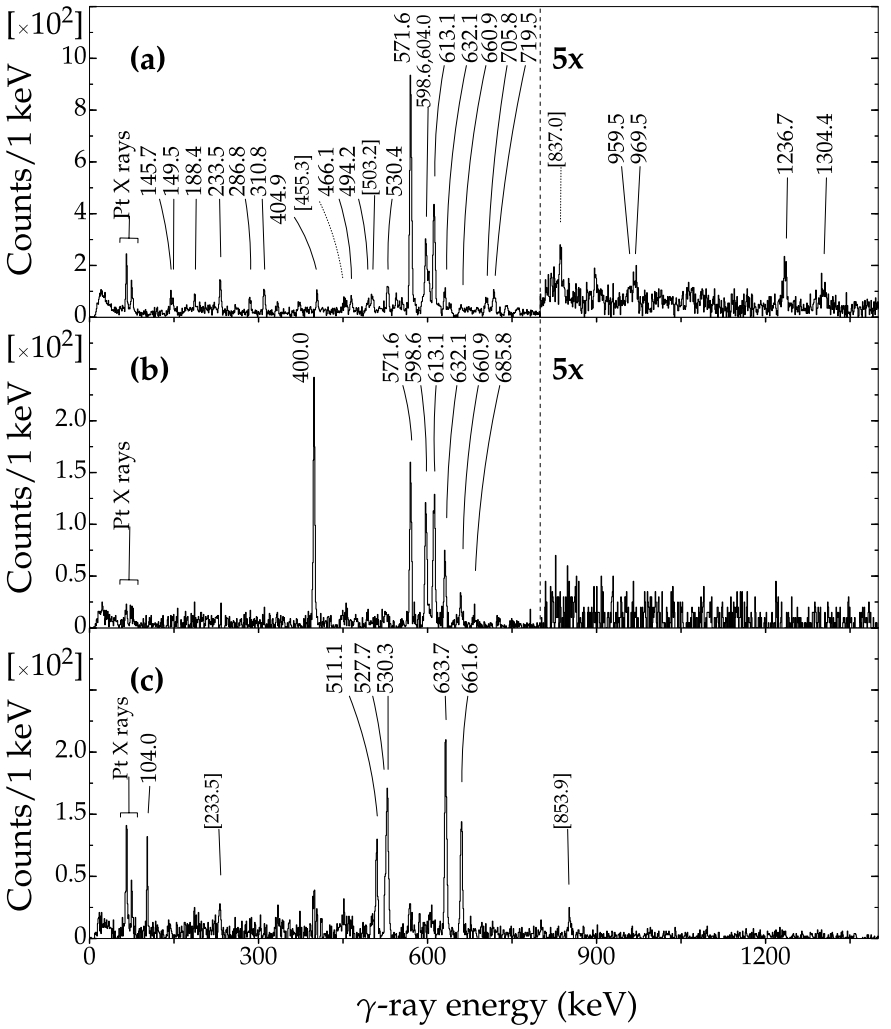

FIGURE 4.9: Prompt γ-rays in coincidence with (a) the 400.0-keV (band 1), (b) 604.0-keV (band 1) and (c) 494.2-keV (band 2) transitions in a ^{173}Pt α-decay-tagged $\gamma\gamma$ matrix. The time-coincidence condition between γ rays in the matrix was 100 ns. Transition energies in square brackets mark γ rays that are seen in coincidence with the applied energy conditions, but it was not possible to place these γ rays in the level scheme of Figure 4.7.

level scheme of ^{173}Pt [Jos06]. In Figure 4.9(c) coincidences are also seen with a 233.5-keV and an 853.9-keV transition. These transitions were observed in coincidence only with the 494.2-keV transition. It is possible that there is another transition in ^{173}Pt with an energy similar to the 494.2-keV transition. The strongest transitions in ^{173}Pt (400.0-keV and 571.6-keV) are seen to be coincident with the 494.2-keV transition in Figure 4.9(c) due to coincidences with Compton-scattering events.

Bands B and C (see Figure 4.7) resemble structures observed in ^{171}Os, where similar structures were tentatively assigned to β and γ vibrations coupled to an $i_{13/2}$ neutron [Bar99a, Fig. 1. Bands 9-10]. The $I = (^{23}/_{2})$ state at 1368 keV (band A) could be the band head of the negative-signature structure of a $\nu i_{13/2}$ band [Bar99a, Fig. 1. Band 8]. Band D is similar to the dipole bands observed in ^{171}Ir [Bar99b]. Bark *et al.* suggested that these bands in ^{171}Ir are created by the tilted-axis cranking of a $\pi h_{11/2} \times \nu i^2_{13/2}$ configuration. Band D in ^{173}Pt, could be based on a neutron 3-quasiparticle configuration, involving a pair of aligned $i_{13/2}$ neutrons. More information on these weak structures, and the high-energy transitions in ^{173}Pt feeding band 1, is needed before specific assignments can be made.

4.4 ^{175}Pt

4.4.1 Alpha decay

The total energy spectrum of α particles emitted by recoils produced in the ^{92}Mo$(^{86}$Sr$, x)$ reaction is shown in Figure 4.10(a). It was not possible to select the ^{175}Pt recoil events using the decay of an isomeric state (as performed for ^{173}Pt). Also, the known α-particle energy of 6038(4) keV for ^{174}Pt [Bag02] overlaps with $E_\alpha = 6038(10)$ keV of ^{175}Pt reported by Hagberg *et al.*[Hag79]. However, it was possible to use the prompt 328.6-keV, 423.2-keV and 436.4-keV ^{175}Pt γ rays observed by the JUROGAM I-Ge detectors to tag the ^{175}Pt recoils. Figure 4.10(b) shows the α-particle energy spectrum observed, when the recoils have been selected using the aforementioned prompt γ rays. A clear reduction in the intensity of ^{172,173,174,176}Pt and ^{175}Au α-particle peaks is achieved. An α-particle energy of 6021(4) keV was obtained for the ground-state to ground-state α-decay of ^{175}Pt. The half-life for this decay was determined to be 2.39(6) s. These values were obtained by tagging the recoils with the above mentioned three γ rays.

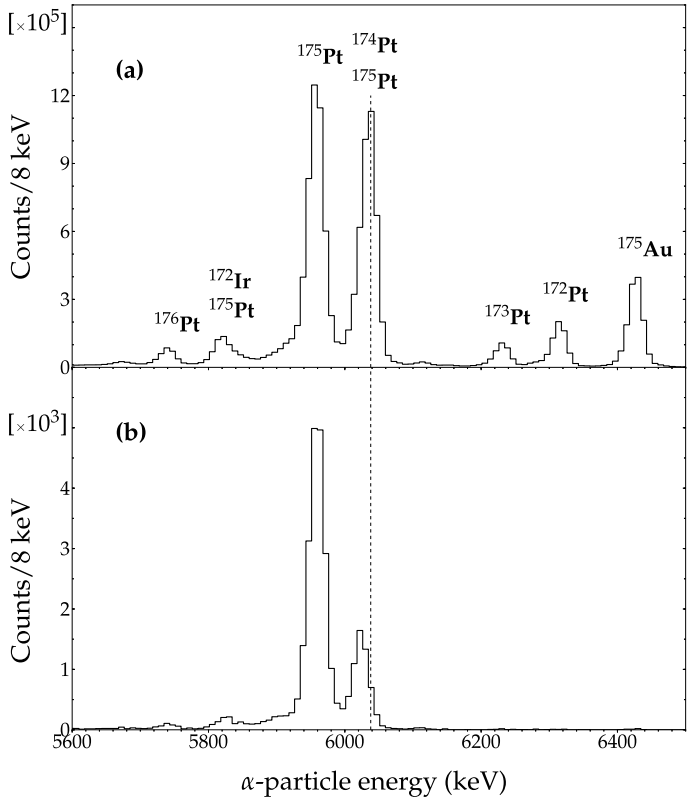

FIGURE 4.10: (a) Alpha-particle energies emitted by the recoils produced in the reaction $^{92}\mathrm{Mo}(^{86}\mathrm{Sr}, x)$. Time-difference condition set to $0 \leq \Delta t_{r,\alpha} \leq 7.5$ s. (b) The recoil-implantation events in the correlated recoil-α chains are demanded to be in coincidence with the prompt 328.6-keV, 423.2-keV or 436.4-keV γ rays observed at the target position. The dashed line marks the position of $E_\alpha = 6038$-keV α-decay branch of ^{174}Pt [Bag02]. Only the peripheral y strips of the DSSDs were used to look for recoil-α correlations. The figure is from [Peu14].

Demanding an observation of γ rays by the planar-Ge detector after an α-decay event, highlighted α decays leading to excited states in the daughter nuclei. Figure 4.11(a) shows γ rays in ^{171}Os in coincidence with the $E_\alpha = 5814$-keV and 5819-keV α-decay branches of ^{175}Pt. In Figure 4.11(b) the α-particle energy condition was set to $E_\alpha = 5948$ keV. The search time between the recoil-implantation and α-decay events was set to 7.5 s, to obtain the events presented in Figures 4.11(a)-(b). A strong 161.6-keV transition, shown in Figure 4.11(a), is correlated with an α decay of $E_\alpha = 5817(4)$ keV and with a α-decay half-life of 1.81(4) s. These values are in agreement with the values published for ^{172}Ir [Bag10], which was produced via the $3p$ evaporation channel.

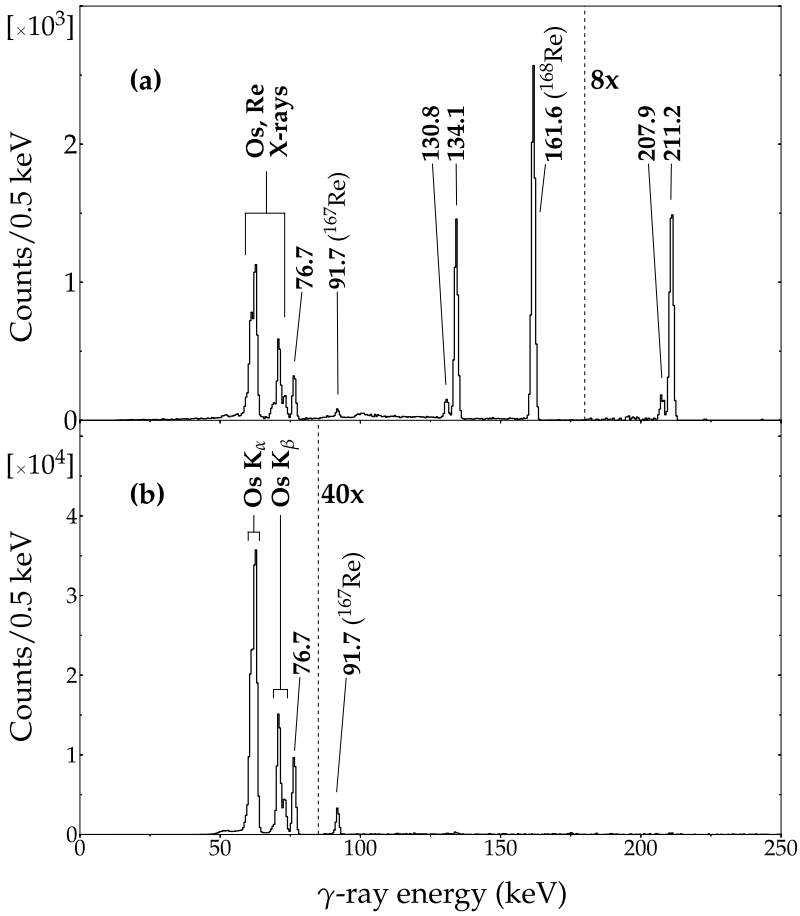

FIGURE 4.11: Gamma rays from ^{171}Os observed by the planar-Ge detector within 150 ns after ^{175}Pt α-decay events. In (a), the α-particle energy condition was set on the decay branch corresponding to $E_\alpha = 5814/5819$ keV, whereas in (b) the α-particle energy condition was set to $E_\alpha = 5948$ keV (see Figure 4.13). All the y strips of the DSSD were used for the α-particle detection. The figure is from [Peu14].

The 91.7-keV transition shown in Figure 4.11(b) is correlated with $E_\alpha = 5919(4)$ keV. The half-life determined for this α decay is 1.14(5) s. These values agree with the published values of ^{171}Ir [Bag00].

The observed 76.7-keV, 134.1-keV and 211.2-keV transition energies shown in Figure 4.11(a) are in accord with the values reported by Hagberg *et al.* [Hag79]. In the present, work the 76.7-keV transition was observed to be in coincidence with the favoured $E_\alpha = 5948$-keV decay branch and with the $E_\alpha = 5814$ and 5819-keV decay branches of ^{175}Pt. Hagberg *et al.* reported the 76.7-keV transition to be in coincidence

only with the favoured decay branch. Observation of the E_γ = 130.8-keV and 207.9-keV transitions, in coincidence with α-decay events, was not reported by Hagberg *et al.*. However, in an in-beam study of ^{171}Os, Bark *et al.* observed γ-ray transitions of 131.1 keV and 208.0 keV [Bar90]. These transitions were assigned to originate from the $I^\pi = (9/2^-)$ state in the $5/2^-$ [523] ground-state band of ^{171}Os. In the present work the $(9/2^-)$ state in ^{171}Os was observed to be fed in α decay, revealing a newly observed α-decay branch.

A matrix of the γ-ray events following ^{175}Pt α-decay events in the DSSD was created. The γ rays were observed by the planar Ge-detector x strips and the $\gamma\gamma$ time-difference condition was set to 90 ns. The α-particle energy condition was set to E_α = 5814 keV. All y strips of the DSSDs were used for the recoil-α correlations when creating the $\gamma\gamma$ matrix. The short 150-ns time condition, together with the α-particle energy condition, makes the observation of γ-ray events from random α-decay events unlikely. Thus a possible false correlation of a recoil-implantation event with the ^{175}Pt α-decay events is not significant for the creation of this $\gamma\gamma$ matrix. The matrix shows the 130.8-keV and 134.1-keV transitions to be in coincidence with the 76.7-keV transition. The total projection of the $\gamma\gamma$ matrix is shown in Figure 4.12(a). Placing an energy condition on the 76.7-keV transition reveals a coincidence with the 130.8-keV and 134.1-keV transitions (Figure 4.12(b)). An $\alpha_K^{\rm exp}$ value of 11.6(9) was obtained for the 76.7-keV transition (see Equation 4.2). This value is a weighted average of the deduced α_K values, when the energy condition was placed separately on the 130.8-keV and 134.1-keV transitions in the matrix. By comparing this result to the theoretical $\alpha_K(M1)$ value of 9.85 [Kib08], the 76.7-keV transition was assigned to have an $M1$ character. For the 130.8-keV and 134.1-keV transitions, only single α_K value could be obtained from the $\gamma\gamma$ analysis, as both transitions are in coincidence with the 76.7-keV transition (see Figure 4.12(b)). An $\alpha_K^{\rm exp}$ value of 2.1(2) was obtained defining $I_\gamma = I(130.8)$ keV + $I(134.1)$ keV in Equation 4.2. Based on the comparison of the experimental and theoretical values in Table 4.4, both transitions are assigned to have an $M1$ character. It was not possible to determine the $\alpha_K^{\rm exp}$ values for the 207.9-keV and 211.2-keV transitions. These two transitions could not be tagged with coincident γ rays, to produce an energy spectrum, free of X rays originating from other transitions observed in coincidence with the α-decay events.

The results of ^{175}Pt decay spectroscopy are presented in Figure 4.13 and in Table 4.5. The fitted α-decay half-lives for ^{175}Pt, given in Table 4.5, agree with the ^{175}Pt

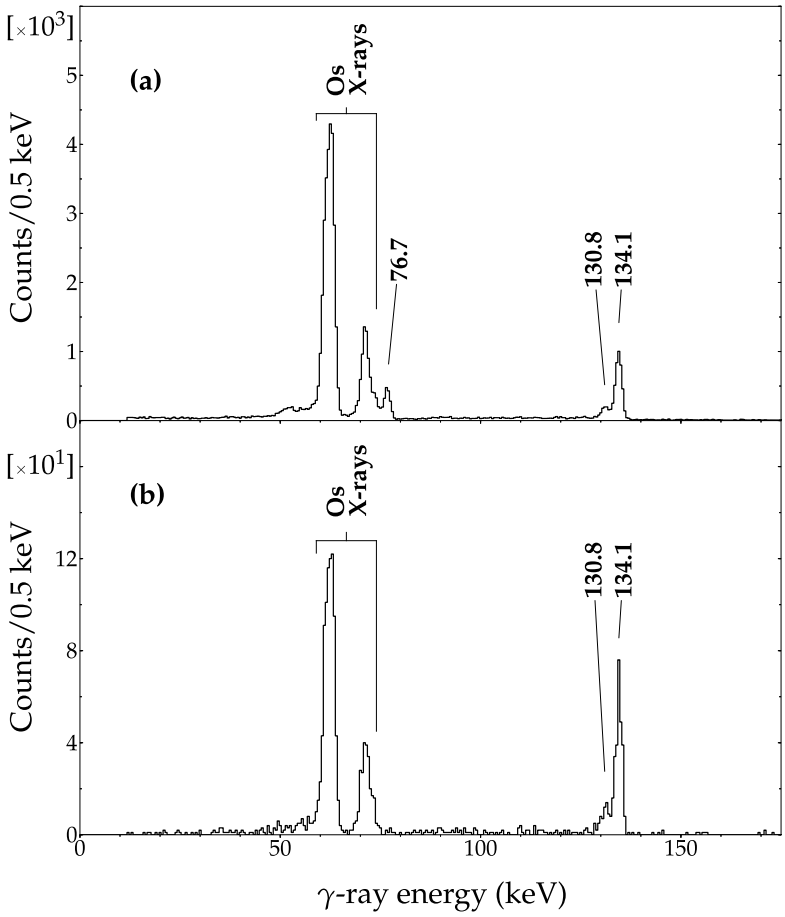

FIGURE 4.12: (a) A total projection of a $\gamma\gamma$ matrix of the ^{171}Os γ rays detected by the planar Ge-detector x strips, following the ^{175}Pt α-decay events observed with the DSSD. (b) The γ rays in coincidence with the 76.7-keV transition in ^{171}Os. All DSSD y strips were used for the α-particle detection. The time-difference condition between an α-decay event and a γ-ray event was 150 ns. Between γ-ray events the time condition was 90 ns. The figure is from [Peu14].

TABLE 4.4: The calculated α_K values from BrIcc v2.3S [Kib08]. The values are given for different sums, from combinations of electric and magnetic multipolarities for the 130.8-keV and 134.1-keV transitions in ^{171}Os. The calculated values are compared with the α_K^{exp} value. The experimental value is from the energy spectrum of Figure 4.12(b) where both transitions and the Os X rays from the internal conversion of these transitions are present. The notation for the BrIcc values in the Table is $\alpha_K(\sigma l;\ 130.8\ \mathrm{keV}) + \alpha_K(\sigma' l';\ 134.1\ \mathrm{keV})$.

α_K^{exp}	$\alpha_K(M1)+\alpha_K(M1)$	$\alpha_K(E2)+\alpha_K(M1)$	$\alpha_K(M1)+\alpha_K(E2)$	$\alpha_K(E2)+\alpha_K(E2)$
2.1(2)	2.04(4)	1.74(3)	0.76(3)	0.46(1)

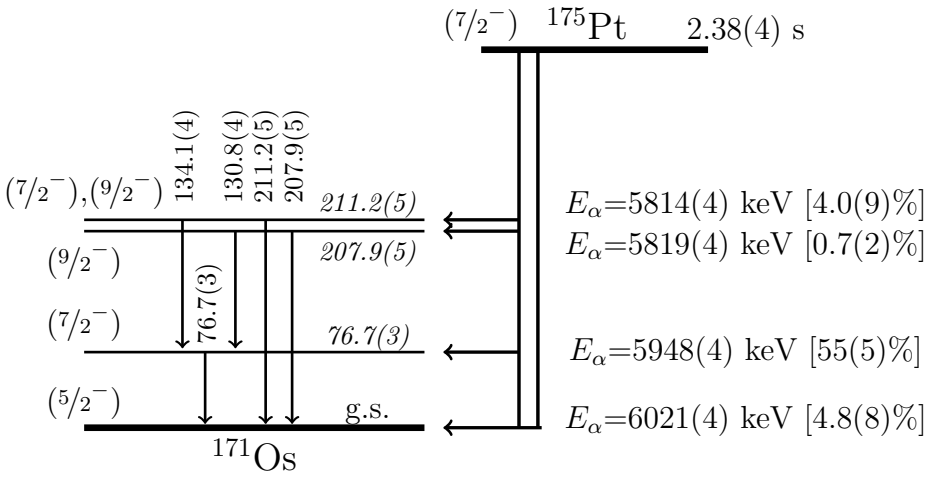

FIGURE 4.13: The ^{175}Pt α-particle energies are presented together with the transitions depopulating the excited states in ^{171}Os. The values in brackets following E_α indicate the α-decay branching ratios b_α. The ^{175}Pt α-decay branching ratios were taken from the work by Hagberg *et al.* [Hag79]; see Table 4.5. The total angular momenta and parities of the states are based on the systematics of the Os and Pt isotopes, α-decay hindrance factors and the deduced γ-ray transition types from the α_K^{exp} values.

ground-state half-life of 2.53 s [Bas04]. Similarly to ^{173}Pt (see Figure 4.6), the α-decay half-lives were obtained from a two-component fit [Sch84] to the data (see Table 4.5 for details). The α-decay branching ratios for ^{175}Pt were taken from the work of Hagberg *et al.* [Hag79]. These branching ratios could not be extracted from the current data set, due to uncertainties caused by the conversion-electron summing to the observed α-particle energies. The b_α values for the E_α = 5814-keV and E_α = 5819-keV decay branches were obtained taking b_α = 4.7 % [Hag79] as the sum of these two decay-branch intensities. Assuming an $M1$ character for the 130.8-keV and 134.1-keV transitions, $b_\alpha(5814\ \mathrm{keV}) = 4.0(9)$ % and $b_\alpha(5819\ \mathrm{keV}) = 0.7(2)$ % were obtained.

TABLE 4.5: Decay spectroscopy data from the ^{92}Mo(^{86}Sr, x) reaction. Only the low event rate y strips of the DSSDs were used; see Figure 4.1. For the ^{175}Pt ground state half-life a weighted-average value of the fitted half-lives is 2.38(4) s. The half-lives were fitted to the recoil-α time-difference spectra where the α-decay event was followed by a γ-ray event within 150 ns. The γ-ray energy conditions used are given in the table (see also Figure 4.13). The reduced widths δ^2 and the hindrance factors F were obtained using Equations (2.23) and (2.25), respectively. The $\delta^2_{\text{Ref}} = \frac{1}{2}\left(\delta^2_1 + \delta^2_2\right) = 109(12)$ keV was obtained from the δ^2 values for the nearest even-even neighbours ^{174,176}Pt.

Nucleus	E_α (keV)	$t_{\frac{1}{2}}$ (s)	b_α (%)	δ^2 (keV)	F	I^π_f	E_γ (keV)	α_K^{exp}
^{174}Pt	6038(4)[a]	0.93(3)						
^{171}Ir	5919(4)	1.14(5)[b]					91.7(4)	
^{172}Ir	5817(4)	1.81(4)[c]					161.6(4)	
^{175}Pt	5814(4)	2.6(3)[d]	4.0(9)[h]	17(4),31(7)	6(2),3.5(8)	$(7/2^-)$,$(9/2^-)$	211.2(5)	
		2.34(8)[e]					134.1(4)	2.1(2)[i]
							76.7(3)	11.6(9)
	5819(4)		0.7(2)[h]	6(2)	20(6)	$(9/2^-)$	207.9(5)	
							130.8(4)	2.1(2)[i]
							76.7(3)	11.6(9)
^{175}Pt	5948(4)	2.39(5)[f]	55(5)[j]	66(7)	1.7(2)	$(7/2^-)$	76.7(3)	
^{175}Pt	6021(4)	2.39(6)[g]	4.8(8)[j]	5.1(9)	21(4)	$(5/2^-)$		

[a] Used for calibration.
[b] E_γ = 91.7 keV in coincidence with E_α = 5919 keV required.
[c] E_γ = 161.6 keV in coincidence with E_α = 5817 keV required.
[d] E_γ = 207.9 keV, 211.2 keV in coincidence with E_α = 5814 keV, 5819 keV required.
[e] E_γ = 130.8 keV, 134.1 keV in coincidence with E_α = 5814 keV, 5189 keV required.
[f] E_γ = 76.7 keV in coincidence with E_α = 5948 keV is demanded.
[g] The prompt E_γ = 328.6 keV in delayed coincidence with E_α = 6021 keV required.
[h] b_α = 4.7 % [Hag79] is divided by the total intensity ratio of the 130.8-keV and 134.1-keV transitions.
[i] This is the deduced value for both, the 130.8 keV and 134.1 keV, transitions together.
[j] The value is from Ref. [Hag79].

4.4.2 Prompt γ-ray spectroscopy

Transition energies, level energies, initial and final angular momenta and parity for ^{175}Pt, from the present work, are listed in Table 4.6. The measured angular distributions and intensity ratios are given in Table 4.7. The proposed level scheme for ^{175}Pt is shown in Figure 4.14. The coincidence analysis for the in-beam γ-ray transitions was performed using an RDT-$\gamma\gamma$ matrix and an RG-$\gamma\gamma\gamma$ cube. For both, all DSSD y strips were used for the RG and RDT methods. Total number of events of 5×10^6

TABLE 4.6: Gamma-ray transition energies and intensities, level energies and I^π assignments for ^{175}Pt obtained in this work. The intensities of the transitions are normalized to the $(\frac{17}{2}^+) \rightarrow (\frac{13}{2}^+)$ 328.6-keV transition.

E_γ (keV)	E_{level} (keV)	I_γ	I_i^π	I_f^π
122.6(7)	546(2)	0.3(2)	$(13/2^-)$	$(11/2^-)$
130.9(6)	130.9(6)	8.2(5)	$(9/2^-)$	$(7/2^-)$
138.6(6)	X+138.6(6)	2.4(4)	$(11/2^+)$	$(13/2^+)$
244.1(4)	X+382.7(8)	8.7(5)	$(15/2^+)$	$(11/2^+)$
257.1(8)	802(2)	3.5(5)	$(15/2^-)$	$(13/2^-)$
291.8(6)	422.7(9)	8(1)	$(11/2^-)$	$(9/2^-)$
328.6(4)	X+328.6(4)	100(2)	$(17/2^+)$	$(13/2^+)$
362.5(5)	X+745.2(9)	24.1(8)	$(19/2^+)$	$(15/2^-)$
380.3(4)	803.5(6)	21(2)	$(15/2^-)$	$(11/2^-)$
382.2(4)	X+382.2(4)	24(4)	$(15/2^+)$	$(13/2^+)$
388.5(4)	1191.9(7)	16.1(8)	$(19/2^-)$	$(15/2^-)$
407.8(4)	X+1173.1(7)	5.8(4)	$(23/2^+)$	$(21/2^+)$
414.3(5)	545.1(8)	35(2)	$(13/2^-)$	$(9/2^-)$
415.8(4)	X+744.6(6)	9.0(5)	$(19/2^+)$	$(17/2^+)$
421.7(4)	1391(1)	22(3)	$(21/2^-)$	$(17/2^-)$
423.2(4)	423.2(4)	12(2)	$(11/2^-)$	$(7/2^-)$
424.3(4)	969.4(9)	28(3)	$(17/2^-)$	$(13/2^-)$
428.6(4)	X+1174(1)	17.0(9)	$(23/2^+)$	$(19/2^+)$
431.4(8)	X+1663(1)	5(2)	$(27/2^+)$	$(25/2^+)$
436.4(4)	X+765.3(6)	63(2)	$(21/2^+)$	$(17/2^+)$
437.3(5)	1629.2(9)	14(2)	$(23/2^-)$	$(19/2^-)$
462.3(5)	1853(1)	21(2)	$(25/2^-)$	$(21/2^-)$
466.4(4)	X+1231.7(7)	44(2)	$(25/2^+)$	$(21/2^+)$
487.4(6)	2117(1)	9(2)	$(27/2^-)$	$(23/2^-)$
490.7(4)	X+1664(1)	11.2(5)	$(27/2^+)$	$(23/2^+)$
502.6(5)	2356(2)	15(2)	$(29/2^-)$	$(25/2^-)$
506.6(4)	X+1738.3(8)	30.8(9)	$(29/2^+)$	$(25/2^+)$
530.1(6)	2647(2)	6(2)	$(31/2^-)$	$(27/2^-)$
533.0(7)	2889(2)	10(3)	$(33/2^-)$	$(29/2^-)$
549.1(5)	X+2214(2)	7.1(8)	$(31/2^+)$	$(27/2^+)$
554.1(7)	3201(2)	4(2)	$(35/2^-)$	$(31/2^-)$
554.6(4)	X+2292.9(9)	19.6(8)	$(33/2^+)$	$(29/2^+)$
556.1(7)	3445(2)	7(2)	$(37/2^-)$	$(33/2^-)$
587.0(7)	3788(2)	3.6(7)	$(39/2^-)$	$(35/2^-)$
587.3(8)	4032(2)	4.4(9)	$(41/2^-)$	$(37/2^-)$
603.1(4)	X+2896(1)	14.3(5)	$(37/2^+)$	$(33/2^+)$
604.4(5)	X+2818(2)	4.2(6)	$(35/2^+)$	$(31/2^+)$
609(1)	4642(2)	2.5(7)	$(45/2^-)$	$(41/2^-)$
618.6(8)	4406(2)	2.6(5)	$(43/2^-)$	$(39/2^-)$
646.2(6)	X+3542(2)	4.2(4)	$(41/2^+)$	$(37/2^+)$
658.8(5)	X+3477(2)	1.3(3)	$(39/2^+)$	$(35/2^+)$
685.5(6)	X+4228(2)	1.8(3)	$(45/2^+)$	$(41/2^+)$
701.6(9)	X+4178(2)	0.6(1)	$(43/2^+)$	$(39/2^+)$
720.1(7)	X+4948(2)	0.8(2)	$(49/2^+)$	$(45/2^+)$
734(2)	X+4912(2)	0.4(1)	$(47/2^+)$	$(43/2^+)$

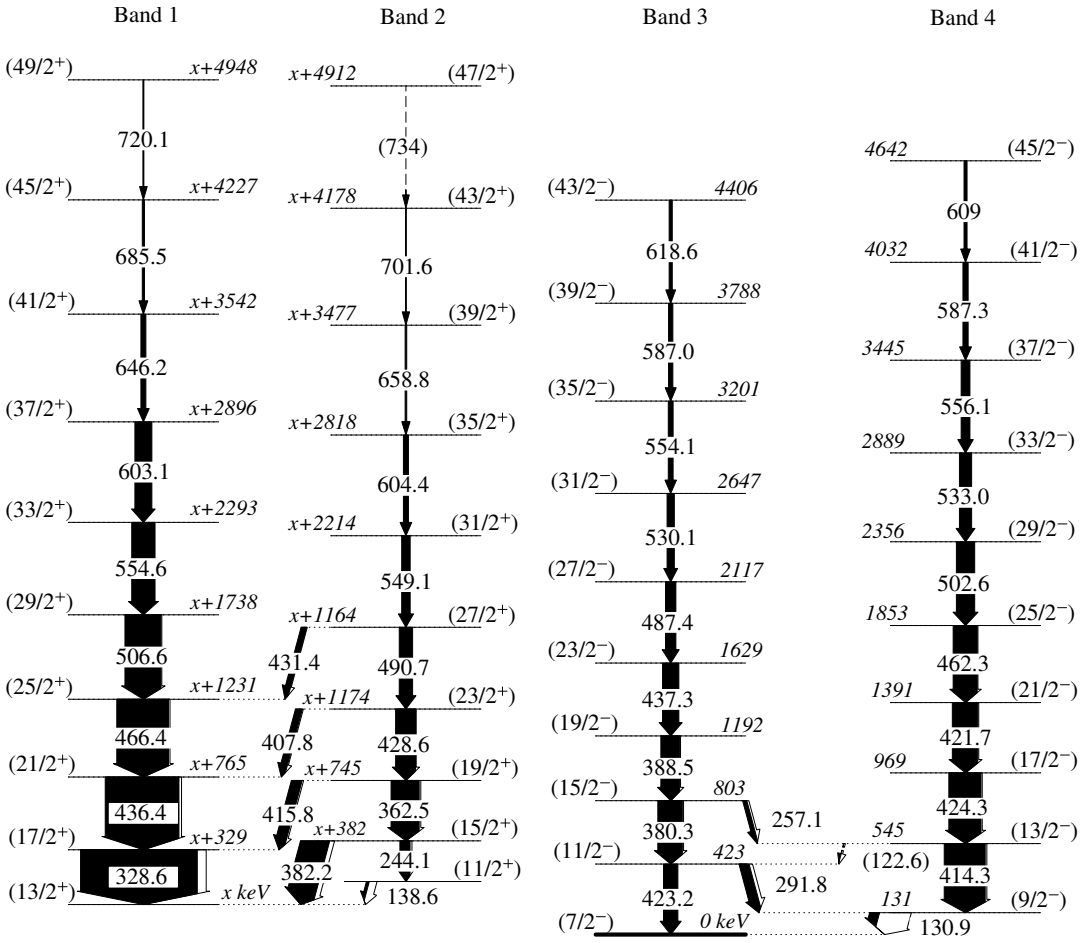

FIGURE 4.14: The proposed level scheme for ^{175}Pt. The width of the arrows show the relative intensity of the transitions. The arrow width consists of the measured γ-ray (black) intensity and of calculated internal-conversion (white) intensity. The transition energies (normal font) and level energies (italics) are given in units of keV. The I^{π} assignments are based on the measured $\gamma\gamma$ and $\gamma\gamma\gamma$ coincidences, intensities and angular distributions for prompt γ rays. Furthermore information on α-decay and ground-state properties of ^{179}Hg, ^{175}Pt and ^{171}Os are considered for the assignment of the $I^{\pi} = (7/2^{-})$ for the ^{175}Pt ground state. The figure is from [Peu14].

TABLE 4.7: Angular distribution coefficients A_2/A_0, A_4/A_0, intensity ratios R_{J1} and the deduced angular momentum l_γ carried away by the photon for prompt γ-ray transitions in ^{175}Pt. The anisotropy ratio R_{J1} was calculated according to Equation 3.3. The results for the A_4/A_0 coefficients were inconclusive, and they are only included in the Table to show the complete results of the fits.

E_γ (keV)	A_2/A_0	A_4/A_0	R_{J1}	l_γ ($\hbar$)
130.9(6)[a]	-0.15(8)	0.0(2)	0.82(6)	1
138.6(6)[a]			1.3(2)	2
244.1(4)[a]	0.09(2)	-0.05(4)	1.16(8)	2
291.8(6)[a]	-0.13(8)	0.1(2)	0.92(8)	1
328.6(4)[a]	0.21(1)	-0.05(2)	1.31(5)	2
362.5(5)[a]	0.09(3)	-0.03(5)	1.11(5)	2
382.2(4)[b]			1.0(2)	-
388.5(4)[a]	0.11(2)	0.01(2)	1.13(7)	2
423.2(4)[b]			0.9(2)	-
428.6(4)[b]			1.1(2)	2
436.4(4)[b]	0.23(4)	-0.03(5)	1.30(8)	2
437.3(5)[b]			1.3(2)	2
466.4(4)[b]	0.29(2)	0.02(3)	1.4(1)	2
487.4(6)[b]			1.0(2)	-
506.6(4)[b]			1.3(2)	2
554.6(4)[b]			1.4(2)	2

[a]The data for these γ rays were obtained from the α-tagged singles γ-ray energy spectra.
[b]The data for these γ rays were obtained from the γ-ray energy spectra obtained from the α-tagged–$\gamma\gamma$ matrix.

and 3×10^7 were collected for the matrix and cube, respectively. A 100-ns–coincidence condition between γ rays allowed the use of all DSSD y strips for recoil-α correlations for this analysis. Nevertheless, the fairly high probability of false recoil-α correlations permitted also a higher percentage of the prompt γ rays from other reaction products into the matrix and the cube. However, these γ rays were not correlated with the γ rays originating from the ^{175}Pt band structures. Observation of bands 3 and 4 is reported, for the first time, in the present work.

Figure 4.15(a) shows the total RDT prompt γ-ray energy spectrum, when $E_\alpha =$ 5968 keV was demanded for the α decays. Six other nuclei produced in the reaction used were still identified from this spectrum, underlining the problem of high event rates (see section 4.1) in the ^{175}Pt experiment. When only the low event-rate DSSD y strips were used (see Figure 4.1) for recoil-α correlations, a significant reduction of false recoil-α correlations was achieved, as shown in Figure 4.15(b). Candidates for newly observed transitions in ^{175}Pt are seen in this figure especially at $E_\gamma = 131, 139, 292, 389$

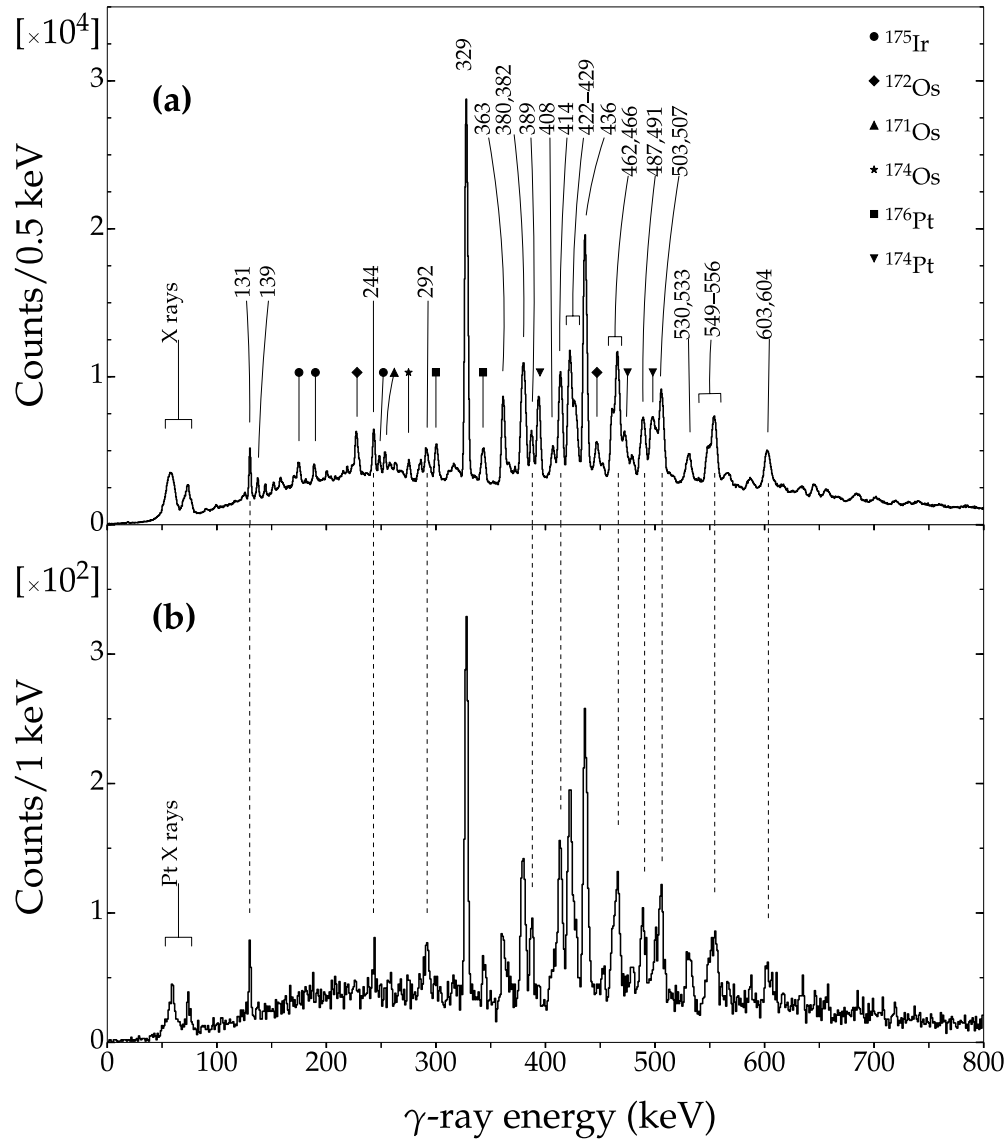

FIGURE 4.15: (a) The total prompt γ-ray energy spectrum of ^{175}Pt obtained with the RDT method using all DSSD y strips. Some of the strongest transitions assigned to ^{175}Pt are labelled in (a) together with transitions belonging to other reaction products marked with symbols. In (b) only the peripheral y strips of the DSSD were used for the recoil-α correlations; see Figure 4.1. Some of the transitions belonging to ^{175}Pt are marked with vertical dashed lines to highlight the reduction of the intensity of the other reaction products of Figure (a) in Figure (b). $E_\alpha = 5968$ keV and time-difference condition $\Delta t_{r,\alpha} \leq 7.5$ s were demanded for the α decays for both Figures.

and 422 keV. These transitions were not reported earlier by Cederwall *et al.* [Ced90].

In Figure 4.16(a) a sum of double-energy condition spectra from the RG-$\gamma\gamma\gamma$ cube is shown. In this Figure, spectra from double-energy conditions, between transitions in band 1 up to $I^{\pi} = (^{45}/_{2}^{+})$, were summed. Similarly, a sum of double-energy condition spectra between transitions in band 2 up to $I^{\pi} = (^{39}/_{2}^{+})$ is shown in Figure 4.16(b). The ordering and the energy of the transitions in bands 1 and 2 is in agreement with the published level scheme of Cederwall *et al.* [Ced90]. In the present work band 1 was extended up to $I^{\pi} = (^{49}/_{2}^{+})$. Band 2 was extended up to $I^{\pi} = (^{47}/_{2}^{+})$. The 138.6-keV and 244.1-keV transitions in band 2 are not seen in coincidence with the interband 382.2-keV transition. Thus the 138.6-keV and 244.1-keV transitions are placed to follow a parallel decay path with the 382.2-keV transition originating from the $(^{15}/_{2}^{+})$ state. Additionally, an inter-band transition with $E_{\gamma} = 431.4$ keV was observed when setting energy conditions on the 436.4-keV and 466.4-keV transitions in the $\gamma\gamma\gamma$ cube; see Figure 4.16(c). The $E_{\gamma} = 138.6$-keV and 431.3-keV transitions were not reported by Cederwall *et al.* [Ced90].

The energy spectrum of the γ rays in coincidence with the newly observed 130.9-keV transition in the RDT-$\gamma\gamma$ matrix is shown in Figure 4.17(a). Based on the measured angular distribution (see Table 4.7) the 130.9-keV transition is assigned to have $M1$ character. It is placed to de-excite an $I^{\pi} = (^{9}/_{2}^{-})$ state, feeding the ground state of ^{175}Pt according to total transition intensity and coincidences with the other transitions in bands 3 and 4. The 291.8-keV transition is seen in coincidence with the 130.9-keV transition and transitions above $I^{\pi} = (^{11}/_{2}^{-})$ state in band 3. The tentatively assigned 122.6-keV transition is very weak and thus the 291.8-keV transition was not seen in coincidence with transitions in band 4. Figure 4.17(b) shows the γ-ray energy spectrum when the energy condition was set on the 421.7-keV transition in the $\gamma\gamma$ matrix. This Figure highlights the newly observed γ rays of band 4 up to $I^{\pi} = (^{45}/_{2}^{-})$. Similarly, the newly observed members of band 3 are shown in Figure 4.17(c). The energy condition was set on 388.5 keV in the $\gamma\gamma$ matrix to obtain the energy spectrum of Figure 4.17(c). Coincidences with the most intense transitions in ^{175}Pt are seen in Figures 4.17(a)-(c) due to the Compton-scattered events, not vetoed by the anti-Compton shields. Additionally, the transitions belonging to band 3 are seen in Figure 4.17(b) as the 421.7-keV energy condition (band 4) overlaps partly with the 423.2-keV transition of band 3.

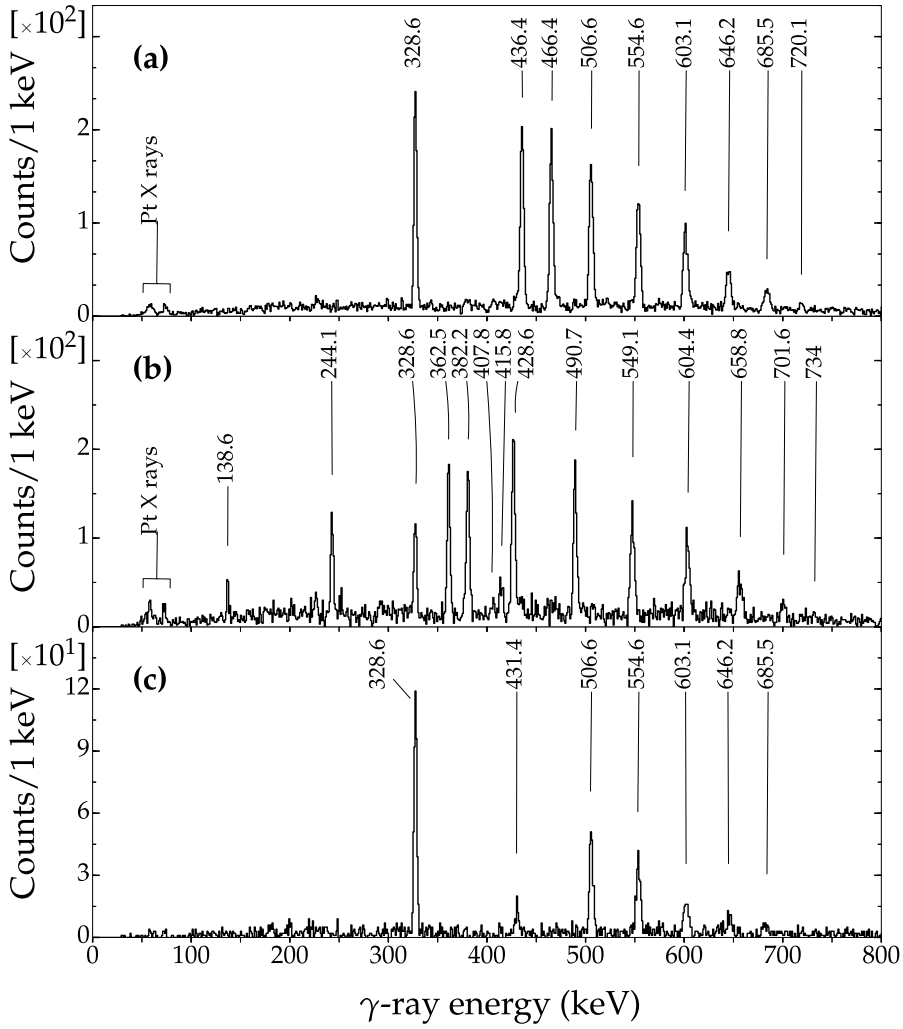

FIGURE 4.16: (a) Double-energy conditions for transitions in band 1 in ^{175}Pt were set up to $I^{\pi} = (^{45}/_{2}^{+})$ in the RG-$\gamma\gamma\gamma$ cube. The energy spectrum in (b) is the result of double-energy conditions set on transitions in band 2 up to $I^{\pi} = (^{39}/_{2}^{+})$. (c) An inter-band 431.4-keV transition is seen with the energy conditions set on the 436.4-keV and 466.4-keV transitions. See Figure 4.14 for the ^{175}Pt level scheme.

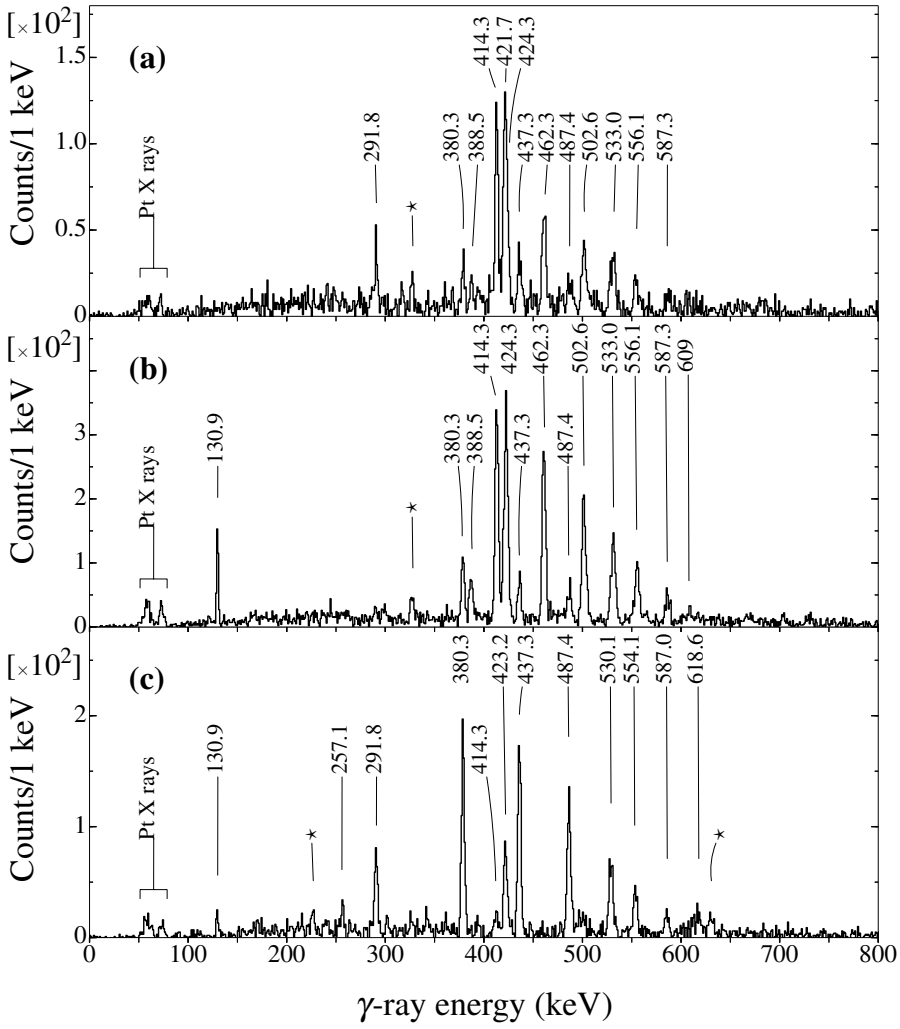

FIGURE 4.17: (a) Energy spectrum of prompt γ rays in ^{175}Pt in coincidence with the 130.9-keV transition in the α-tagged-$\gamma\gamma$ matrix. (b) Gamma rays assigned to band 4 in coincidence with the 421.7-keV γ-ray energy. (c) The γ-ray energy condition was set on the 388.5-keV transition, highlighting transitions in band 3 and inter-band transitions between bands 3 and 4. The α-particle energy condition was set to 5948 keV and the recoil-α time-coincidence window was $0 \leq \Delta t_{r,\alpha} \leq 7.5$ s. The highlighted coincidences (stars) in (a)-(c) are due to Compton-scattered events.

4.4.3 Search for an isomeric state in ^{175}Pt

No candidates for transitions originating from a possible isomeric state in ^{175}Pt were observed in this work. For ^{173}Pt, the observed $I^{\pi} = (13/2^{+})$ isomeric state was placed at an excitation energy of 248.5 keV, 145 keV above the $(9/2^{-})$ state (see Section 4.3.1). An $I^{\pi} = (13/2^{+})$ isomeric state was also observed to feed the $(9/2^{-})$ state in ^{171}Pt [Sch10]. In ^{177}Pt [Dra90] and ^{179}Pt [Bag09], the $13/2^{+}$ state, within the positive-parity band, is observed 68 keV and 162 keV above the $9/2^{-}$ state of the $5/2^{-}$ [512] band, respectively. In Figure 4.18 the level energy of the $13/2^{+}$ state is compared to that of the $9/2^{-}$ state for ^{171,173,177,179}Pt. Based on this systematic behaviour of the $13/2^{+}$–state level energy, this state was assumed to be at most 200 keV above the $9/2^{-}$ state in ^{175}Pt. A Weisskopf estimate for a $\leq$ 200-keV $M2$-type γ-ray transition probability was calculated [Kra88, p. 332]. Taking into account the corresponding total-conversion coefficient $\alpha(M2)$ [Kib08], a $t_{\frac{1}{2}} \approx 10$ μs for the $13/2^{+}$ state is obtained. Already with a transition energy of 100 keV, this $M2$ transition would proceed mainly via internal conversion, as the conversion coefficient would be $\approx$ 60 [Kib08]. However, if this transition would feed the $(9/2^{-})$ state at an excitation energy of 130.9-keV, the transition from this state would most

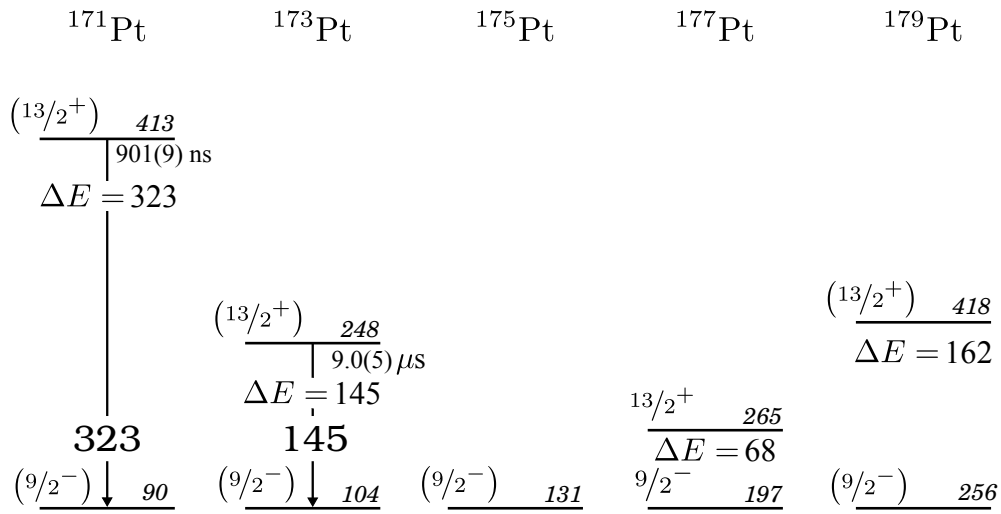

FIGURE 4.18: The level energy of the $13/2^{+}$ state is compared to the level energy of the $9/2^{-}$ state for ^{171,173,177,179}Pt. The energy differences between the states (ΔE) and the level and transition energies are given in units of keV. In ^{171,173}Pt isotopes an $M2$ transition, originating from the $13/2^{+}$ state, feeds the $9/2^{-}$ state. In the present work, the $13/2^{+}$ state was not observed in ^{175}Pt. The data for ^{171}Pt, ^{177}Pt and ^{179}Pt were taken from [Sch10], [Dra90] and [Bag09], respectively. Data for ^{173}Pt and ^{175}Pt are from the present work.

likely have been detected by the focal-plane Ge detectors. Correlation times up to 10 ms between recoil-implantation events in the DSSD and γ-ray events at the focal plane were used, while a search for a possible decay from an isomeric-state was carried out. No candidate or a sign of a 130.9-keV transition were found.

It is also possible that the $^{13}/_{2}^{+}$ state is below the $^{9}/_{2}^{-}$ state in ^{175}Pt. In this case the $^{13}/_{2}^{+}$ state could decay via an $E3$ transition to the $^{7}/_{2}^{-}$ ground state of ^{175}Pt. The estimated half-life for this transition ($E_{\mathrm{ex}} \leq 130.9$-keV) is approximately 50 ms. The Weisskopf estimate for an $E3$-type γ-ray transition probability [Kra88, p. 332] and the corresponding total-conversion coefficient [Kib08] were used to estimate the half-life. No candidates for an $E3$-type transition were found. The GREAT-detector setup in this experiment was far less sensitive to detect a highly-converted ($\alpha_L > 10$) $t_{\frac{1}{2}} \approx 50$-ms transition than a ≈ 10-μs $M2$-type transition followed by a 130.9-keV $M1$-type transition. The conversion-electron detection threshold for the PIN detectors was (70-90) keV in the experiment. Therefore an $E3$-type transition of < 100 keV would not have been detected in the PIN diodes, as the conversion-electron energy after the internal L conversion would be less than 88 keV. The high conversion coefficient ($\alpha_L \approx 20 - 300$) also makes the γ-ray transition intensity weak. Due to the long search time required between a recoil-implantation event and a γ-ray event, these weak γ rays would not be seen above the γ-ray background. Thus, it is likely, that in ^{175}Pt, the $^{13}/_{2}^{+}$ state lies at an excitation energy of ≤ 131 keV.

Chapter 5

Discussion

5.1 Alpha decay

The ground-state $I^{\pi}_{gs} = (7/2^-)$ assignments for ^{173}Pt and ^{175}Pt are based on the results obtained from α-decay spectroscopy. For both nuclei, the unhindered α decays (see Table 4.2 and 4.5) were used for these deduced assignments. The details for these conclusions are discussed below.

The ^{173}Pt ground-state is observed to α decay mainly to a $(7/2^-)$ state in ^{169}Os. Hild *et al.* assigned the ^{169}Os ground-state I^{π} to be $5/2^-$, based on the unhindered α decay to a $5/2^-$ state in ^{165}W [Hil95]. The excited state at 35.0 keV in ^{169}Os has $I^{\pi} = (7/2^-)$, as the 35.0-keV transition was assigned an $M1$ type in the present work. Previously [Bag08, Goo04a] an unhindered α-decay branch was assigned to connect the ground-states of ^{173}Pt and ^{169}Os. In the present work, the unhindered α decay to the $I^{\pi} = (7/2^-)$ state is firmly established. The 135.7-keV transition in ^{169}Os was reported earlier to be in coincidence with the $E_{\alpha} = 6100$-keV decay branch [Goo04a]. In the present work this coincidence between the reported α decay and the subsequent γ-ray transition was not observed. It can be argued that the coincidence observed by Goon [Goo04a], is due to summing of $E_{\alpha} = 6063$ keV and conversion electrons from the 35-keV transition in the DSSD (see Figure 4.3(c)). No sign of the reported $E_{\alpha} = 6133$-keV α decay in coincidence with a $E_{\gamma} = 101$-keV transition [Goo04a] was observed in the present work. The $b_{\alpha} \approx 2$ % value of this decay branch, reported by Goon, is twice as large as the b_{α} values reported for the decays with $E_{\alpha} = 6067$ keV and $E_{\alpha} = 6100$ keV [Goo04a, Bag08]. A 101-keV $M1$ or $E2$ transition, following an α

decay of the reported intensity, would have been detected by the Ge detectors in the GREAT spectrometer. The E_α = 6063-keV decay branch is assigned, in the present work, to feed a $I^\pi = (9/2^-)$ state in ^{169}Os, based on the $M1$-type assignment of the 35.0-keV and 135.7-keV transitions.

The unhindered α decay of the ^{175}Pt ground state was assigned to feed a $(7/2^-)$ state in ^{171}Os. The ^{171}Os ground state has been assigned to have $I^\pi = (5/2^-)$ by Bark *et al.*. This assignment was based on the largest calculated contribution to the wave function originating from the $5/2^-$ [523] Nilsson orbital [Bar90]. As an $M1$ character was deduced for the 76.7-keV transition in the present work, it is assigned to originate from a $(7/2^-)$ state in ^{171}Os. Thus, the unhindered α decay connects the $I^\pi = (7/2^-)$ ground state of ^{175}Pt with the $(7/2^-)$ state in ^{171}Os. This I^π assignment of the ^{175}Pt ground state has already been pointed out by Kondev *et al.* [Kon02], and is confirmed here by the measured $M1$ character of the 76.7-keV transition in ^{171}Os.

The ground-state I^π assignments for ^{173}Pt and ^{175}Pt are also supported by the results published for A = 177 and 179 isotopes of Hg, respectively. For ^{177}Hg, only one α-decay branch was reported by Hagberg *et al.* [Hag79]. The large reduced width of this decay suggests an unhindered decay to ^{173}Pt. In an α-decay study of ^{181}Pb by Andreyev *et al.*, an assignment of $I^\pi_{gs} = (7/2^-)$ for ^{177}Hg was made [And09]. Their assignment is based on an unhindered ^{181}Pb α decay to a $(9/2^-)$ excited state in ^{177}Hg and the observation of a 77.2-keV $M1$ transition in ^{177}Hg following the α-decay events. The 77-keV transition was also reported to be in coincidence with a 246-keV $M2$ transition originating from a $I^\pi = (13/2^+)$ state by Melerangi *et al.* [Mel03].

For ^{183}Pb, the unhindered α decay from a $13/2^+$ state was reported by Jenkins *et al.* to be in delayed coincidence with a 111-keV $M2$ and a 61-keV $M1$ transitions in ^{179}Hg [Jen02]. The $I^\pi_{gs} = 7/2^-$ assignment for ^{179}Hg supports the $I^\pi_{gs} = (7/2^-)$ assignment for ^{175}Pt, as the known α decay from ^{179}Hg is unhindered [Hag79]. To conclude, the ^{173}Pt and ^{175}Pt ground states can be assigned to have $I^\pi_{gs} = (7/2^-)$ based on their α-decay parent lineage.

The hindered ($F > 4$) α-decay branches of ^{173}Pt and ^{175}Pt are assumed to take place between initial and final states having different configurations. The E_α = 5819-keV decay branch observed in this work for ^{175}Pt has $F = 20(6)$. This hindrance factor agrees with $F = 21(4)$, for the E_α = 6021-keV ground-state to ground-state decay. This points towards similar configurations for the $9/2^-$ and $5/2^-$ states of ^{171}Os. The α decay leading to the 211.2-keV state in ^{171}Os has a considerably smaller hindrance factor F

of $\approx 4-6$. The value extracted for F depends on the assumed final state I^π, and thus on the angular momentum carried away by the α particle. The $E_\alpha = 6063$-keV decay branch of ^{173}Pt, to the $I^\pi = (9/2^-)$ state in ^{169}Os, is also hindered. Based on these observed hindrance factors of the α decays, it appears that these $I^\pi = (9/2^-)$ states both in ^{169}Os and ^{171}Os have a different configuration compared to the $I^\pi = (7/2^-)$ states in both nuclei.

5.2 Isomeric $13/2^+$ state in ^{173,175}Pt

A reduced transition probability of $B(M2) = 0.070(4)$ W.u. is extracted for the observed 145.0-keV $M2$ transition in ^{173}Pt. Equation 2.17 was used to obtain the $B(M2)$ value, together with a total conversion coefficient of $\alpha\,(M2; 145.0\text{ keV}) = 14.73$ [Kib08]. Observation of $M2$-type transitions depopulating isomeric $I^\pi = 13/2^+$ states have been reported by Scholey *et al.* for ^{171}Pt, ^{167}Os and ^{163}W [Sch10]. The corresponding $B(M2)$ values are 0.105(2) W.u., 0.118(2) W.u. and 0.11(4) W.u., respectively. Also in ^{175}Hg [O'D09] and ^{177}Hg [Mel03] a $13/2^+$ isomeric state has been observed. For these two nuclei, $B(M2)$ values of 0.10(2) W.u. and 0.14(2) W.u., respectively, were calculated. These isomeric states are shown in Figure 5.1 together with $B(M2)$ values, half-lives and transitions depopulating the $13/2^+$ and $9/2^-$ states. The $B(M2)$ value, obtained in the present work for the decay of the $13/2^+$ state in ^{173}Pt, is of the same order of magnitude as the corresponding values for the nuclei mentioned above.

The Weisskopf estimates for the γ-ray transition probabilities are only order-of-magnitude estimates, or upper limits, for the transition probabilities due to a single-proton transition [Bla60, p.627]. Thus, the observed hindrance is assumed to highlight the single-particle character of the observed $M2$-type transition in ^{173}Pt.

The nonobservation of an isomeric state in ^{175}Pt points towards the possibility that in ^{175}Pt, the yrast–$13/2^+$ state lies below the $9/2^-$ state. A trend of decreasing excitation energy of the $13/2^+$ state compared to the $9/2^-$ state is observed, when going from ^{171}Pt to ^{173}Pt (see Figure 4.18). Additionally, in ^{177}Pt the $13/2^+$ state is observed at excitation energy of only 67.3-keV compared to the $9/2^-$ state (see Section 4.4.3). These observations support the assumption of the $13/2^+$ state having a smaller excitation energy than the $9/2^-$ state in ^{175}Pt.

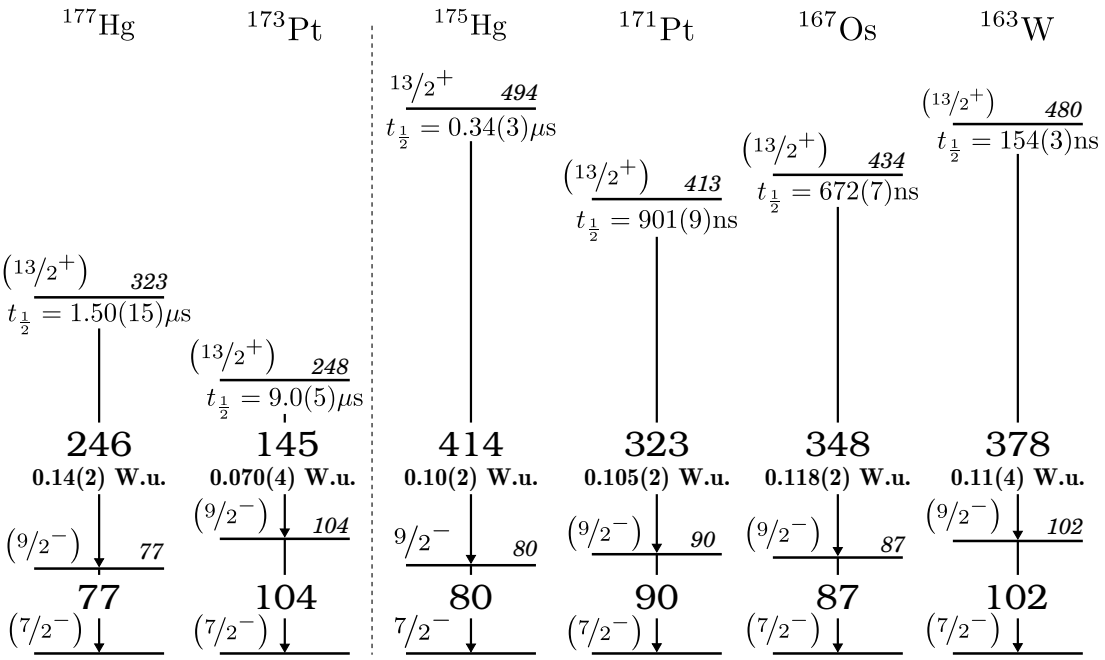

FIGURE 5.1: The $^{13}/_{2}^{+}$ and $^{9}/_{2}^{-}$-state excitation energies with respect to the observed $^{7}/_{2}^{-}$ states for ^{171,173}Pt, ^{175,177}Hg, ^{167}Os and ^{163}W. For the $^{13}/_{2}^{+}$ states, also the measured half-lives are given. $B(M2)$ values are given below the transitions that depopulate the isomeric $^{13}/_{2}^{+}$ states. $B(M2)$ values were calculated using Equation 2.17. The total conversion coefficients for the calculations were taken from BrIcc [Kib08]. The dashed line separates the two α-decay chains considered. Data were taken from [Sch10] (^{171}Pt, ^{167}Os and ^{163}W), [O'D09] (^{175}Hg) and [Mel03] (^{177}Hg). The energies of the transitions and excited states are given in keV units.

5.3 Prompt γ-ray spectroscopy

For ^{175}Pt, the experimental $^{B(M1)}/_{B(E2)}$ ratios of reduced transition probabilities of the negative-parity band were compared with theoretical predictions of Dönau and Frauendorf [Dön83, Dön87]. Theoretical values were calculated for a negative-parity band of ^{175}Pt, assuming $^{7}/_{2}^{-}$ [514] and $^{7}/_{2}^{-}$ [503] configurations for the band heads. These configurations originate from the $h_{9/2}$ and $f_{7/2}$ single-particle orbitals, respectively. In the

equation [Dra90]

$$\frac{B(M1, I \to I-1)}{B(E2, I \to I-2)} = \frac{12}{5}\frac{K^2}{Q_0^2 \cos^2(30^\circ+\gamma)}\left[1-\frac{K^2}{(I-1/2)^2}\right]^{-2} \times \left[(g_a - g_R)\left(\sqrt{1-\frac{K^2}{I^2}} - \frac{i_a}{I} \pm \frac{\Delta e'}{\omega}\right) - (g_b - g_R)\frac{i_b}{I}\right]^2, \tag{5.1}$$

a quadrupole moment of $Q_0 = 6$ e·b and a γ deformation of -21° were used for the calculations. The γ-deformation value is based on calculations by Cederwall *et al.* [Ced90, Fig.11] and Joss [Jos14]. Aligned angular momentum of the strongly coupled neutron (i_a) was taken to be 1 $\hbar$, based on the observed aligned angular momentum (see Figure 5.3(d)). A quasiparticle alignment was not assumed to take place at the low ω values considered, thus i_b of the aligned quasiparticles was taken to be zero. The rotating core g-factor was taken to be $g_R \approx Z/A = 0.45$ [Boh73, p.54]. Additionally, single-particle g-factors were calculated, within the Schmidt model, to be[a] $g_a\left(\nu h_{9/2}\right) = 0.243$, $g_a\left(\nu f_{7/2}\right) = -0.383$ for neutrons (ν) [Bla60, pp.38–39]. The signature splitting term $\Delta e'$ was taken to be zero.

The experimental ratio can be written as [Dra90]

$$\frac{B(M1, I \to I-1)}{B(E2, I \to I-2)} = 0.0693\frac{16\pi}{5}\frac{[E_\gamma(I \to I-2)]^5}{[E_\gamma(I \to I-1)]^3\,\lambda(1+\delta^2)}, \tag{5.2}$$

where the $^{M1}/_{E2}$-mixing ratio $\delta = 0$ is assumed for the $\Delta I = 1$ transition. The branching ratio λ is defined as

$$\lambda = \frac{I_\gamma\,(I \to I-2)}{I_\gamma(I \to I-1)}. \tag{5.3}$$

Experimental $^{B(M1)}/_{B(E2)}$ ratios are compared with the theoretical predictions in Figure 5.2. The experimental values at $I = {}^{17}/_2$ and $I = {}^{19}/_2$ are upper-limits. They are based on the estimated maximum intensity the corresponding unobserved $M1$ transitions could have had. According to Figure 5.2, the $^7/_2^-$ [514] configuration, of $h_{9/2}$ single-particle origin, is the favoured configuration for the ground-state band of ^{175}Pt. At $I = {}^{11}/_2$ the experimental $^{B(M1)}/_{B(E2)}$ ratio is seen to be ≈ 3 times larger than the theoretical prediction for the $^7/_2^-$ [514] configuration. Similar behaviour of the $^{B(M1)}/_{B(E2)}$ ratios has been reported by Bark *et al.* for ^{171}Os and ^{173}Os [Bar90, Fig.14].

[a] g_s (eff) $= 0.7 \times g_s$ (free) was assumed [Boh73, p.304].

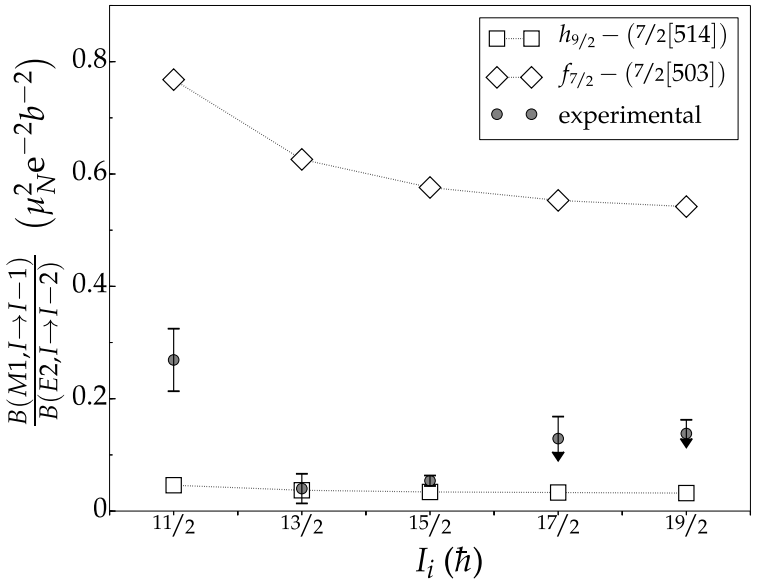

FIGURE 5.2: The theoretical $^{B(M1)}/_{B(E2)}$ ratios (open symbols) are compared with the experimental values (filled circles) for the negative-parity band in ^{175}Pt. Experimental values at $I = {}^{17}/_{2}$ and $I = {}^{19}/_{2}$ are upper-limit estimates for the maximum intensity of the unobserved $M1$-type transitions. The theoretical values are connected with the dotted lines to guide the eye. Experimental values were extracted from the RDT-$\gamma\gamma$ matrix.

In ^{175}Pt the $^{7}/_{2}^{-}$ band-head wave function may have a larger component of the $^{7}/_{2}^{-}$ [503] Nilsson configuration, compared with the states at higher angular momentum.

5.3.1 Aligned angular momenta

The aligned angular momenta (see section 2.4) for the $N = 95$ and $N = 97$ isotones of Pt, Os, W and Hf are shown in Figures 5.3(a)-(d). For the $N = 95$ isotones reference-configuration parameters, $J_0 = 13$ MeV$^{-1}\hbar^2$ and $J_1 = 85$ MeV$^{-3}\hbar^4$, of ^{171}Os [Bar90] were used. The parameters $J_0 = 35$ MeV$^{-1}\hbar^2$ and $J_1 = 45$ MeV$^{-3}\hbar^4$ were used for the $N = 97$ isotones [Esp94]. Additionally, cranked shell-model calculations for ^{175}Pt were performed, using deformation parameters $\beta_2 = 0.18$, $\beta_4 = 0$ and $\gamma = -21°$ [Ced90, Jos14]. These calculations were performed according to references [Naz85, Cwi87, Wys88], using a universal Woods-Saxon single-particle potential. The results of the calculations as quasiparticle Routhians are shown in Figures 5.4(a)-(b). The labelling used for the neutron and proton quasiparticle orbitals is given in Table 5.1.

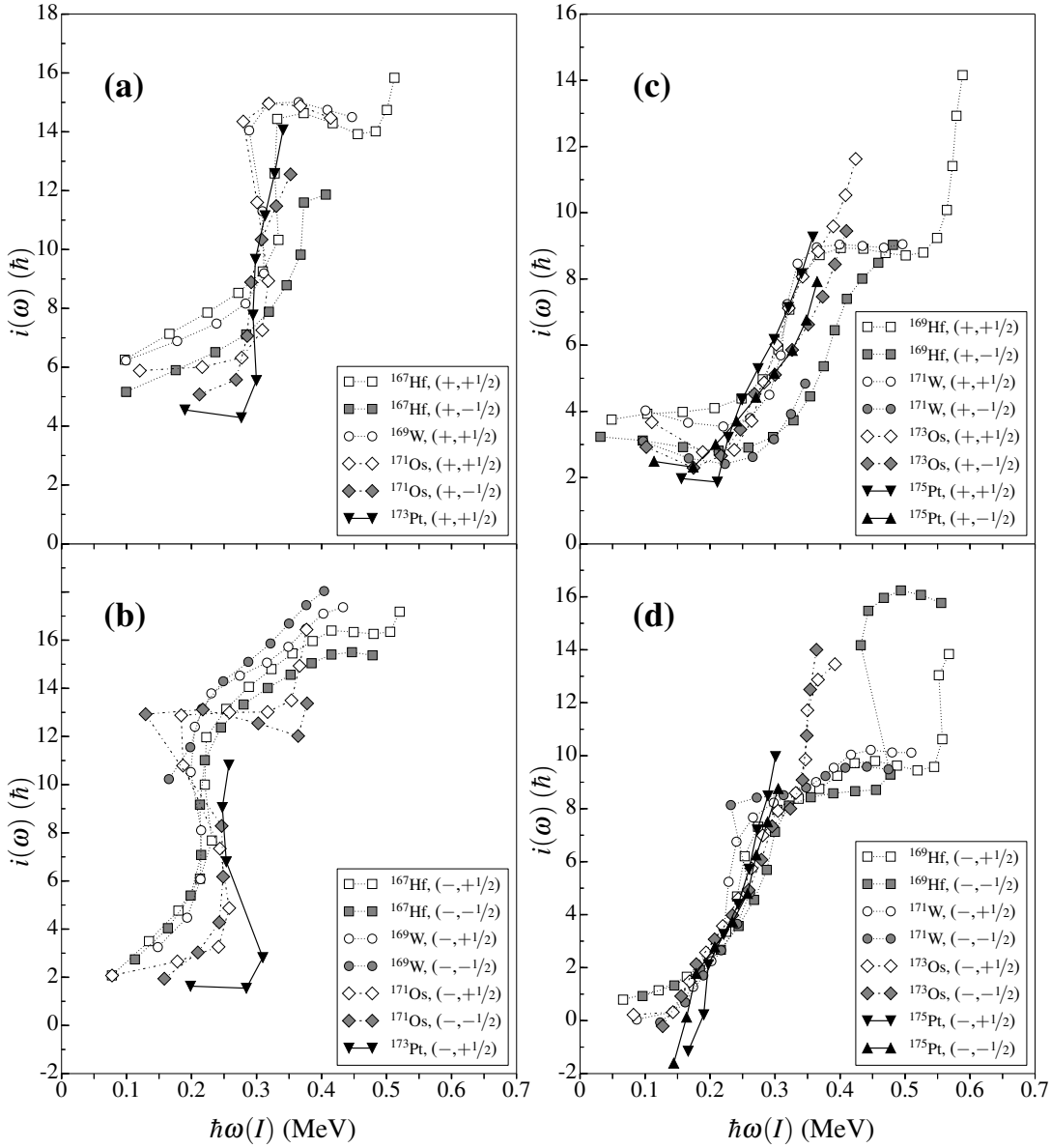

FIGURE 5.3: Aligned angular momenta are plotted for the $N = 95$ isotones (a & b) and $N = 97$ isotones (c & d) of Pt, Os, W and Hf. In (a) and (c) $i(\omega)$ for the positive-parity bands are plotted, whereas in (b) and (d) $i(\omega)$ for the negative-parity bands are plotted. For the $N = 95$ isotones the data are from [Bar90, Bar99a] (^{171}Os), [Rec85] (^{169}W) and [Cro99] (^{167}Hf). For the $N = 97$ the data are from [Bar90, Kal91] (^{173}Os), [Esp94] (^{171}W) and [Sch01] (^{169}Hf). The reference-configuration parameters $J_0 = 13$ MeV$^{-1}\hbar^2$, $J_1 = 85$ MeV$^{-3}\hbar^4$ [Bar90] and $J_0 = 35$ MeV$^{-1}\hbar^2$, $J_1 = 45$ MeV$^{-3}\hbar^4$ [Esp94] were used for $N = 95$ and $N = 97$ isotones, respectively.

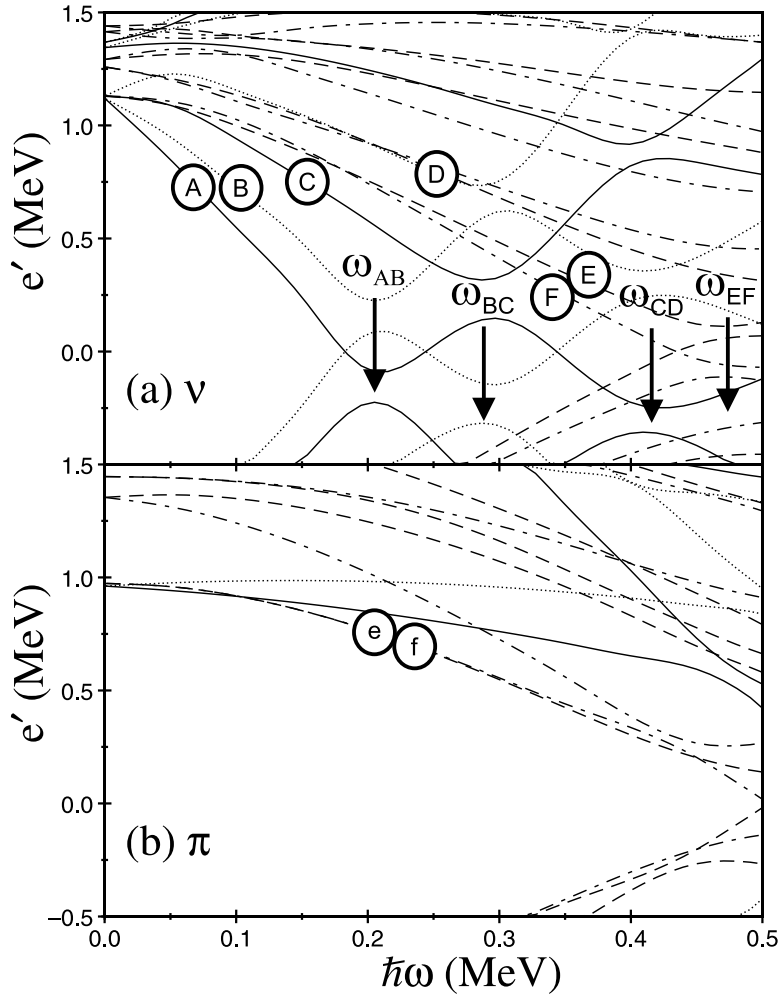

FIGURE 5.4: Calculated energy in the rotating coordinate system (Routhian) of the single-particle states in ^{175}Pt as a function of $\hbar\omega$ for neutrons (a) and protons (b). The crossing frequencies of AB, BC, CD and EF neutron-quasiparticle configurations are marked by arrows in (a). The calculation was performed using $\beta_2 = 0.18$, $\beta_4 = 0$ and $\gamma = -21°$. The quasiparticle labelling used in (a) and (b) is explained in Table 5.1. (Figure and corresponding calculations by D.T. Joss [Jos14]).

TABLE 5.1: The labelling of neutron (ν) and proton (π) quasiparticle orbitals in this work. The index numbering for (π,α), orders the orbitals according to excitation energy, separately for positive and negative-parity. Furthermore, the index numbering is separate for neutrons and protons.

Label	Parity, Signature (π,α)	Main shell-model component
A	$\nu(+,+\frac{1}{2})_1$	$i_{13/2}$
B	$\nu(+,-\frac{1}{2})_1$	$i_{13/2}$
C	$\nu(+,+\frac{1}{2})_2$	$i_{13/2}$
D	$\nu(+,-\frac{1}{2})_2$	$i_{13/2}$
E	$\nu(-,-\frac{1}{2})_1$	$h_{9/2}/f_{7/2}$
F	$\nu(-,+\frac{1}{2})_1$	$h_{9/2}/f_{7/2}$
e	$\pi(-,-\frac{1}{2})_1$	$h_{9/2}/h_{11/2}$
f	$\pi(-,+\frac{1}{2})_1$	$h_{9/2}/h_{11/2}$

In ^{173}Pt, the $(\pi,\alpha) = (+,+\frac{1}{2})$[b] band structure gains at least 10 $\hbar$ of alignment at $\hbar\omega \approx 0.30$ MeV (Figure 5.3(a)). A similar alignment for the positive-parity bands is seen in all the $N = 95$ isotones of Figure 5.3(a). In ^{171}Os this has been attributed to the BC neutron alignment with an estimated 9 $\hbar$ contribution to the aligned angular momentum [Bar90, Bar99a]. The rotational alignment of the second and third $i_{13/2}$ neutrons is attributed to this BC crossing. The BC neutron alignment was assumed to be responsible for the observed alignment gain also in ^{169}W [Rec85] and ^{167}Hf [Cro99]. Based on these similarities, the alignment in the $(+,+\frac{1}{2})$ band of ^{173}Pt is attributed to a BC alignment. The calculated neutron BC-crossing frequency $\hbar\omega \approx 0.28$ MeV (Figure 5.4(a)) for ^{175}Pt also agrees with the frequency of the observed alignment in ^{173}Pt. The neutron-AB alignment is seen to occur before the BC alignment in Figure 5.4(a). However, this AB alignment is blocked for the $i_{13/2}$ $\nu(+,+\frac{1}{2})$ and $\nu(+,-\frac{1}{2})$ bands as a neutron already occupies either the A or B orbital.

In the $(-,+\frac{1}{2})$ band of ^{173}Pt, an alignment shown in Figure 5.3(b) is seen to occur at a somewhat lower frequency compared with the $(+,+\frac{1}{2})$ band. This frequency ($\hbar\omega \approx 0.25$ MeV) is comparable to the observed frequencies for the lighter $N = 95$ isotones. For the negative-parity bands, the neutron-AB alignment is not blocked,

[b]Later on in this section a shorthand notation is used, where the symbols (π,α) for parity and signature are not repeated.

making it a likely candidate for the observed alignment. In the $N = 95$ isotones of Os, W and Hf, the AB alignment is assumed to take place in the negative-parity bands, with a $\Delta i \approx 9\ \hbar$ gain in the alignment [Bar99a, Rec85, Cro99]. In ^{173}Pt the negative-parity band is not observed to high enough angular momentum to determine the total gain (Δi) to the initial alignment. However, based on the similar alignment frequency, which is lower than the observed frequency for the BC alignment, an AB neutron alignment is assigned to occur also in the ^{173}Pt $(-, +\frac{1}{2})$ band.

The picture of the observed alignments for the $\pi = +$ bands in the $N = 97$ isotones is similar to the $N = 95$ isotones discussed above. In ^{169}Hf [Sch01], ^{171}W [Esp94] and ^{173}Os [Bar90] the observed alignments in the $i_{13/2}$ bands have been attributed to the $A \rightarrow ABC$ and $B \rightarrow BAD$ alignments. The ^{175}Pt $(+, +\frac{1}{2})$ and $(+, -\frac{1}{2})$ bands in Figure 5.3(c) can be seen to gain at least 6 $\hbar$ of alignment at $\hbar\omega \approx 0.30$ MeV. A corresponding alignment gain is observed also for the lighter $N = 97$ isotones. The calculated neutron BC and AD alignment frequencies of $\hbar\omega \approx 0.28$ MeV shown in Figure 5.4(a) agree with the observed alignments. Hence the picture of $i_{13/2}$ BC and AD neutron alignments is seen to prevail also in ^{175}Pt.

When compared with each other, the negative-parity bands of the $N = 97$ isotones show much the same alignment frequency ($\hbar\omega \approx 0.25$ MeV, Figure 5.3(d)). The calculations shown in Figure 5.4(a) predict this alignment to occur at $\hbar\omega \approx 0.21$ MeV, which is in reasonable agreement with the observations. These alignments have been attributed to the neutron-AB alignment in all three mentioned $N = 97$ isotones lighter than Pt [Sch01, Esp94, Bar90]. Based on the CSM-calculation results and on the observations in the lighter isotones, an AB neutron alignment is assumed to take place in the negative-parity band of ^{175}Pt.

In the $N = 95$ isotones the alignments are seen to be more sudden, compared with the more gradual alignments observed for the $N = 97$ isotones (see Figure 5.3). This signifies a stronger interaction between the 1-quasiparticle (1-qp) and 3-qp band structures in the $N = 97$ isotones compared to those in the $N = 95$ isotones [Ste75]. A proton-quasiparticle alignment below $\hbar\omega = 0.4$ MeV is not probable according to CSM-calculation results presented in Figure 5.4(b). This has been discussed earlier by McGowan *et al.* [McG91, pp.501–504] along with similar results obtained for the calculated proton-quasiparticle Routhians for ^{169}Hf [Sch01], ^{171}W [Esp94] and ^{173}Os [Bar90].

It should be noted that in the present work, the CSM reference-configuration parameters J_0 and J_1 used for the $N = 97$ isotones in Figures 5.3(c)-(d) differ from the

parameters used by Peura *et al.* [Peu14]. This difference in the reference parameters is due to the choice to compare the $N = 95$ and $N = 97$ isotones with the same parameters for each isotone group. However, this does not change the interpretation of the frequency of alignment in ^{175}Pt. The choice of neighbouring reference configuration for ^{173,175}Pt is not obvious as ^{174}Pt [Dra91, Goo04b] and ^{176}Pt [Dra86, Ced90] have been interpreted to have shapes of different deformation at low excitation energy.

5.4 Deformation considerations

The observation of rotational bands can be taken as a fingerprint for deformation in both nuclei studied in this work. Additionally, the nonobservation of negative-signature bands in ^{173}Pt, points toward a decreasing β_2 deformation compared with ^{175}Pt. As the nuclear deformation decreases, the Coriolis force can readily align nucleons along the rotational axis. Especially when the Fermi surface is located near the low-Ω deformed shell-model orbitals, the rotational alignment is predicted to be possible even at low rotational frequencies [Ste75]. The effect of the rotational alignment of a single-particle is manifest in increased signature splitting. For ^{173}Pt the Fermi surface lies low in the $i_{13/2}$ orbital. Additionally, the ground state of ^{173}Pt is predicted to have a positive β_2 deformation value [GR14b]. This situation is similar to the example given by Stephens for a single-particle state based on an $h_{11/2}$ orbital, where the decoupled band is predicted for a prolate nucleus (see [Ste75, Fig.12]). Compared with the rotational bands observed in ^{175}Pt, the signature splitting in ^{173}Pt causes the unfavoured-signature band to be weakly populated. Thus, in the region of the nuclear chart where ^{173,175}Pt lie, the strong coupling of single-particle motion competes with weak-coupling and rotation-decoupling modes as the neutron number decreases.

For ^{177}Pt the spectroscopic results can be explained assuming the nucleus to be a well-deformed rotor with $\beta_2 \approx 0.2$ [Dra90]. As the low-lying excited states in ^{171,172}Pt are already seen to be predominantly vibrational in character [Ced98], it is reasonable to assume that ^{173}Pt and ^{175}Pt could have shapes of different deformation coexisting at low excitation energies. Total Routhian surface (TRS) calculations for ^{174,176}Pt show that both nuclei are soft along the axis of γ deformation (γ soft) when $\hbar\omega = 0$ MeV [Ced90, Fig.6(a)]. When the TRS calculation is performed above the $i_{13/2}$ neutron-crossing frequency of 0.33 MeV, both nuclei are seen to have a well-deformed minimum at $\gamma \approx 0°$, $\beta_2 \approx 0.2$ [Ced90, Fig.6(b)]. More recent theoretical calculations

predict the prolate ground-state deformations of $\beta_2 \approx 0.17 - 0.3$ for ^{172,174,176}Pt to coexist with a γ-soft triaxial shape [GR14b]. A TRS calculation for odd-mass Pt isotopes predicts the ^{175}Pt ground state to be γ soft with $\beta_2 \approx 0.15 - 0.2$ [Hil92], in agreement with the results obtained for the even-A Pt isotopes. The irregularities at $\hbar\omega \approx 0.2$ MeV in the $i\,(\omega)$ plots for ^{175}Pt (Figures 5.3(c)-(d)) can be taken as a sign of a changing deformation, as the rotational frequency increases. These low-frequency alignments ($\hbar\omega < 0.2$ MeV) of the observed negative-parity bands in ^{175}Pt could be due to a deformed configuration, which is different from the configuration (E or F; see Table 5.1) where the assumed neutron-AB alignment takes place.

In Hg and Pb isotopes these low-lying deformed structures are assigned to be based on intruding multi-particle multi-hole (*mp-mh*) excitations. These excitations are across the $Z = 82$ energy gap between major shells [Hey11]. Also for neutron-deficient Os and Re isotopes, this proton *mp-mh* excitation has been suggested to be the cause of the observed low-frequency alignment changes [Bar91]. The irregularities in the positive- and negative-parity bands in ^{175}Pt occur at similar rotational frequencies. This could be taken as a sign of a *mp-mh* excitation.

$B(E2)$ values, obtained from lifetime measurements of the low-lying excited states in ^{173,175}Pt, could provide more direct information on the deformation in these nuclei. $B(E2)$ values for the $^{17}/_{2}^{+} \rightarrow {}^{13}/_{2}^{+}$ and $^{21}/_{2}^{+} \rightarrow {}^{17}/_{2}^{+}$ transitions in ^{175}Pt have been reported by Watkins [Wat11]. The increase of the $B(E2)$ values, when the angular momentum increases, was attributed to a change in the deformation of ^{175}Pt. Both ^{173}Pt and ^{175}Pt have many γ-ray transition energies that are doublets. For this reason, the lifetime measurements would need to be performed using $\gamma\gamma$ matrices. Thus, although the cross sections for producing these Pt isotopes are relatively large, the $\gamma\gamma$-coincidence requirement makes these experiments challenging.

Coulomb-excitation studies can be utilized to yield information on the low-lying excited state configurations [Hey11, p.1502]. However, Coulomb-excitation experiments are currently not feasible for ^{173,175}Pt, as studying these nuclei would require a radioactive ^{173}Pt ion beam with high intensity. Moreover, experiments employing laser spectroscopy would be desirable for the determination of the ground-state angular momentum and parity for Pt isotopes below $A = 178$.

Chapter 6

Summary

Transitions de-exciting the negative-parity states at $E_{\rm ex}$ = 35-keV and 171-keV in ^{169}Os have been observed in coincidence with the α decay of ^{173}Pt. These states are assigned to have $I^{\pi} = (7/2^{-})$ and $I^{\pi} = (9/2^{-})$, respectively. The ground-state $I^{\pi} = (7/2^{-})$ for ^{173}Pt was established, based on the α-decay fine structure of ^{173}Pt. Also for ^{175}Pt, the fine-structure α-decay results presented, confirm the ground-state $I^{\pi} = (7/2^{-})$ assignment. In addition, a newly observed α-decay branch in ^{175}Pt, with $E_{\alpha} = 5819$ keV, was established. This decay feeds an $I^{\pi} = (7/2^{-})$ excited state at 207.9-keV in ^{171}Os, which has been observed before only in an in-beam γ-ray study [Bar90].

In ^{173}Pt, an $I^{\pi} = (13/2^{+})$ isomeric state was observed with $t_{\frac{1}{2}} = 9.0(5)$ μs. The extracted value for the reduced transition probability for the 145.0-keV $M2$ transition, depopulating the isomeric state, is $B(M2) = 0.070(4)$ W.u. This is similar to the corresponding values obtained in this region of nuclei. The hindered $B(M2)$ value is assumed to be a sign of a single-particle type transition between states based on the $i_{13/2}$ and $h_{9/2}$ shell-model orbitals. In ^{175}Pt this isomeric state was not observed, and it is assumed to lie below the $9/2^{-}$ state in ^{175}Pt. This assumption is based on the systematic behaviour of the $13/2^{+}$-state excitation energy with respect to the $9/2^{-}$ state in the neighbouring Pt isotopes, together with the capabilities of the experimental setup in the present work.

For both ^{173}Pt and ^{175}Pt, the previously reported [Ced90, Jos06] positive-parity band structures were confirmed and extended. Negative-parity bands were observed for both nuclei, in the present work. The differences in band structures, observed between ^{175}Pt and ^{173}Pt (for both $\pi = +$ and $\pi = -$ bands), were assumed to arise due

to decreasing β_2 deformation as the neutron number decreases. The aligned angular momenta for ^{173}Pt and ^{175}Pt display similar alignment frequencies compared with the $N = 95$ and $N = 97$ isotones of Os, W and Hf, respectively. Quasiparticle neutron-AB alignment for the negative-parity bands in ^{173}Pt and ^{175}Pt is assumed. For the positive-parity bands BC and AD neutron alignments are taken to be responsible for the observed alignments in the favoured ($\alpha = +\frac{1}{2}$) and unfavoured ($\alpha = -\frac{1}{2}$) signature bands, respectively.

It would be very interesting to see lifetime measurements of the low-lying excited states in ^{173,175}Pt in the future. Especially in ^{175}Pt at $\hbar\omega \approx 0.20$ MeV there is a clear discontinuity observed in the aligned angular momenta (Figures 5.3(c)-(d)). The intruding deformed configuration, based on mp-mh excitations across the $Z = 82$ shell gap, is a likely cause of the observed irregularities. Lifetime measurements would provide valuable information on the possible change of the β_2 deformation of ^{173,175}Pt at low excitation energies.

The combination of the in-beam γ-ray spectroscopy results and the results obtained from the decay spectroscopy, reveals a more complete picture of the properties of nuclei, compared with just one experimental setup. The flexibility of the TDR data-acquisition system, together with the high radiation-detection efficiencies of the detectors, enables a comprehensive analysis of the possible correlations in the data.

Bibliography

[And00] A. N. Andreyev, M. Huyse, P. Van Duppen, L. Weissman, D. Ackermann, J. Gerl, F. P. Heßberger, S. Hofmann, A. Kleinböhl, G. Münzenberg, S. Reshitko, C. Schlegel, H. Schaffner, P. Cagarda, M. Matos, S. Saro, A. Keenan, C. Moore, C. D. O'Leary, R. D. Page, M. Taylor, H. Kettunen, M. Leino, A. Lavrentiev, R. Wyss, K. Heyde. "A triplet of differently shaped spin-zero states in the atomic nucleus ^{186}Pb." *Nature*, 405:430–433 (2000). ISSN 0028-0836. doi:10.1038/35013012. URL http://dx.doi.org/10.1038/35013012.

[And04] A. N. Andreyev, P. A. Butler, R. D. Page, D. E. Appelbe, G. D. Jones, D. T. Joss, R.-D. Herzberg, P. H. Regan, J. Simpson, R. Wadsworth. "GEANT Monte Carlo simulations for the GREAT spectrometer." *Nuclear Instruments and Methods in Physics Research Section A: Accelerators, Spectrometers, Detectors and Associated Equipment*, 533(3):422–434 (2004). ISSN 0168-9002. doi:http://dx.doi.org/10.1016/j.nima.2004.07.205. URL http://www.sciencedirect.com/science/article/pii/S0168900204017462.

[And09] A. N. Andreyev, S. Antalic, D. Ackermann, T. E. Cocolios, V. F. Comas, J. Elseviers, S. Franchoo, S. Heinz, J. A. Heredia, F. P. Heßberger, S. Hofmann, M. Huyse, J. Khuyagbaatar, I. Kojouharov, B. Kindler, B. Lommel, R. Mann, R. D. Page, S. Rinta-Antila, P. J. Sapple, Š. Šaro, P. Van Duppen, M. Venhart, H. Watkins. "α decay of ^{180,181}Pb." *Phys. Rev. C*, 80:054322 (2009). doi:10.1103/PhysRevC.80.054322. URL http://link.aps.org/doi/10.1103/PhysRevC.80.054322.

[Bag00] C. M. Baglin. "Nuclear data sheets for $A = 167$." *Nuclear Data Sheets*, 90(3):431–644 (2000). ISSN 0090-3752. doi:10.1006/ndsh.2000.0012. URL http://www.sciencedirect.com/science/article/pii/S0090375200900127.

[Bag02] C. M. Baglin. "Nuclear data sheets for $A = 170$." *Nuclear Data Sheets*, 96(4):611–873 (2002). ISSN 0090-3752. doi:10.1006/ndsh.2002.0015. URL http://www.sciencedirect.com/science/article/pii/S0090375202900153.

[Bag08] C. M. Baglin. "Nuclear data sheets for $A = 169$." *Nuclear Data Sheets*, 109(9):2033–2256 (2008). ISSN 0090-3752. doi:10.1016/j.nds.2008.08.001. URL http://www.sciencedirect.com/science/article/pii/S0090375208000628.

[Bag09] C. M. Baglin. "Nuclear data sheets for $A = 179$." *Nuclear Data Sheets*, 110(2):265–506 (2009). ISSN 0090-3752. doi:10.1016/j.nds.2009.01.001. URL http://www.sciencedirect.com/science/article/pii/S0090375209000027.

[Bag10] C. M. Baglin. "Nuclear data sheets for $A = 168$." *Nuclear Data Sheets*, 111(7):1807–2080 (2010). ISSN 0090-3752. doi:10.1016/j.nds.2010.07.001. URL http://www.sciencedirect.com/science/article/pii/S0090375210000682.

[Bar90] R. A. Bark, G. D. Dracoulis, A. E. Stuchbery. "Shape coexistence or particle alignment in the light osmium isotopes ^{171}Os, ^{172}Os and ^{173}Os." *Nuclear Physics A*, 514(3):503–544 (1990). ISSN 0375-9474. doi:10.1016/0375-9474(90)90154-E. URL http://www.sciencedirect.com/science/article/pii/037594749090154E.

[Bar91] R. A. Bark. "A shape coexistence interpretation of the phenomenology of alignment curves in Os and Re isotopes." *Journal of Physics G: Nuclear and Particle Physics*, 17(8):1209 (1991). doi:10.1088/0954-3899/17/8/011. URL http://dx.doi.org/10.1088/0954-3899/17/8/011.

[Bar99a] R. A. Bark, S. Törmänen, T. Bäck, B. Cederwall, S. W. Ødegård, J. F. C. Cocks, K. Helariutta, P. Jones, R. Julin, S. Juutinen,

H. Kankaanpää, H. Kettunen, P. Kuusiniemi, M. Leino, M. Muikku, P. Rahkila, A. Savelius. "Bandcrossings in ^{171}Os." *Nuclear Physics A*, 646(4):399–413 (1999). ISSN 0375-9474. doi:10.1016/S0375-9474(98)00645-9. URL http://www.sciencedirect.com/science/article/pii/S0375947498006459.

[Bar99b] R. A. Bark, S. Törmänen, T. Bäck, B. Cederwall, S. W. Ødegård, J. F. C. Cocks, K. Helariutta, P. Jones, R. Julin, S. Juutinen, H. Kankaanpää, H. Kettunen, P. Kuusiniemi, M. Leino, M. Muikku, P. Rahkila, A. Savelius, M. Bergström, F. Ingebretsen, A. Maj, M. Mattiuzzi, W. Mueller, L. L. Riedinger, T. Saitoh, P. O. Tjøm. "Coexistence of triaxial and prolate shapes in ^{171}Ir." *Nuclear Physics A*, 657(2):113–133 (1999). ISSN 0375-9474. doi:10.1016/S0375-9474(99)00319-X. URL http://www.sciencedirect.com/science/article/pii/S037594749900319X.

[Bas04] M. S. Basunia. "Nuclear data sheets for $A = 175$." *Nuclear Data Sheets*, 102(4):719–900 (2004). ISSN 0090-3752. doi:10.1016/j.nds.2004.09.002. URL http://www.sciencedirect.com/science/article/pii/S0090375204000626.

[Bea92] C. W. Beausang, S. A. Forbes, P. Fallon, P. J. Nolan, P. J. Twin, J. N. Mo, J. C. Lisle, M. A. Bentley, J. Simpson, F. A. Beck, D. Curien, G. deFrance, G. Duchêne, D. Popescu. "Measurements on prototype Ge and BGO detectors for the Eurogam array." *Nuclear Instruments and Methods in Physics Research Section A: Accelerators, Spectrometers, Detectors and Associated Equipment*, 313(1-2):37–49 (1992). ISSN 0168-9002. doi:10.1016/0168-9002(92)90084-H. URL http://www.sciencedirect.com/science/article/B6TJM-470F4PY-NX/2/9c311095a5518fab63dbe7476a7bcf94.

[Bel59] S. T. Belyaev. "Effect of pairing correlations on nuclear properties." *Matematisk-fysiske Skrifter udgivet af Det Kongelige Danske Videnskabernes Selskab*, 31:1–54 (1959).

[Ben79a] R. Bengtsson, S. Frauendorf. "An interpretation of backbending in terms of the crossing of the ground state band with an aligned two-quasiparticle band." *Nuclear Physics A*, 314(1):27–36 (1979). ISSN 0375-9474. doi:10.1016/0375-9474(79)90552-9. URL http://www.sciencedirect.com/science/article/pii/0375947479905529.

[Ben79b] R. Bengtsson, S. Frauendorf. "Quasiparticle spectra near the yrast line." *Nuclear Physics A*, 327:139–171 (1979). ISSN 0375-9474. doi:10.1016/0375-9474(79)90322-1. URL http://www.sciencedirect.com/science/article/pii/0375947479903221.

[Ben86a] R. Bengtsson, S. Frauendorf, F.-R. May. "Quasiparticle levels in rotating rare earth nuclei: A cranked shell-model dictionary." *Atomic Data and Nuclear Data Tables*, 35(1):15–122 (1986). ISSN 0092-640X. doi:10.1016/0092-640X(86)90028-8. URL http://www.sciencedirect.com/science/article/pii/0092640X86900288.

[Ben86b] R. Bengtsson, J.-y. Zhang, J. H. Hamilton, L. K. Peker. "Potential energy surface calculations of nuclear shape transitions and shape coexistence in ^{176,178,180}Pt." *Journal of Physics G: Nuclear Physics*, 12(10):L223–L227 (1986). doi:10.1088/0305-4616/12/10/002. URL http://dx.doi.org/10.1088/0305-4616/12/10/002.

[Ben87] R. Bengtsson, T. Bengtsson, J. Dudek, G. Leander, W. Nazarewicz, J.-y. Zhang. "Shape coexistence and shape transitions in even-even Pt and Hg isotopes." *Physics Letters B*, 183(1):1–6 (1987). ISSN 0370-2693. doi:10.1016/0370-2693(87)91406-7. URL http://www.sciencedirect.com/science/article/pii/0370269387914067.

[Bes76] S. Beshai, K. Fransson, S. A. Hjorth, A. Johnson, Th. Lindblad, J. Sztarkier. "Band crossing in ^{184}Pt." *Zeitschrift für Physik A Atoms and Nuclei*, 277(4):351–356 (1976). ISSN 0939-7922. doi:10.1007/BF01545972. URL http://dx.doi.org/10.1007/BF01545972.

[Bla60] J. M. Blatt, V. F. Weisskopf. *Theoretical Nuclear Physics*. John Wiley & Sons, Inc., New York, 5th edition (1960).

[Boa83] M. L. Boas. *Mathematical methods in the physical sciences*. John Wiley & Sons, Inc., New York, 2nd edition (1983). ISBN 0-471-09960-0.

[Boh36] N. Bohr. "Neutron capture and nuclear constitution." *Nature*, 137:344–348 (1936). doi:10.1038/137344a0. URL http://www.nature.com/nature/journal/v137/n3461/abs/137344a0.html.

[Boh51] A. Bohr. "On the quantization of angular momenta in heavy nuclei." *Phys. Rev.*, 81:134–138 (1951). doi:10.1103/PhysRev.81.134. URL http://link.aps.org/doi/10.1103/PhysRev.81.134.

[Boh52] A. Bohr. "The coupling of nuclear surface oscillations to the motion of individual nucleons." *Kgl. Danske Videnskab. Selskab, Mat.-fys. Medd.*, 26:1–40 (1952).

[Boh53a] A. Bohr, B. R. Mottelson. "Collective and individual-particle aspects of nuclear structure." *Kgl. Danske Videnskab. Selskab, Mat.-fys. Medd.*, 27:1–174 (1953).

[Boh53b] A. Bohr, B. R. Mottelson. "Interpretation of isomeric transitions of electric quadrupole type." *Phys. Rev.*, 89:316–317 (1953). doi:10.1103/PhysRev.89.316. URL http://link.aps.org/doi/10.1103/PhysRev.89.316.

[Boh53c] A. Bohr, B. R. Mottelson. "Rotational states in even-even nuclei." *Phys. Rev.*, 90:717–719 (1953). doi:10.1103/PhysRev.90.717.2. URL http://link.aps.org/doi/10.1103/PhysRev.90.717.2.

[Boh73] A. Bohr, B. R. Mottelson. *Nuclear Structure, Volume II: Nuclear Deformations*. W.A. Benjamin, Inc., Massachusetts, 1st edition (1973). ISBN 0-8053-1016-9.

[Bur67] J. Burde, R. M. Diamond, F. S. Stephens. "Ground state (quasi-) rotational levels in light Os, Pt and Hg nuclei." *Nuclear Physics A*, 92(2):306–318 (1967). ISSN 0375-9474. doi:10.1016/0375-9474(67)90220-5. URL http://www.sciencedirect.com/science/article/pii/0375947467902205.

[Ced90] B. Cederwall, R. Wyss, A. Johnson, J. Nyberg, B. Fant, R. Chapman, D. Clarke, F. Khazaie, J. Lisle, J. Mo, J. Simpson, I. Thorslund. "Shape coexistence and strong shape changes in very neutron deficient platinum isotopes." *Zeitschrift für Physik A Atomic Nuclei*, 337:283–292 (1990). ISSN 0939-7922. doi:10.1007/BF01289694. URL http://dx.doi.org/10.1007/BF01289694.

[Ced98] B. Cederwall, T. Bäck, R. Bark, S. Törmänen, S. Ødegård, S. King, J. Simpson, R. D. Page, N. Amzal, D. M. Cullen, P. T. Greenlees, A. Keenan, R. Lemmon, J. Cocks, K. Helariutta, P. M. Jones, R. Julin, S. Juutinen, H. Kettunen, H. Kankaanpää, P. Kuusiniemi, M. Leino, M. Muikku, P. Rahkila, A. Savelius, J. Uusitalo, P. Magierski, R. Wyss. "Collective rotational – vibrational transition in the very neutron-deficient nuclei ^{171,172}Pt." *Physics Letters B*, 443(1–4):69–76 (1998). ISSN 0370-2693. doi:10.1016/S0370-2693(98)01334-3. URL http://www.sciencedirect.com/science/article/pii/S0370269398013343.

[Cro99] M. Cromaz, J. DeGraaf, T. E. Drake, D. Ward, A. Galindo-Uribarri, V. P. Janzen, D. C. Radford, S. Flibotte, S. M. Mullins, J. Rodriguez, S. Pilotte. "High spin spectroscopy of ^{167}Hf." *Phys. Rev. C*, 59:2406–2415 (1999). doi:10.1103/PhysRevC.59.2406. URL http://link.aps.org/doi/10.1103/PhysRevC.59.2406.

[Cwi87] S. Cwiok, J. Dudek, W. Nazarewicz, J. Skalski, T. Werner. "Single-particle energies, wave functions, quadrupole moments and g-factors in an axially deformed Woods-Saxon potential with applications to the two-centre-type nuclear problems." *Computer Physics Communications*, 46(3):379–399 (1987). ISSN 0010-4655. doi:10.1016/0010-4655(87)90093-2. URL http://www.sciencedirect.com/science/article/pii/0010465587900932.

[Della Negra81] S. Della Negra, C. Deprun, D. Jacquet, Y. Le Beyec. "Alpha decay characteristics of neutron deficient isotopes of Pt isotopes produced in ^{63}Cu induced reactions on ^{112}Sn and ^{113}In targets." *Zeitschrift für*

Physik A Atoms and Nuclei, 300(2–3):251–252 (1981). ISSN 0939-7922. doi:10.1007/BF01412302. URL http://dx.doi.org/10.1007/BF01412302.

[De Voigt90] M. J. A. De Voigt, R. Kaczarowski, H. J. Riezebos, R. F. Noorman, J. C. Bacelar, M. A. Deleplanque, R. M. Diamond, F. S. Stephens. "Rotational bands in ^{181}Pt." *Nuclear Physics A*, 507(2):447–471 (1990). ISSN 0375-9474. doi:10.1016/0375-9474(90)90303-4. URL http://www.sciencedirect.com/science/article/pii/0375947490903034.

[Dia66] R. M. Diamond, E. Matthias, J. O. Newton, F. S. Stephens. "Nuclear alignment in heavy-ion reactions." *Phys. Rev. Lett.*, 16:1205–1207 (1966). doi:10.1103/PhysRevLett.16.1205. URL http://link.aps.org/doi/10.1103/PhysRevLett.16.1205.

[Dön83] F. Dönau, S. Frauendorf. "Magnetic moments as a probe for rotational alignment." In N. Johnson, editor, "High Angular Momentum Properties of Nuclei," pages 143–160. Hardwood Academic Publishers, New York (1983). ISSN 0250-4375.

[Dön87] F. Dönau. "Electromagnetic radiation of rotating nuclei." *Nuclear Physics A*, 471(3–4):469–488 (1987). ISSN 0375-9474. doi:10.1016/0375-9474(87)90094-7. URL http://www.sciencedirect.com/science/article/pii/0375947487900947.

[Dra86] G. D. Dracoulis, A. E. Stuchbery, A. P. Byrne, A. R. Poletti, S. J. Poletti, J. Gerl, R. A. Bark. "Shape coexistence in very neutron-deficient Pt isotopes." *Journal of Physics G: Nuclear Physics*, 12(3):L97 (1986). doi:10.1088/0305-4616/12/3/005. URL http://dx.doi.org/10.1088/0305-4616/12/3/005.

[Dra90] G. D. Dracoulis, B. Fabricius, R. A. Bark, A. E. Stuchbery, D. G. Popescu, T. Kibédi. "Intrinsic states and rotational bands in ^{177}Pt." *Nuclear Physics A*, 510(3):533–556 (1990). ISSN 0375-9474. doi:10.1016/0375-9474(90)90065-T. URL http://www.sciencedirect.com/science/article/pii/037594749090065T.

[Dra91] G. D. Dracoulis, B. Fabricius, A. E. Stuchbery, A. O. Macchiavelli, W. Korten, F. Azaiez, E. Rubel, M. A. Deleplanque, R. M. Diamond, F. S. Stephens. "Shape coexistence from the structure of the yrast band in ^{174}Pt." *Phys. Rev. C*, 44:R1246–R1249 (1991). doi: 10.1103/PhysRevC.44.R1246. URL http://link.aps.org/doi/10.1103/PhysRevC.44.R1246.

[Duc99] G. Duchêne, F. A. Beck, P. J. Twin, G. de France, D. Curien, L. Han, C. W. Beausang, M. A. Bentley, P. J. Nolan, J. Simpson. "The Clover: a new generation of composite Ge detectors." *Nuclear Instruments and Methods in Physics Research Section A: Accelerators, Spectrometers, Detectors and Associated Equipment*, 432(1):90–110 (1999). ISSN 0168-9002. doi:10.1016/S0168-9002(99)00277-6. URL http://www.sciencedirect.com/science/article/pii/S0168900299002776.

[Eng82] H. A. Enge, M. Salomaa, A. Sperduto, J. Ball, W. Schier, A. Graue, A. Graue. "Neutron deficient platinum and osmium isotopes produced in the ^{32}S + ^{144}Sm fusion reaction." *Phys. Rev. C*, 25:1830–1837 (1982). doi:10.1103/PhysRevC.25.1830. URL http://link.aps.org/doi/10.1103/PhysRevC.25.1830.

[Esp94] J. Espino, J. D. Garrett, G. B. Hagemann, P. O. Tjøm, C.-H. Yu, M. Bergström, L. Carlén, L. P. Ekström, J. Lyttkens-Lindén, H. Ryde, R. Bengtsson, T. Bengston, R. Chapman, D. Clarke, F. Khazaie, J. C. Lisle, J. N. Mo. "Rotational band structures in ^{171,172}W: Aspects on signature partnership at high spin." *Nuclear Physics A*, 567(2):377–413 (1994). ISSN 0375-9474. doi:10.1016/0375-9474(94)90155-4. URL http://www.sciencedirect.com/science/article/pii/0375947494901554.

[Eva72] R. D. Evans. *The Atomic Nucleus*. McGraw-Hill, Inc., 14th edition (1972).

[Fir96] R. B. Firestone, V. S. Shirley. *Table of Isotopes*. Wiley Interscience, 8th edition (1996). ISBN 0471-14918-7.

[Frö96] P. Fröbrich, R. Lipperheide. *Theory of nuclear reactions*. Oxford University Press, 1st edition (1996). ISBN 978-0-19-853783-0.

[Gam28] G. Gamow. "Zur quantentheorie des atomkernes." *Z. Phys.*, 51:204–212 (1928).

[Gar86] U. Garg, A. Chaudhury, M. W. Drigert, E. G. Funk, J. W. Mihelich, D. C. Radford, H. Helppi, R. Holzmann, R. V. F. Janssens, T. L. Khoo, A. M. Van Den Berg, J. L. Wood. "Lifetime measurements in ^{184}Pt and the shape coexistence picture." *Physics Letters B*, 180(4):319–323 (1986). ISSN 0370-2693. doi:10.1016/0370-2693(86)91195-0. URL http://www.sciencedirect.com/science/article/pii/0370269386911950.

[Gau73] H. Gauvin, R. L. Hahn, Y. Le Beyec, M. Lefort, J. Livet. "Reactions of ^{40}Ar with ^{159}Tb, ^{142}Nd and ^{144}Sm; new α-activities from ^{189}Bi, ^{173}Pt and ^{177}Au." *Nuclear Physics A*, 208(2):360–370 (1973). ISSN 0375-9474. doi:10.1016/0375-9474(73)90381-3. URL http://www.sciencedirect.com/science/article/pii/0375947473903813.

[GH09] M. B. Gómez Hornillos, D. O'Donnell, J. Simpson, D. T. Joss, L. Bianco, B. Cederwall, T. Grahn, P. T. Greenlees, B. Hadinia, P. Jones, R. Julin, S. Juutinen, S. Ketelhut, M. Labiche, M. Leino, M. Nyman, R. D. Page, E. S. Paul, M. Petri, P. Peura, P. Rahkila, P. Ruotsalainen, M. Sandzelius, P. J. Sapple, J. Sarén, C. Scholey, J. Sorri, J. Thomson, J. Uusitalo. "γ-ray spectroscopy approaching the limits of existence of atomic nuclei: A study of the excited states of ^{168}Pt and ^{169}Pt." *Phys. Rev. C*, 79:064314 (2009). doi:10.1103/PhysRevC.79.064314. URL http://link.aps.org/doi/10.1103/PhysRevC.79.064314.

[Gla12] K. A. Gladnishki, P. Petkov, A. Dewald, C. Fransen, M. Hackstein, J. Jolie, Th. Pissulla, W. Rother, K. O. Zell. "Yrast electromagnetic transition strengths and shape coexistence in ^{182}Pt." *Nuclear Physics A*, 877(0):19–34 (2012). ISSN 0375-9474. doi:10.1016/j.nuclphysa.2012.01.001. URL http://www.sciencedirect.com/science/article/pii/S0375947412000036.

[Goo04a] J. TM. Goon. *Alpha and gamma-ray spectroscopic studies of Au, Pt and Ir nuclei near the proton dripline*. Ph.D. thesis, University of Tennessee, Knoxville (2004).

[Goo04b] J. TM. Goon, D. J. Hartley, L. L. Riedinger, M. P. Carpenter, F. G. Kondev, R. V. F. Janssens, K. H. Abu Saleem, I. Ahmad, H. Amro, J. A. Cizewski, C. N. Davids, M. Danchev, T. L. Khoo, A. Heinz, T. Lauritsen, W. C. Ma, G. L. Poli, J. Ressler, W. Reviol, D. Seweryniak, M. B. Smith, I. Wiedenhöver, J.-y. Zhang. "Shape coexistence and band crossings in ^{174}Pt." *Phys. Rev. C*, 70:014309 (2004). doi:10.1103/PhysRevC.70.014309. URL http://link.aps.org/doi/10.1103/PhysRevC.70.014309.

[GR11] J. E. García-Ramos, V. Hellemans, K. Heyde. "Platinum nuclei: Concealed configuration mixing and shape coexistence." *Phys. Rev. C*, 84:014331 (2011). doi:10.1103/PhysRevC.84.014331. URL http://link.aps.org/doi/10.1103/PhysRevC.84.014331.

[GR14a] J. E. García-Ramos, K. Heyde. "Nuclear shape coexistence: A study of the even-even Hg isotopes using the interacting boson model with configuration mixing." *Phys. Rev. C*, 89:014306 (2014). doi:10.1103/PhysRevC.89.014306. URL http://link.aps.org/doi/10.1103/PhysRevC.89.014306.

[GR14b] J. E. García-Ramos, K. Heyde, L. M. Robledo, R. Rodríguez-Guzmán. "Shape evolution and shape coexistence in Pt isotopes: Comparing interacting boson model configuration mixing and Gogny mean-field energy surfaces." *Phys. Rev. C*, 89:034313 (2014). doi:10.1103/PhysRevC.89.034313. URL http://link.aps.org/doi/10.1103/PhysRevC.89.034313.

[Gre55] A. E. S. Green. *Nuclear Physics*. McGraw-Hill, Inc., 1st edition (1955).

[Gur28] R. W. Gurney, E. U. Condon. "Wave mechanics and radioactive disintegration." *Nature*, 122:439–439 (1928). doi:10.1038/122439a0. URL http://dx.doi.org/10.1038/122439a0.

[Hag79] E. Hagberg, P. G. Hansen, P. Hornshøj, B. Jonson, S. Mattsson, P. Tidemand-Petersson. "Alpha decay of neutron-deficient mercury isotopes and their daughters." *Nuclear Physics A*, 318(1-2):29–44 (1979). ISSN 0375-9474. doi:10.1016/0375-9474(79)90467-6. URL http://www.sciencedirect.com/science/article/pii/0375947479904676.

[Han71] P. G. Hansen, B. Jonson, J. Żylicz, M. Alpsten, Å. Appelqvist, G. Nyman. "The alpha decay of ^{179}Hg and ^{178}Hg." *Nuclear Physics A*, 160(2):445–448 (1971). ISSN 0375-9474. doi:10.1016/0375-9474(71)90144-8. URL http://www.sciencedirect.com/science/article/pii/0375947471901448.

[Har65] S. M. Harris. "Higher order corrections to the cranking model." *Phys. Rev.*, 138:B509–B513 (1965). doi:10.1103/PhysRev.138.B509. URL http://link.aps.org/doi/10.1103/PhysRev.138.B509.

[Hax49] O. Haxel, J. H. D. Jensen, H. E. Suess. "On the "magic numbers" in nuclear structure." *Phys. Rev.*, 75:1766–1766 (1949). doi:10.1103/PhysRev.75.1766.2. URL http://link.aps.org/doi/10.1103/PhysRev.75.1766.2.

[Hey11] K. Heyde, J. L. Wood. "Shape coexistence in atomic nuclei." *Rev. Mod. Phys.*, 83:1467–1521 (2011). doi:10.1103/RevModPhys.83.1467. URL http://link.aps.org/doi/10.1103/RevModPhys.83.1467.

[Hil92] Th. Hilberath, St. Becker, G. Bollen, H.-J. Kluge, U. Krönert, G. Passler, J. Rikovska, R. Wyss. "Ground-state properties of neutron-deficient platinum isotopes." *Zeitschrift für Physik A Hadrons and Nuclei*, 342(1):1–15 (1992). ISSN 0939-7922. doi:10.1007/BF01294481. URL http://dx.doi.org/10.1007/BF01294481.

[Hil95] T. Hild, W.-D. Schmidt-Ott, V. Kunze, F. Meissner, C. Wennemann, H. Grawe. "α and β decays of $^{169-173}$Os and the nuclear structure of the daughter isotopes." *Phys. Rev. C*, 51:1736–1744 (1995). doi:10.1103/PhysRevC.51.1736. URL http://link.aps.org/doi/10.1103/PhysRevC.51.1736.

[Ing54] D. R. Inglis. "Particle derivation of nuclear rotation properties associated with a surface wave." *Phys. Rev.*, 96:1059–1065 (1954). doi:10.1103/PhysRev.96.1059. URL http://link.aps.org/doi/10.1103/PhysRev.96.1059.

[Jan88] V. P. Janzen, M. P. Carpenter, L. L. Riedinger, W. Schmitz, S. Pilotte, S. Monaro, D. D. Rajnauth, J. K. Johansson, D. G. Popescu, J. C. Waddington, Y. S. Chen, F. Dönau, P. B. Semmes. "Evidence for a low-frequency $\pi h_{\frac{9}{2}}$ band crossing in ^{185}Pt and ^{183}Ir." *Phys. Rev. Lett.*, 61:2073–2076 (1988). doi:10.1103/PhysRevLett.61.2073. URL http://link.aps.org/doi/10.1103/PhysRevLett.61.2073.

[Jen02] D. G. Jenkins, A. N. Andreyev, R. D. Page, M. P. Carpenter, R. V. F. Janssens, C. J. Lister, F. G. Kondev, T. Enqvist, P. T. Greenlees, P. M. Jones, R. Julin, S. Juutinen, H. Kettunen, P. Kuusiniemi, M. Leino, A.-P. Leppänen, P. Nieminen, J. Pakarinen, P. Rahkila, J. Uusitalo, C. D. O'Leary, P. Raddon, A. Simons, R. Wadsworth, D. T. Joss. "Confirmation of triple shape coexistence in ^{179}Hg: Focal plane spectroscopy of the α decay of ^{183}Pb." *Phys. Rev. C*, 66:011301 (2002). doi:10.1103/PhysRevC.66.011301. URL http://link.aps.org/doi/10.1103/PhysRevC.66.011301.

[Joh71] A. Johnson, H. Ryde, J. Sztarkier. "Evidence for a "singularity" in the nuclear rotational band structure." *Physics Letters B*, 34(7):605–608 (1971). ISSN 0370-2693. doi:10.1016/0370-2693(71)90150-X. URL http://www.sciencedirect.com/science/article/pii/037026937190150X.

[Jos01] D. T. Joss, S. L. King, R. D. Page, J. Simpson, A. Keenan, N. Amzal, T. Bäck, M. A. Bentley, B. Cederwall, J. F. C. Cocks, D. M. Cullen, P. T. Greenlees, K. Helariutta, P. M. Jones, R. Julin, S. Juutinen, H. Kankaanpää, H. Kettunen, P. Kuusiniemi, M. Leino, M. Muikku, A. Savelius, J. Uusitalo, S. J. Williams. "Identification of excited states in ^{167}Os and ^{168}Os: shape coexistence at extreme neutron deficiency."

Nuclear Physics A, 689(3–4):631–654 (2001). ISSN 0375-9474. doi:10.1016/S0375-9474(00)00692-8. URL http://www.sciencedirect.com/science/article/pii/S0375947400006928.

[Jos05] D. T. Joss, J. Simpson, D. E. Appelbe, K. Lagergren, C. J. Barton, B. Cederwall, S. Eeckhaudt, T. Grahn, P. M. Jones, R. Julin, S. Juutinen, B. Hadinia, H. Kettunen, M. Leino, A.-P. Leppänen, P. Nieminen, R. D. Page, J. Pakarinen, E. S. Paul, J. Perkowski, P. Rahkila, M. A. Riley, C. Scholey, J. Uusitalo, K. Van de Vel, D. D. Warner, D. R. Wiseman. "Yrast structures in the light Pt isotopes $^{169-173}$Pt." *Journal of Physics G: Nuclear and Particle Physics*, 31(10):S1715–S1718 (2005). doi:10.1088/0954-3899/31/10/060. URL http://stacks.iop.org/0954-3899/31/i=10/a=060.

[Jos06] D. T. Joss, J. Simpson, D. E. Appelbe, C. J. Barton, D. D. Warner, K. Lagergren, B. Cederwall, B. Hadinia, S. Eeckhaudt, T. Grahn, P. T. Greenlees, P. M. Jones, R. Julin, S. Juutinen, H. Kettunen, M. Leino, A.-P. Leppänen, P. Nieminen, J. Pakarinen, J. Perkowski, P. Rahkila, C. Scholey, J. Uusitalo, K. Van de Vel, R. D. Page, E. S. Paul, D. R. Wiseman, M. A. Riley. "Yrast states and band crossings in the neutron-deficient platinum isotopes $^{169-173}$Pt." *Phys. Rev. C*, 74:014302 (2006). doi:10.1103/PhysRevC.74.014302. URL http://link.aps.org/doi/10.1103/PhysRevC.74.014302.

[Jos14] D. T. Joss. private communication (2014).

[Kal91] C. A. Kalfas, S. Kossionides, C. T. Papadopoulos, R. Vlastou, L. Hildingsson, W. Klamra, Th. Lindblad, C. G. Lindén, R. Wyss, J. Gizon, S. Juutinen, R. Chapman, D. Clarke, F. Khazaie, J. C. Lisle, J. N. Mo. "Study of high spins in ^{173}Os." *Nuclear Physics A*, 526(1):205–223 (1991). ISSN 0375-9474. doi:10.1016/0375-9474(91)90306-Q. URL http://www.sciencedirect.com/science/article/pii/037594749190306Q.

[Kel86] J. G. Keller, K.-H. Schmidt, F. P. Heßberger, G. Münzenberg, W. Reisdorf, H.-G. Clerc, C.-C. Sahm. "Cold fusion in symmetric ^{90}Zr-induced reactions." *Nuclear Physics A*, 452(1):173–204 (1986). ISSN

0375-9474. doi:10.1016/0375-9474(86)90514-2. URL http://www.sciencedirect.com/science/article/pii/0375947486905142.

[Kib08] T. Kibédi, T. W. Burrows, M. B. Trzhaskovskaya, P. M. Davidson, C. W. Nestor Jr. "Evaluation of theoretical conversion coefficients using BrIcc." *Nuclear Instruments and Methods in Physics Research Section A: Accelerators, Spectrometers, Detectors and Associated Equipment*, 589(2):202–229 (2008). ISSN 0168-9002. doi:10.1016/j.nima.2008.02.051. URL http://www.sciencedirect.com/science/article/pii/S0168900208002520.

[Kon02] F. G. Kondev, M. P. Carpenter, R. V. F. Janssens, C. J. Lister, K. Abu Saleem, I. Ahmad, H. Amro, J. Caggiano, C. N. Davids, A. Heinz, B. Herskind, T. L. Khoo, T. Lauritsen, W. C. Ma, J. J. Ressler, W. Reviol, L. L. Riedinger, D. G. Sarantites, D. Seweryniak, S. Siem, A. A. Sonzogni, P. G. Varmette, I. Wiedenhöver. "First observation of excited structures in neutron-deficient ^{179}Hg: evidence for multiple shape coexistence." *Physics Letters B*, 528(3–4):221–227 (2002). ISSN 0370-2693. doi:10.1016/S0370-2693(02)01221-2. URL http://www.sciencedirect.com/science/article/pii/S0370269302012212.

[Kra65] V. A. Kravtsov, N. N. Skachkov. "Influence of nuclear structure on binding energy." *Nuclear Data Sheets*, 1:491–519 (1965). doi:10.1016/S0550-306X(65)80013-1. URL http://www.sciencedirect.com/science/article/pii/S0550306X65800131.

[Kra88] K. S. Krane. *Introductory nuclear physics*. John Wiley & Sons, rev. 2nd edition (1988). ISBN 0-471-85914-1.

[Laz01] I. H. Lazarus, D. E. Appelbe, P. A. Butler, P. J. Coleman-Smith, J. R. Cresswell, S. J. Freeman, R. D. Herzberg, I. Hibbert, D. T. Joss, S. C. Letts, R. D. Page, V. F. E. Pucknell, P. H. Regan, J. Sampson, J. Simpson, J. Thornhill, R. Wadsworth. "The GREAT triggerless total data readout method." *Nuclear Science, IEEE Transactions on*, 48(3):567–569 (2001). ISSN 0018-9499. doi:10.1109/23.940120. URL http://dx.doi.org/10.1109/23.940120.

[Le Blanc99] F. Le Blanc, D. Lunney, J. Obert, J. Oms, J. C. Putaux, B. Roussière, J. Sauvage, S. Zemlyanoi, J. Pinard, L. Cabaret, H. T. Duong, G. Huber, M. Krieg, V. Sebastian, J. E. Crawford, J. K. P. Lee, M. Girod, S. Péru, J. Genevey, J. Lettry. "Large odd-even radius staggering in the very light platinum isotopes from laser spectroscopy." *Phys. Rev. C*, 60:054310 (1999). doi:10.1103/PhysRevC.60.054310. URL http://link.aps.org/doi/10.1103/PhysRevC.60.054310.

[Lei95] M. Leino, J. Äystö, T. Enqvist, P. Heikkinen, A. Jokinen, M. Nurmia, A. Ostrowski, W. H. Trzaska, J. Uusitalo, K. Eskola, P. Armbruster, V. Ninov. "Gas-filled recoil separator for studies of heavy elements." *Nuclear Instruments and Methods in Physics Research Section B: Beam Interactions with Materials and Atoms*, 99(1-4):653–656 (1995). ISSN 0168-583X. doi:10.1016/0168-583X(94)00573-7. URL http://www.sciencedirect.com/science/article/B6TJN-43JWW5R-67/2/47f1773b6eb6b4121236943396feef57. Application of Accelerators in Research and Industry '94.

[Lei97] M. Leino. "In-flight separation with gas-filled systems." *Nuclear Instruments and Methods in Physics Research Section B: Beam Interactions with Materials and Atoms*, 126(1–4):320–328 (1997). ISSN 0168-583X. doi:10.1016/S0168-583X(96)01001-4. URL http://www.sciencedirect.com/science/article/pii/S0168583X96010014. International Conference on Electromagnetic Isotope Separators and Techniques Related to Their Applications.

[May49] M. G. Mayer. "On closed shells in nuclei. II." *Phys. Rev.*, 75:1969–1970 (1949). doi:10.1103/PhysRev.75.1969. URL http://link.aps.org/doi/10.1103/PhysRev.75.1969.

[May50] M. G. Mayer. "Nuclear configurations in the spin-orbit coupling model. I. Empirical evidence." *Phys. Rev.*, 78:16–21 (1950). doi:10.1103/PhysRev.75.1969. URL http://link.aps.org/doi/10.1103/PhysRev.75.1969.

[McG91] F. K. McGowan, N. R. Johnson, I. Y. Lee, C. Baktash, J. W. McConnell, M. N. Rao, M. Oshima, J. C. Wells, A. Larabee, L. L. Riedinger, R. Bengtsson, Z. Xing. "Transition quadrupole moments of high-spin states in ^{172}W and their implications for the interpretation of band crossings in the light isotopes of W to Pt." *Nuclear Physics A*, 530(2):490–506 (1991). ISSN 0375-9474. doi:10.1016/0375-9474(91)90815-N. URL http://www.sciencedirect.com/science/article/pii/037594749190815N.

[Mel03] A. Melerangi, D. Appelbe, R. D. Page, H. J. Boardman, P. T. Greenlees, P. Jones, D. T. Joss, R. Julin, S. Juutinen, H. Kettunen, P. Kuusiniemi, M. Leino, M. H. Muikku, P. Nieminen, J. Pakarinen, P. Rahkila, J. Simpson. "Shape isomerism and spectroscopy of ^{177}Hg." *Phys. Rev. C*, 68:041301 (2003). doi:10.1103/PhysRevC.68.041301. URL http://link.aps.org/doi/10.1103/PhysRevC.68.041301.

[Moh12] P. J. Mohr, B. N. Taylor, D. B. Newell. "CODATA recommended values of the fundamental physical constants: 2010." *Rev. Mod. Phys.*, 84:1527–1605 (2012). doi:10.1103/RevModPhys.84.1527. URL http://link.aps.org/doi/10.1103/RevModPhys.84.1527.

[Mot55] B. R. Mottelson, S. G. Nilsson. "Classification of the nucleonic states in deformed nuclei." *Phys. Rev.*, 99:1615–1617 (1955). doi:10.1103/PhysRev.99.1615. URL http://link.aps.org/doi/10.1103/PhysRev.99.1615.

[Mot59] B. R. Mottelson, S. G. Nilsson. "The intrinsic states of odd-A nuclei having ellipsoidal equilibrium shape." *Matematisk-fysiske Skrifter udgivet af Det Kongelige Danske Videnskabernes Selskab*, 1:1–105 (1959).

[Naz85] W. Nazarewicz, J. Dudek, R. Bengtsson, T. Bengtsson, I. Ragnarsson. "Microscopic study of the high-spin behaviour in selected $A \simeq 80$ nuclei." *Nuclear Physics A*, 435(2):397–447 (1985). ISSN 0375-9474. doi:10.1016/0375-9474(85)90471-3. URL http://www.sciencedirect.com/science/article/pii/0375947485904713".

[New67] J. O. Newton, F. S. Stephens, R. M. Diamond, K. Kotajima, E. Matthias. "Angular distributions of gamma rays produced in reactions with heavy ions." *Nuclear Physics A*, 95(2):357–376 (1967). ISSN 0375-9474. doi:10.1016/0375-9474(67)90507-6. URL http://www.sciencedirect.com/science/article/pii/0375947467905076.

[Nil55] S. G. Nilsson. "Binding states of individual nucleons in strongly deformed nuclei." *Kgl. Danske Videnskab. Selskab, Mat.-fys. Medd.*, 29:1–69 (1955).

[Nil69] S. G. Nilsson, C. F. Tsang, A. Sobiczewski, Z. Szymański, S. Wycech, C. Gustafson, I.-L. Lamm, P. Möller, B. Nilsson. "On the nuclear structure and stability of heavy and superheavy elements." *Nuclear Physics A*, 131(1):1–66 (1969). ISSN 0375-9474. doi:10.1016/0375-9474(69)90809-4. URL http://www.sciencedirect.com/science/article/pii/0375947469908094.

[Nil95] S. G. Nilsson, I. Ragnarsson. *Shapes and shells in nuclear structure*. Cambridge Univerity Press, 1st edition (1995). ISBN 0-521-37377-8.

[Nyb90] J. Nyberg, A. Johnson, M. P. Carpenter, C. R. Bingham, L. H. Courtney, V. P. Janzen, S. Juutinen, A. J. Larabee, Z.-M. Liu, L. L. Riedinger, C. Baktash, M. L. Halbert, N. R. Johnson, I. Y. Lee, Y. Schutz, J. C. Waddington, D. G. Popescu. "High-spin states in ^{183}Pt." *Nuclear Physics A*, 511(1):92–116 (1990). ISSN 0375-9474. doi:10.1016/0375-9474(90)90028-K. URL http://www.sciencedirect.com/science/article/pii/037594749090028K.

[O'D09] D. O'Donnell, J. Simpson, C. Scholey, T. Back, P. T. Greenlees, U. Jakobsson, P. Jones, D. T. Joss, D. S. Judson, R. Julin, S. Juutinen, S. Ketelhut, M. Labiche, M. Leino, M. Nyman, R. D. Page, P. Peura, P. Rahkila, P. Ruotsalainen, M. Sandzelius, P. J. Sapple, J. Sarén, J. Thomson, J. Uusitalo, H. V. Watkins. "First observation of excited states in ^{175}Hg$_{95}$." *Phys. Rev. C*, 79(5):051304 (2009). doi:10.1103/PhysRevC.79.051304. URL http://link.aps.org/doi/10.1103/PhysRevC.79.051304.

[Pag96] R. D. Page, P. J. Woods, R. A. Cunningham, T. Davinson, N. J. Davis, A. N. James, K. Livingston, P. J. Sellin, A. C. Shotter. "Radioactivity of neutron deficient isotopes in the region $N > 82 > Z$." *Phys. Rev. C*, 53:660–670 (1996). doi:10.1103/PhysRevC.53.660. URL http://link.aps.org/doi/10.1103/PhysRevC.53.660.

[Pag03] R. D. Page, A. N. Andreyev, D. E. Appelbe, P. A. Butler, S. J. Freeman, P. T. Greenlees, R. D. Herzberg, D. G. Jenkins, G. D. Jones, P. Jones, D. T. Joss, R. Julin, H. Kettunen, M. Leino, P. Rahkila, P. H. Regan, J. Simpson, J. Uusitalo, S. M. Vincent, R. Wadsworth. "The GREAT spectrometer." *Nuclear Instruments and Methods in Physics Research Section B: Beam Interactions with Materials and Atoms*, 204:634–637 (2003). ISSN 0168-583X. doi:10.1016/S0168-583X(02)02143-2. URL http://www.sciencedirect.com/science/article/B6TJN-47MHV52-B/2/5407c5ba07f5804725a2636a7bc02384. 14th International Conference on Electromagnetic Isotope Separators and Techniques Related to their Applications.

[Per57] I. Perlman, J. Rasmussen. "Alpha radioactivity." In S. Flügge, editor, "Encyclopedia of Physics, Nuclear Reactions III," volume XLII, pages 109–202. Springer-Verlag, 1st edition (1957).

[Peu14] P. Peura, C. Scholey, D. T. Joss, S. Juutinen, R. Julin, T. Bäck, B. Cederwall, P. T. Greenlees, U. Jakobsson, P. Jones, D. S. Judson, S. Ketelhut, M. Labiche, M. Leino, M. Nyman, D. O'Donnell, R. D. Page, P. Rahkila, P. Ruotsalainen, M. Sandzelius, P. J. Sapple, J. Sarén, J. Simpson, J. Thomson, J. Uusitalo, H. V. Watkins. "Quasiparticle alignments and α-decay fine structure of ^{175}Pt." *Phys. Rev. C*, 89:024316 (2014). doi:10.1103/PhysRevC.89.024316. URL http://link.aps.org/doi/10.1103/PhysRevC.89.024316.

[Pii75] M. Piiparinen, J. C. Cunnane, P. J. Daly, C. L. Dors, F. M. Bernthal, T. L. Khoo. "High-spin level systematics in $^{186-194}$Pt and rotation-alignment coupling." *Phys. Rev. Lett.*, 34:1110–1113 (1975). doi:10.1103/PhysRevLett.34.1110. URL http://link.aps.org/doi/10.1103/PhysRevLett.34.1110.

[Rad72] V. Radeka. "Trapezoidal filtering of signals from large germanium detectors at high rates." *Nuclear Instruments and Methods*, 99(3):525–539 (1972). ISSN 0029-554X. doi:10.1016/0029-554X(72)90666-0. URL http://www.sciencedirect.com/science/article/pii/0029554X72906660.

[Rad95a] D. C. Radford. "Background subtraction from in-beam HPGe coincidence data sets." *Nuclear Instruments and Methods in Physics Research Section A: Accelerators, Spectrometers, Detectors and Associated Equipment*, 361(1-2):306–316 (1995). ISSN 0168-9002. doi:10.1016/0168-9002(95)00184-0. URL http://www.sciencedirect.com/science/article/pii/0168900295001840.

[Rad95b] D. C. Radford. "ESCL8R and LEVIT8R: Software for interactive graphical analysis of HPGe coincidence data sets." *Nuclear Instruments and Methods in Physics Research Section A: Accelerators, Spectrometers, Detectors and Associated Equipment*, 361(1-2):297–305 (1995). ISSN 0168-9002. doi:10.1016/0168-9002(95)00183-2. URL http://www.sciencedirect.com/science/article/pii/0168900295001832.

[Rah08] P. Rahkila. "Grain - A java data analysis system for Total Data Readout." *Nuclear Instruments and Methods in Physics Research Section A: Accelerators, Spectrometers, Detectors and Associated Equipment*, 595(3):637–642 (2008). ISSN 0168-9002. doi:10.1016/j.nima.2008.08.039. URL http://www.sciencedirect.com/science/article/pii/S0168900208011698.

[Rai50] J. Rainwater. "Nuclear energy level argument for a spheroidal nuclear model." *Phys. Rev.*, 79:432–434 (1950). doi:10.1103/PhysRev.79.432. URL http://link.aps.org/doi/10.1103/PhysRev.79.432.

[Ras59a] J. O. Rasmussen. "Alpha-decay barrier penetrabilities with an exponential nuclear potential: Even-even nuclei." *Phys. Rev.*, 113:1593–1598 (1959). doi:10.1103/PhysRev.113.1593. URL http://link.aps.org/doi/10.1103/PhysRev.113.1593.

[Ras59b] J. O. Rasmussen. "Alpha-decay barrier penetrabilities with an exponential nuclear potential: Odd-mass nuclei." *Phys. Rev.*, 115:1675–1679 (1959). doi:10.1103/PhysRev.115.1675. URL http://link.aps.org/doi/10.1103/PhysRev.115.1675.

[Rec85] J. Recht, Y. K. Agarwal, K. P. Blume, M. Guttormsen, H. Hübel, H. Kluge, K. H. Maier, A. Maj, N. Roy, D. J. Decman, J. Dudek, W. Nazarewicz. "High-spin structure in ^{169}W and ^{170}W." *Nuclear Physics A*, 440(2):366–396 (1985). ISSN 0375-9474. doi:10.1016/0375-9474(85)90345-8. URL http://www.sciencedirect.com/science/article/pii/0375947485903458.

[Ros93] C. Rossi Alvarez. "The GASP array." *Nuclear Physics News*, 3(3):10–13 (1993). URL http://www.informaworld.com/10.1080/10506899308221154.

[Row02] M. W. Rowe, J. C. Batchelder, T. N. Ginter, K. E. Gregorich, F. Q. Guo, F. P. Heßberger, V. Ninov, J. Powell, K. S. Toth, X. J. Xu, J. Cerny. "Decay of ^{178}Tl." *Phys. Rev. C*, 65:054310 (2002). doi:10.1103/PhysRevC.65.054310. URL http://link.aps.org/doi/10.1103/PhysRevC.65.054310.

[Sch84] K.-H. Schmidt, C.-C. Sahm, K. Pielenz, H.-G. Clerc. "Some remarks on the error analysis in the case of poor statistics." *Zeitschrift für Physik A Atoms and Nuclei*, 316:19–26 (1984). ISSN 0939-7922. doi:10.1007/BF01415656. URL http://dx.doi.org/10.1007/BF01415656.

[Sch86] K.-H. Schmidt, R. S. Simon, J.-G. Keller, F. P. Hessberger, G. Münzenberg, B. Quint, H.-G. Clerc, W. Schwab, U. Gollerthan, C.-C. Sahm. "Gamma-spectroscopic investigations in the radiative fusion reaction ^{90}Zr + ^{90}Zr." *Physics Letters B*, 168(1-2):39–42 (1986). ISSN 0370-2693. doi:10.1016/0370-2693(86)91456-5. URL http://www.sciencedirect.com/science/article/B6TVN-470MKVK-NS/2/41a796b4a989076489993733eeeb232f.

[Sch01] K. A. Schmidt, M. Bergström, G. B. Hagemann, B. Herskind, G. Sletten, P. G. Varmette, J. Domscheit, H. Hübel, S. W. Ødegård, S. Frattini, A. Bracco, B. Million, M. P. Carpenter, R. V. F. Janssens, T. L. Khoo, T. Lauritsen, C. J. Lister, S. Siem, I. Wiedenhöver, D. J. Hartley, L. L. Riedinger, A. Maj, W. C. Ma, R. Terry. "Study of ^{169}Hf at high rotational frequency." *The European Physical Journal A - Hadrons and Nuclei*, 12(1):15–28 (2001). ISSN 1434-6001. doi:10.1007/s100500170035. URL http://dx.doi.org/10.1007/s100500170035.

[Sch10] C. Scholey, K. Andgren, L. Bianco, B. Cederwall, I. G. Darby, S. Eeckhaudt, S. Ertürk, M. G. Hornillos, T. Grahn, P. Greenlees, B. Hadinia, E. Ideguchi, P. Jones, D. Joss, R. Julin, S. Juutinen, S. Ketelhut, M. Leino, A.-P. Leppänen, P. Nieminen, M. Niikura, M. Nyman, D. O'Donnell, R. D. Page, J. Pakarinen, P. Rahkila, J. Sarén, M. Sandzelius, J. Simpson, J. Sorri, J. Thomson, J. Uusitalo, M. Venhart. "Isomeric and ground-state properties of $^{171}_{78}$Pt, $^{167}_{76}$Os, and $^{163}_{74}$W." *Phys. Rev. C*, 81:014306 (2010). doi:10.1103/PhysRevC.81.014306. URL http://link.aps.org/doi/10.1103/PhysRevC.81.014306.

[Sii66] A. Siivola. "Alpha-active platinum isotopes." *Nuclear Physics*, 84(2):385–397 (1966). ISSN 0029-5582. doi:10.1016/0029-5582(66)90377-4. URL http://www.sciencedirect.com/science/article/pii/0029558266903774.

[Sim86] R. S. Simon, K.-H. Schmidt, F. P. Heßberger, S. Hlavac, M. Honusek, G. Münzenberg, H.-G. Clerc, U. Gollerthan, W. Schwab. "Evidence for nuclear shape coexistence ^{180}Hg." *Zeitschrift für Physik A Hadrons and Nuclei*, 325:197–202 (1986). ISSN 0939-7922. doi:10.1007/BF01289651. URL http://dx.doi.org/10.1007/BF01289651.

[Ste72] F. S. Stephens, R. S. Simon. "Coriolis effects in the yrast states." *Nuclear Physics A*, 183(2):257–284 (1972). ISSN 0375-9474. doi:10.1016/0375-9474(72)90658-6. URL http://www.sciencedirect.com/science/article/pii/0375947472906586.

[Ste75] F. S. Stephens. "Coriolis effects and rotation alignment in nuclei." *Rev. Mod. Phys.*, 47:43–65 (1975). doi:10.1103/RevModPhys.47.43. URL http://link.aps.org/doi/10.1103/RevModPhys.47.43.

[Tow49] C. H. Townes, H. M. Foley, W. Low. "Nuclear quadrupole moments and nuclear shell structure." *Phys. Rev.*, 76:1415–1416 (1949). doi:10.1103/PhysRev.76.1415. URL http://link.aps.org/doi/10.1103/PhysRev.76.1415.

[Wal12] J. C. Walpe, U. Garg, S. Naguleswaran, J. Wei, W. Reviol, I. Ahmad, M. P. Carpenter, T. L. Khoo. "Lifetime measurements in ^{182,186}Pt." *Phys. Rev. C*, 85:057302 (2012). doi:10.1103/PhysRevC.85.057302. URL http://link.aps.org/doi/10.1103/PhysRevC.85.057302.

[Wat11] H. Watkins. *Lifetime measurements probing shape coexistence in ^{175}Pt, ^{174}Pt and ^{175}Pt.* Ph.D. thesis, Oliver Lodge Laboratory, University of Liverpool (2011).

[Wei51] V. F. Weisskopf. "Radiative transition probabilities in nuclei." *Phys. Rev.*, 83:1073–1073 (1951). doi:10.1103/PhysRev.83.1073. URL http://link.aps.org/doi/10.1103/PhysRev.83.1073.

[Wil06] E. Williams, C. Plettner, E. A. McCutchan, H. Levine, N. V. Zamfir, R. B. Cakirli, R. F. Casten, H. Ai, C. W. Beausang, G. Gürdal, A. Heinz, J. Qian, D. A. Meyer, N. Pietralla, V. Werner. "Revisiting anomalous $B(E2;4_1^+ \rightarrow 2_1^+)/B(E2;2_1^+ \rightarrow 0_1^+)$ values in ^{98}Ru and ^{180}Pt." *Phys. Rev. C*, 74:024302 (2006). doi:10.1103/PhysRevC.74.024302. URL http://link.aps.org/doi/10.1103/PhysRevC.74.024302.

[Wys88] R. Wyss, J. Nyberg, A. Johnson, R. Bengtsson, W. Nazarewicz. "Highly deformed intruder bands in the $A \approx 130$ mass region." *Physics Letters B*, 215(2):211–217 (1988). ISSN 0370-2693. doi:10.1016/0370-2693(88)91422-0. URL http://www.sciencedirect.com/science/article/pii/0370269388914220.